A Modelling and Experimental Study of Locomotion-Induced Hyperpolarization of Voltage Threshold in Cat Lumbar Motoneurones

BY

YUE DAI

A Thesis
Submitted to the Faculty of Graduate Studies
in Partial Fulfillment of the Requirements
for the Degree of

DOCTOR OF PHILOSOPHY

Department of Physiology
University of Manitoba
Winnipeg, Manitoba

THE UNIVERSITY OF MANITOBA

FACULTY OF GRADUATE STUDIES

*****

COPYRIGHT PERMISSION PAGE

A Modelling and Experimental Study of Locomotion-Induced Hyperpolarization of Voltage Threshold in Cat Lumbar Motoneurones

BY

Yue Dai

A Thesis/Practicum submitted to the Faculty of Graduate Studies of The University of Manitoba in partial fulfillment of the requirements of the degree

of

Doctor of Philosophy

Abstract

Cat lumbar motoneurones display changes in excitability during fictive locomotion induced by stimulation of the mesencephalic locomotor region (MLR). A novel finding reported recently is a ~8.0 mV hyperpolarization of voltage threshold (Vth) for action potential generation in motoneurones during fictive locomotion (Krawitz et al. 2001). Mechanisms underlying this phenomenon are still unknown.

In this thesis we use computer models combined with single cell recording technique to investigate possible mechanisms responsible for the hyperpolarization of Vth. Three types of model motoneurons (S, FR and FF) were built using GENESIS based on cat spinal motoneurone properties. A large-scale population model (Bashor, 1998) was used to reveal potential effects on the output of motoneurone pools during fictive locomotion.

Simulation results with the motoneurone models show that Vth could be hyperpolarized by either increasing the fast sodium conductance or by decreasing the fast potassium conductance (delayed rectifier) in the initial segment. Fluctuations of membrane potential could also produce Vth hyperpolarization, but unlike the state-dependent hyperpolarization of Vth observed during fictive locomotion, this effect on Vth is limited to the first few spikes in the spike train. The network modeling shows that hyperpolarization of Vth could enhance the output of the motor system through increasing the recruitment of motoneurones and the average firing frequency of motoneurone pools. The simulation results suggest that enhancement of the initial

segmental sodium conductance is a possible mechanism underlying the hyperpolarization of Vth during fictive locomotion and that this increased excitability of motoneurones would enhance the output of spinal motor systems mainly through an increment of recruited motoneurons. These results suggest the hypothesis that motoneurone recruitment during locomotion is determined, at least in part, by modulation of voltage threshold.

Acknowledgments

I would like to take this opportunity to express my deepest gratitude and appreciation to my supervisor Dr. Larry Jordan. I thank him for providing me with an opportunity to enter a wonderful world of neuroscience from mathematics where I had ever worked for many years for my bachelor and master degrees. I thank him for his continuous guidance and helpful suggestions and for giving me a great independency in my graduate work with his kindness and patience over the course of my Ph.D program. I thank him for not only introducing me to the neuroscience world that has become a part of my life, but also bringing me into a wider world that is built with loyalty and dedication to sciences for developing curiosity to sciences, encouraging creative ability, promoting scientific research, and seeking the truth of sciences. His attitude toward science and spirit of devoting to scientific research is my lifetime example and will inspire me constantly in my future career.

I would also like to express enormous thanks and appreciation to Dr. David McCrea for standing behind me to give strong support and encouragement to me. I thank him for shaping me with his "scientific axe", enlightening me with his philosophic thoughts, and guiding me with his endless wisdom and knowledge.

I would like to extend special thanks to Dr. Brent Fedirchuk for his suggestions, conversations, and helpful inputs that helped me undertake my studies and complete my publications and thesis. For the same reasons I am especially grateful to Dr. Kelvin Jones and Dr. David Bashor.

I would also like to convey my special thanks to Dr. Shawn Hochman and Dr. Peter Aitchison for their long-term support and cares not only to my graduate studies but also to my personal development and my children and family.

I am indebted to Dr. Dean Kriellaars for introducing me to Dr. Larry Jordan and for serving as my committee member for my thesis defense.

I would also like to thank Gilles Detillieux, Kim Madec, Maria Setterbom, Matt Ellis, and Nancy Eidsvig for their excellent technique support during my Ph.D program training.

I would like to acknowledge the Manitoba Neurotrauma Program for studentship support.

Finally, I would like to express my all thanks and loves to my wife Lingou who has been standing with me throughout the years to give me the strength to pursue my educational and life goals. Lingou, it is my great honor and pleasure to dedicate this thesis to you !

Contents

General Introduction

Overview of Motoneurone Physiology

Motoneurones are the final common path which links the central nervous system (CNS) and motor behaviour (Sherrington, 1947). Motoneurones receive synaptic inputs from descending systems (forebrain, some brain stem nuclei, raphe nucleus, locus coeruleus, and other pontine and brainstem nuclei) and from various afferent fibers (from muscle, joints, and skin, etc.), and integrate the synaptic inputs for coding of the output signals. Motoneurones also receive synaptic inputs from the interneuron circuitry serving as the "central pattern generation" for a motor behaviour. The resulting motor output is determined by the final integration of synaptic sources occurring at the motoneurones. Mechanisms capable of altering the firing or integrative properties of motoneurones will therefore to be expected to have profound effects on motoneurone recruitment and the total motor output.

Anatomy and membrane properties of motoneurones

Spinal motoneurones are mainly distributed in lamina IX of the ventral horn. They are among the largest of spinal neurones. In cat, the spinal motoneurones have a large dendritic tree and a large soma. The dendritic membrane accounts for more than 97% (Cullheim et al., 1987) of the total membrane area, with 61% of the stem dendrites and 12-33% of distal dendrites covered by synaptic boutons (örnung et al., 1998; see Rekling et al. 2000 for review). In adult cat, the hindlimb motoneurones have a soma diameter of 30-70 μm, 5-20 stem dendrites with diameters of 0.5-19 μm, and a mean

length of ~1200 μm (Cullheim et al., 1987; Ulfhake et al., 1981;Van Buren and Frank, 1965; Zwaagstra and Kernell, 1980. See Rekling et al. 2000 for review).

The anatomical structure of motoneurones determines some aspects of their passive membrane electrical properties. Cat spinal motoneurones have an input resistance (R_N) of ~1.5 MΩ (ranging from 0.3 to 6), specific membrane resistivity (R_M) of ~0.25 Ωm^2 (0.1-1), specific membrane capacitance (C_M) of ~0.02 F/m^2 (0.01-0.04), specific cytoplasmic resistivity (R_A) of ~0.7 Ωm (0.5-1), time constant (τ) of ~5 ms (3-12), and electrotonic length (L_N) of ~1.5λ (1-2), (See Rall, 1977 for review).

Active conductances in cat, mouse and neonatal rat spinal motoneurones include fast sodium conductance (g_{Na}), fast potassium conductance-delayed rectifier ($g_{K(DR)}$), A-current conductance (g_{KA}), calcium-dependent potassium conductance ($g_{K(AHP)}$, both fast and slow), h-current conductance (g_h, mixed currents of sodium and potassium), leak conductance (potassium current g_{K_l} and chloride current g_{Cl_l}), and three types of calcium conductances, including T-type (g_{Ca_T}, LVA), L-type (g_{Ca_L}, HVA), and N-type (g_{Ca_N}, HVA). The P-type calcium conductance (g_{Ca_P}, HVA) has been found in hypoglossal motoneurones, and the persistent sodium conductance (g_{NaP}) has been found in trigeminal, hypoglossal, and facial motoneurones in guinea pig. (Rekling et al., 2000 and Binder et al., 1996).

A motoneurone and the population of muscle fibers that it innervates are called a "motor unit". In vertebrates, the skeletal muscles are generally classified into three types: slow fibers with high level of aerobic metabolism & slow contraction (slow type), fast glycolytic fibers with high level of glycolysis & rapid contraction (fast type), and fast oxidative fibers with intermediate properties between the slow and fast type. The

different types of muscle fibers are organized into different types of motor units, and there is a close correlation between the types of muscle fibers and the types of motoneurones that innervates it. Studies by Robert Burke's group therefore demonstrated that motor units could be divided into three types: S-type (slow-twitch & fatigue resistant), FF-type (fast-twitch & fatiguable), and FR type (fast-twitch & fatigue resistant), according to their different rate of contraction, force generation, fatigue resistant ability, and glycolytic & oxidative capacity (see Burke R.E. 1981 for details).

Studies by Burke and his colleagues (Burke, R.E., Levine, D.N., Salcman, M., and Tsairis, P., 1974) showed that force generations by the three types of motor units were different. The S-type motor unit generated the smallest force (contraction) in response to single volley stimulation while the FF-type generated the largest one (~25 times larger than the S-type). In response to tetanic stimulation, however, the S-type motor unit maintained a prolonged contractile state, which is called a muscle tetanus, while the FF-type activated tetanically and faded rapidly to no contractile force at all. The FR-type showed intermediate properties between the S- and FF-types: a modest contractile response to a single volley (~5 times larger than the S-type) and only modest fading with tetanic stimulation.

Correspondingly, motoneurones are divided into S, FF and FR types according to the motor units they belong to. Different types of motoneurones have different sizes and electrophysiological properties. The S-type motoneurones have a relatively small somatic and dendritic membrane area (e.g. 456900 μm^2, Cullheim et al., 1987), low rheobase current of ~5 nA (in a range of $\leq$ 8.5 nA, Zengel et al., 1985), large input resistance of ~1.6 MΩ ($\geq$ 1.3MΩ, Zengel et al., 1985), and large membrane time constant of ~10 ms ($\geq$

9.5 ms, Zengel et al., 1985), while the FF-type motoneurones have a large membrane area (e.g. 726600 μm^2, Cullheim et al., 1987), high rheobase of ~20 nA (≥15 nA, Zengel et al., 1985), small input resistance of ~0.6 MΩ (≤ 0.85 MΩ, Zengel et al., 1985), and small membrane time constant of ~6.0 ms (≤ 7.4 ms, Zengel et al., 1985). The FR-type motoneurones fall between the S- and F-type units with a mediate somatic and dendritic area (e.g. 617300 μm^2, Cullheim et al., 1987), rheobase current of ~12 nA (in a range of 8.5-15 nA, Zengel et al., 1985), input resistance of ~1.0 MΩ (0.85-1.3 MΩ, Zengel et al., 1985), and membrane time constant of 8.0 ms (7.4-9.5 ms, Zengel et al., 1985). There is another type called FI type (fast-twitch & intermediate fatigue) which falls between the FF- and FR-type units. See Zengel et al. (1985), Clements et al. (1989), and Cullheim et al. (1987) for details of properties of all four types of motoneurones.

Excitability of motoneurones

The excitability of motoneurones is determined by their intrinsic membrane properties and modulated by pre-motor networks. Normally, the action potential is initiated in the unmyelinated initial axon segment because it has higher density of fast sodium channels than the soma (Catterall 1981; Dodge and Cooley, 1973; Moore et al., 1983). Then the initial segmental action potential invades the soma-dendritic membrane and generates the somatodendritic action potential, the SD spike. The initial segment spike that causes an inflection of the somatic membrane potential is referred to as IS spike (See Fig. 1A, Section I).

In cat lumbar motoneurones, the relation between the steady-state firing frequency and the amount of injected current (f-I relation) can be described as one or two

ranges with the slopes of the first range (primary range) of 1-3 Hz/nA and the secondary range of 3-8 Hz/nA (Kernell 1965). Further increasing the injected current may result in a third range with lower slope (Baldissera and Gustafsson, 1974a,b,c; Kernell, 1965; Schwindt, 1973; Schwindt and Calvin, 1972; Schwindt and Crill, 1982).

Motoneurone excitability can be influenced by many factors including (1) anatomical structure; (2) passive and active membrane properties; (3) afferent and segmental inputs; and (4) neuronal modulators. Almost every active conductance listed above has an effect on motoneurone excitability. However, the conductances that have direct and major influences on the excitability of spinal motoneurones include (1) the calcium-dependent potassium conductance, which produces the afterhyperpolarization (AHP) and regulates the firing frequency of the motoneurones; (2) the fast o conductance, which initiates the action potentials, determines voltage threshold for action potential generation, and has an effect on the current threshold for firing; (3) high voltage activated non-inactivating calcium conductance (L-type), which facilitates non-linear integration of synaptic inputs, plateau potentials, and bi-stable firing motoneurone firing; and (4) leak conductance which is a major contributor to the input resistance, rheobase current, and resting membrane potential.

Synaptic inputs from sensory fibers and pre-motor neuronal networks produce both post synaptic excitation and inhibition. For example, the excitatory monosynaptic input to spinal motoneurones from group Ia afferent uses glutamate as neurotransmitter, and Ia inhibitory interneurons (IaIN), which mediate reciprocal inhibition, release glycine as transmitter. Aslo, Renshaw cells mediate recurrent inhibition through GABAergic and glycinergic projections to the motoneurone pools (See Rekling et al., 2000 for review).

Neuronal modulators exert potent effects on motoneurone excitability. The major modulators for cat, mouse, and neonatal rat motoneurones include glutamate, 5-HT, NE (norepinephrine), ACh, and dopamine. Modulation of motoneuronal excitability includes both pre- and post-synaptic modulations and act both via ionotropic and metabotropic receptors. Actions at ionotropic receptors alter local membrane currents that are determined by membrane properties and cellular morphology. Actions at metabotropic receptors initiate second messenger cascades that have various effects including altering the function of ionotropic channels and/or receptors (Rekling et al., 2000). Details of putative mechanisms altering motoneurone excitability are discussed in Section I (discussion) and General Discussion of this thesis.

Motoneurone excitability is increased during fictive locomotion

Cat lumbar motoneurones display enhanced in excitability during fictive locomotion induced by stimulation of mesencephalic locomotor region (MLR). Previous experiments have shown that during fictive locomotion, motoneurones display (1) changes in the input resistance (Shefchyk et al 1985); (2) a reduction in afterhyperpolarization (Brownstone et al 1992, similar observations are also reported in the isolated neonatal rat spinal cord preparation (Schmidt, 1994) during pharmacologically induced locomotor like activity); (3) hyperpolarization of voltage threshold for action potential generation (Krawitz et al., 2000); and (4) changes in the relation of firing frequency and injected current (Brownstone et al., 1992; Fedirchuk et al., 1998). All these changes in membrane properties are state-dependent. Mechanisms underlying these phenomena are still unknown. However, some factors that have

influence on the motoneurone excitability at rest would be excluded. For example, the morphology or size of the motoneurones can be excluded because no relation between the types of motoneurone and the above-mentioned changes in excitability has been reported during fictive locomotion. Some transient changes in membrane conductance could be also excluded because of their limited effects on motoneurone membrane properties. For examples, the accommodation of action potential generation, which is mainly due to an inactivation of sodium channels during a slow depolarization of membrane potential, and adaptation of repetitive firing, which mainly results from an accumulation of calcium dependent-potassium currents, would not be responsible for the above mentioned phenomena. The synaptic inputs from afferent fibers could be also excluded as a possible mechanism because the above mentioned changes in motoneurone excitability are observed during fictive locomotion in the absence of afferent activity. Therefore, the question of what mechanisms underlying the changes in cat lumbar motoneurone excitability during fictive locomotion remains open. A further investigation of these mechanisms will enhance our knowledge of the motoneurone properties and help us to better understand the mechanisms that the motor system uses to regulate the output for locomotion. The purpose of this thesis is to investigate putative mechanisms underlying the hyperpolarization of voltage threshold for action potential generation in cat lumbar motoneurones during fictive locomotion using modelling and experimental approaches.

Modeling of neuronal activity

Computer modeling is a useful tool in unraveling the complex workings of neuronal systems. Neurone models are widely used for studies of membrane properties

and excitability of neurons in different species. Early excitability models were focused on action potential propagation in nerve and the gating of the ions permeable to the membrane. An important early proposal was made by Bernstein (1902) based on the work of Nernst and others. Bernstein proposed that the membrane was a site of diffusion potential primarily due to a potassium concentration gradient and that a sharp increase in permeability and the loss of ion specificity permitted the membrane potential temporarily to depolarize to zero. Based on these ideas some phenomenological models were later developed for the studies of electrical changes in membrane property and threshold for excitation (Hill 1910; Rashevsky 1931). Our knowledge of neuronal electrical and anatomical properties has greatly improved over many decades of research, and now the channel-based biophysical models can be built much more accurately to reflect the detailed membrane properties of neurons. The ability to build a neuron model with increasingly realistic properties is mainly attributed to the contributions by Hodgkin, Huxley, and Rall. Their pioneering work has become a basis for today's neuronal modeling.

Hodgkin-Huxley (HH) model

The Hodgkin-Huxley model includes two parts: (1) the parallel-conductance model of the axon membrane, and (2) the mathematical model which was constructed to describe the voltage and time dependencies of the fast potassium and fast sodium conductances responsible for the action potential in squid axons (Hodgkin and Huxley, 1952d). The original HH model was intended to account for the voltage-clamp experimental observations, where the currents carried by Na^+ and K^+ ions could be

separated. During the action potential produced by a step depolarization, the sodium conductance turned on and then inactivated and the potassium conductance turned on with a sigmoid time course following a step depolarization. The assumption for the HH model is that there are separate channels for potassium, sodium, and other ions so that the total ionic current is a sum of the currents generated by each of the channels (Hodgkin and Huxley, 1952c). In HH model, potassium conductance (g_K) is computed by a coefficient (n) multiplied by the maximum value (g_{K_max}) of the conductance (i.e. $g_K = n^4 g_{K\_max}$), and sodium conductance (g_{Na}) is calculated in a similar way with two coefficients (m and h) multiplying the maximum value (g_{Na_max}) of the conductance (i.e. $g_{Na} = m^3h\, g_{Na\_max}$). State variables n, m, and h are time- and voltage-dependent and satisfy a first order of an ordinary differential equation with a form of $dX/dt = \alpha(1-X)-\beta X$, where X is the state variable; α and β are rate constants that are voltage dependent. Solutions to this ordinary differential equation suggest that n and m exponentially increase with time and voltage depolarization while h exponentially decays with time and voltage depolarization. The n and m are called the activation state variables, and h is called the inactivation state variable. The introduction of h to the description of the gating behaviour of sodium channels distinguishes the kinetics of sodium currents from that of the potassium currents (details of the HH model are described in method in Section I).

The HH model describes the permeability changes of the excitable membrane and predicts action potential generation and propagation. "The success of HH models is a triumph of the classical biophysical method in answering a fundamental biological question. Sodium and potassium ion fluxes account for excitation and conduction in the squid giant axon. Voltage-dependent permeability mechanisms and ionic gradients

suffice to explain electrical excitability. The membrane hypothesis is correct. A new era began in which an ionic basis was sought for every electrical response of every cell." (Hill, 1992).

Rall model of spinal motoneurones

The Rall model (Rall 1959; Rall 1962) was established in the quest for a theory for analyzing how electrical currents spread in dendritic trees when the single R-C neuron model (resistor-capacitor model) could not correctly interpret the decay of synaptic potentials measured in motoneurones. The Rall model can be used to simplify the complex dendritic structure into a series of electrically equivalent "cylinders" without losing the electrical properties of the dendrites. A neuron can be represented by the Rall model if the equation $d_{parent}^{3/2} = \Sigma\, d_{daughter}^{3/2}$ holds, where d_{parent} is the diameter of parent dendrite and $d_{daughter}$ is the diameter of daughter dendrites. Using the Rall model a neuron can be modeled as an isopotential soma attached to cable segments representing dendritic trees. In the Rall model the passive electric properties of a neuron are described by four parameters: input resistance (R_N), time constant (τ), ratio of somatic R_N to dendritic R_N (ρ), and electrotonic length ($L=l/\lambda$, where, l is the physical length of the dendrite, and λ is the space constant).

To overcome the restrictive assumption imposed on cable theory that the membrane is passive, Rall (1964) developed a compartmental approach. With this approach dendritic segments are assumed to be isopotential and are lumped into a single electrically short R-C compartment. Compartments are connected to each other through longitudinal resistivity. Using the compartment approach, dendritic trees can be modeled

with active conductances, and the input/output properties of neurons can be computed with synaptic perturbation rather than synaptic current. Cable and compartmental models provide the essential tools for linking the structure of neurons to their electrical function. The Rall model has become the groundwork for a quantitative biophysical approach for exploring the functional role of dendrites as well as a basis of neuron modeling at both the single neuron level and the level of large-scale networks.

The HH-model describes the mechanisms underlying the gating behaviours of the voltage dependent conductances, while the Rall model links neuronal structure to electrical function. Both models (or theories) have become an essential basis for today's modeling framework for models comprising a single neuron to a large-scale neuronal network.

Constraints and contributions of the Rall model

The cable equation was first derived by Hermann and Weber in 1870s and applied to the problem of electrotonic propagation along a cylinder cable. Their work was later known as the cable theory. Rall was the first person to apply the cable theory to dendritic neurons in 1950s. Although at that time Coombs, Eccles, and Fatt did consider current flow to dendrites in their interpretation of measured input resistance, they neglected the transient cable properties of the dendrites. This resulted in erroneously low value for membrane time constant (τ_m) and misinterpretations of how synaptic potential could decay more slowly than would be expected. Rall applied cable theory to dendritic neurones to correct these errors and misinterpretations (See Rall 1977 for review). Rall's work refuted the notions made by Eccles and others that the distal dendritic tree was

essentially electrically invisible from the soma. Instead, Rall showed that the entire dendritic tree of motoneurones was important for synaptic integration. Rall's work made some important contributions, including a way of estimating electrotonic length (L) and membrane time constant (τ_m) from intracellular recordings and an estimation of C_M, R_M and L using an electrical model with dendrites represented by electrically equivalent cables (See section *Measurement of electrical properties of motoneurones* in general discussion). The reduction of the neuron to a simpler electrical geometry has been one of the great accomplishments in neural modelling research.

Representation of a branched dendritic tree as an equivalent cylinder is based on several assumptions including (1) the values of R_M and R_A are the same in all branches; (2) all terminal branches end with the same boundary conditions; (3) all terminal branches have the same electrotonic length (L); (4) at every branch point, the diameters of the two daughter branches must follow the 3/2 power law (Rall 1989.). It is obvious that natural dendritic trees are unlikely to satisfy all of these constraints, which were used to define an idealized mathematical representation that provides a valuable reference case. However, some dendrite trees such as those of cat spinal motoneurones have been reported to approximately satisfy the 3/2 power law, and some (e.g. cells in hippocampus) satisfy the 3/2 power law fairly well. Studies (Lux et al., 1970; Redman 1976) showed that there was about 20% variation in the electrotonic lengths of major dendritic branches from the same motoneurone in cat spinal cord, but collapsing ten or more dendrite trees into an equivalent cylinder with a single electrotonic length is unlikely to cause a significant error (see Carlen et al. 1984 for review). The assumption of uniform membrane resistivity for entire soma-dendritic membrane (i.e. the same value

of R_M) is not necessary; theoretical solutions could be carried out with a different R_M value for the soma and for each cylinder branch component. Since the input conductance is dominated by the combined dendritic trees the input conductance of the whole neuron is not sensitive to the changes in the value of R_M.

Despite its limitations the Rall model has enhanced our understanding of how the neuron's morphology, membrane properties, and synaptic architecture determine its input/output properties and provides us a way of extracting key parameters of the neurons (such as τ_m and L) from a set of simple intracellular recordings. The simplification of a neuron to an electrically equivalent cylinder has been one of the great accomplishments in the modelling. This approach is one of the bases upon which our single cell models are built.

Single neurone models

According to Segev (1992), neurone models can be divided into phenomenological models and channel-based biophysical models. Phenomenological models include the 'integrated-and-fire' model (due to the membrane capacitance), in which the threshold is arbitrarily assumed, and the FHN-type (Fitz, Hugh and Nagumo) model, in which the electrical properties of the membrane are represented by two variables (two coupled differential equations) - the membrane voltage and a slow recovery variable, each satisfies a differential equation with polynomial non-linearity. Threshold in the FHN model is not arbitrarily predefined but an emergent property of the model. The Hodgkin and Huxley (1952d) three-channel model is the prominent channel-based model. In this class of models the various membrane currents, characterized using

voltage clamp techniques, are described mathematically. The model is then used to study the contribution of the various ion currents to overall complex electrical behaviour of the modeled neurone. Neurone models can also be divided into morpho-less models (Segev, 1992) and morpho-complex models. In morpho-less models, the geometrical complexities of nerve cells are neglected, and the neurones are represented as a point unit. In contrast, morpho-complex models retain the complexity of the morphology of the modeled neurone to a certain degree. The neuronal dendritic trees can be reduced at any level using the Rall model, and the degree of reduction depends on the questions that the model is designed to answer.

Single cell models could provide us with an effective tool to study the neuronal properties in an idealized condition and help us better understand how the behaviour of neurons relates to their membrane properties and morphological and biophysical features. Kernell et al built the first HH-type motoneurone model based on cat spinal motoneurone properties (Kernell, D., and H. Sjöholm, 1972). This model was a modification of the Frankenhaeuser-Huxley model (1964) for voltage clamp data from the amphibian nerve fiber and was later used to study the repetitive firing properties of cat spinal motoneurones. One year later, Dodge and Cooley (1973) built another HH-type motoneurone model with more realistic properties based on cat spinal motoneuronal structure and voltage-clamp data (Araki and Terzuolo, 1962), for a study of action potential generation in cat spinal motoneurones. This model was further developed by Traub (1977) to study the different geometry of cat spinal motoneurones in relation to the "size principle". Traub's model (1977) is the basis upon which I have built the cat lumbar motoneurone models presented in this thesis.

Over the last 50 years different forms of cat spinal motoneurone models with different degree of complexity have been developed for various studies of electrical properties, repetitive firing properties and excitability of the cat spinal motoneurones and input/output relation of the motoneurone pools (e.g. Kernell, 1968; Lux et al., 1970; Kernell, D., and H. Sjöholm, 1972; Dodge and Cooley, 1973; Barrett and Crill, 1974; Baldissera and Gustafsson, 1974a,b,c; Traub, 1977; Traub and Llinas, 1977; Pinter et al., 1983; Fleshman et al., 1988; Cullheim et al., 1987; Clements and Redman, 1989; Heckman and Binder, 1991; 1993a; 1993b; Powers, 1993; Heckman 1994; Jones and Bawa 1997, Dai et al., 1998). The degree of complexity of the models depends on the question posed and the problems that the models are applied to. However, a model based on anatomic structure and physiological characteristics of the actual neurones has some advantages. For example, Wilson and Bower (1989), using known anatomic and physiological data, showed that one can constrain the values of model parameters that need to be explored to tune and characterize the behaviour of the model. These biologically accurate simulations can more readily produce results that are comparable to data from experiments, thus increasing the likelihood that predictions of the models will be testable. For this reason, building neurone models with more realistic properties of the modeled neurones is one of the goals of this thesis. There is always a balance between the modeled neurones and the realistic neurones.

"A model is something simple made by the scientists to help them understand something complicated. A good model is one that succeeds to reduce the complexity of the modeled system significantly while still preserving its essential features." (Segev, 1992).

The purpose of this thesis

The purpose of this thesis is to use modeling approaches combining cat experimental data to probe answers to the following three questions:

(1) What are possible mechanisms underlying the hyperpolarization of voltage threshold for action potential generation in cat lumbar motoneurones observed during fictive locomotion induced by stimulation of midbrain locomotion region (MLR) ?

(2) Will locomotor drive potentials (LDPs), the periodic fluctuations of membrane potential, have an effect on the voltage threshold for action potential generation during fictive locomotion ?

(3) How does voltage threshold hyperpolarization change the output of motoneurone pools ?

The thesis is composed of three sections. Each section focuses on each of the above questions.

Rational for choosing the models in each section

Studies presented in Section I and II focused on an investigation of the possible ionic bases that might account for hyperpolarization of Vth in cat lumbar motoneurones during fictive locomotion. To this end, the Hodgkin-Huxley (HH) type of the single cell model was chosen for these studies. There are many benefits for using the HH-type model motoneurones. In general, the HH-type model motoneurones could be built with more realistic properties of the real motoneurones based on the anatomic structure and passive properties of the real motoneurones and properties of ionic channels that have been found in mammalian spinal motoneurones. The behaviour of the HH-type model

motoneurones could be easily adjusted by appropriately setting the passive and active membrane properties. In addition, it is also easy to simulate the effect of modulation of the ionic conductances by either altering the maximum conductance or shifting the voltage dependency of the conductances and to measure the resulting effects on the output of the model motoneurones such as the action potential generation and the firing frequency/injected current (f-I) relationships, etc.

Study in Section III focused on the effect of lowing of Vth on the output of motoneurone pools. The active membrane properties determined by ionic conductances were not the target of this study. Therefore, a large-scale population model was chosen in this section. The model was built with point neurones that had simple membrane properties and an easy control of Vth. The output of the model in this study consisted of the mean firing frequency and the number of recruited cells in the model motoneurone pools.

Section I

A modelling study of locomotion-induced hyperpolarization of voltage threshold in cat lumbar motoneurones.

YUE DAI, KELVIN E. JONES, BRENT FEDIRCHUK,

DAVID A. McCREA, LARRY M. JORDAN

Department of Physiology,

University of Manitoba,

Winnipeg, MB, R3E 3J7, Canada

Summary

1. During fictive locomotion the voltage threshold for action potential initiation (Vth) in adult cat, lumbar motoneurones becomes hyperpolarized. This threshold lowering (mean of 6.2 mV, Krawitz et al. 2001) occurs in the absence of or with only small changes in action potential height and width. Potential ionic mechanisms of this locomotor state-dependent increase in excitability were examined using a five compartment model of the motoneurone. The input resistance, rheobase, membrane time constant, voltage threshold, and firing frequency-current (f-I) relation of the model cells were similar to those observed in adult cat motoneurones. Models were constructed to represent motoneurones innervating fast fatigable, fast fatigue resistant and slow muscle fibers.
2. Parameters of ten active conductances were altered to determine which might be modified during fictive locomotion to produce the lowering of action potential Vth that occurs in real motoneurones. Changes in several currents were either ineffective in altering Vth or resulted in gross changes in the amplitude or duration of the somatic action potential. This included currents underlying the afterhyperpolarization, the persistent Na^+ current, the leak current, three Ca^{2+} currents and 'h' and 'a' potassium currents. These were then eliminated as likely candidates for lowering the Vth during fictive locomotion.
3. Changing only one modelled conductance did not fully replicate the Vth lowering seen experimentally. A greater than 5 mV hyperpolarization of Vth with minimum changes in the action potential was obtained, however, by either increasing the

conductance or hyperpolarizing the voltage dependency of fast sodium channels located in the initial segment compartment. Similar but smaller changes were produced by reducing the conductance or decreasing the activation of delayed rectifier potassium channels.

4. These simulations show that changes in several conductances can alter the current threshold of motoneurons, but the lowering of Vth can be most easily accomplished by affecting the voltage dependency of fast Na^+ channels. This suggests a potential target for as yet unknown neuromodulators that are released as part of the transition from the quiescent to the locomotor state.

Introduction

Spinal motoneurones exhibit changes in intrinsic membrane properties during the transition from the resting to the locomotor state. These state-dependent changes include a reduction in the post-spike afterhyperpolarization (AHP) (Brownstone et al., 1992; Schmidt, 1994) and a change in the relation between intracellular current injection and firing frequency (Brownstone et al., 1992; Fedirchuk et al., 1998). Krawitz et al. (2001) recently described another state-dependent change in motoneurone excitability accompanying the transition to locomotion: a hyperpolarization of the voltage threshold (Vth) for action potential initiation. While the mechanisms for this enhancement of motoneuronal excitability are unknown, the authors postulated that this effect may be mediated by neuromodulators released during locomotor activity (Krawitz et al., 2001).

The primary aim of the present study was to determine possible ionic mechanisms that might account for hyperpolarization of Vth in cat lumbar motoneurones during

fictive locomotion. To this end, we built three models corresponding to the three biophysical types of motoneurons (S, slow; FR, fast, fatigue resistant; FF, fast fatigable) with properties resembling those of real motoneurones recorded in *vivo*. The models were built with five compartments (axon, initial segment, soma, proximal dendrite, and distal dendrite) based on a simplification of the anatomic structure of real motoneurones. The passive parameters of the models were based on data from cat spinal motoneurones. Parameters of the ten active conductances included in the models were taken primarily from literature for mammalian spinal motoneurones. They are conductances of the fast sodium (g_{Na}), persistent sodium (g_{NaP}), delayed rectifier potassium ($g_{K(DR)}$), A-current ($g_{K(A)}$), calcium-dependent potassium ($g_{K(AHP)}$), T-type calcium (g_{Ca_T}), L-type calcium (g_{Ca_L}), N-type calcium (g_{Ca_N}), h-current (g_h), and potassium leak current (g_{leak}). The models were constrained to the biophysical properties of adult cat spinal motoneurones, and target values for the simulations were taken from *in vivo* electrophysiological recordings. Because the hyperpolarization of Vth has been observed in all types of motoneurons (Krawitz et al., 2001), models of the three types of motoneurones (FF, FR, and S) were constructed and used to detect common changes in active properties that might yield the Vth hyperpolarization during locomotion. It was shown in our recent study (Krawitz et al., 2001) that the Vth hyperpolarization occurs in both the excitatory and inhibitory phases of the fictive step cycle. This suggests that a modulation of ion channels during the locomotor state was responsible for the hyperpolarization of Vth rather than direct postsynaptic effects in only one phase of the step sycle.

The simulation results predict that the selective modulation of sodium and/or delayed-rectifier channels in the axon hillock/initial segment are likely ionic mechanisms

through which Vth may be controlled in all types of motoneurons. Portions of this work have been presented in abstract form (Dai et al., 1998a; 1998b).

Methods

Anatomic structure

The geometry of the models was that of a simplified cylinder structure (Fig. 1A). Since the hyperpolarization of Vth was shown to be not directly linked to the periodic synaptic excitation and inhibition during fictive locomotion (see Results in this paper), the effect of synaptic input was not considered in this paper. The dendrites of the model motoneurones were simplified as two compartments. The diameter and length of the proximal dendrite compartment were adjusted to make the amplitude of the SD spike appropriate. The size of the distal dendrite was set arbitrarily because it had a relative small effect on spike generation and action potential shape in these models. In addition to the two dendritic compartments, the models had an axon, initial segment (IS), and soma for a total of five compartments conserved the surface membrane area of initial segment and soma (Conradi 1969; Cullheim et al., 1987). The size of the axon compartment was adjusted to produce an appropriate IS spike.

Three types of model motoneurones were built based on the assumption that the different properties of the biophysical types of motoneurone were determined by their anatomic structure (size) and passive and active properties. Studies by Cullheim et al (1987) suggested that there is little difference in the averaged soma diameters of the F- and S-type cells, but the dendritic trees of F-type motoneurones have more complex branching than S-type. Our models followed the same principle. The structure of F- and

S-type of model motoneurones had the same size of axon, initial segment, and soma compartments. The only difference was the size of dendrite compartments (Table 1).

Our simplification of the dendrites ignored electrotonic properties resulting from branching and termination of the dendrites. The total electrotonic lengths are 0.59, 0.79, and 0.89 for S-, FR- and FF-type model motoneurones respectively. These values are smaller than those reported for real motoneurones and reflect the rather small distal dendritic compartments in the present models. Such a reduction while not appropriate for a consideration of the response to synaptic inputs is unlikely to influence spike initiation in the initial segment and soma.

Table 1

Passive parameters

Each compartment (Table 1) had a specific membrane capacitance (C_M) of 1.0 $\mu F/cm^2$. Specific membrane resistance (R_M) was the same in all five compartments and was set to 7000, 5000, and 4000 Ωcm^2 for S-, FR-, and FF-type respectively. Its value was chosen to give a theoretical value of the membrane time constant ($R_M C_M$) of the model motoneurone equal to that of the corresponding type of cat lumbar motoneurones reported by Hochman and McCrea (1994a and 1994b). Specific axial resistance (R_A) was set to 20 Ωcm in the axon, initial segment, and soma compartments for all three types of model motoneurones and was adjusted to 60 Ωcm in the dendrite compartments to make the models produce an appropriate spike height and repetitive firing properties. These parameters are summarized in Table 1.

Active parameters

To model the repetitive firing behaviour of motoneurones, a variety of ionic currents were introduced into some or all compartments. We first chose nine major active conductances (g_{Na}, $g_{K(DR)}$, $g_{K(A)}$, $g_{K(AHP)}$, g_{Ca_T}, g_{Ca_L}, g_{Ca_N}, g_h, g_{leak}) for the models that have been widely found in mammalian motoneurones, including cat, rat and mouse motoneurones (Binder et al., 1996). In addition, a tenth conductance, a persistent sodium conductance (g_{NaP}), was added to the models to test its effect on Vth on the basis of a recent report that this conductance was essential for initiation of spikes during rhythmic firing in cat spinal motoneurones (Lee and Heckman 2001). As the actual kinetics of these conductances are not known in adult cat spinal motoneurone, we have drawn the parameters for the equations from a wide range of experimental and theoretical results.

1) g_{Na}: The fast sodium conductance was included in the axon, initial segment and soma compartments. The state variable of this conductance was based on Traub's model (1977), where the voltage dependency of the IS g_{Na} was about 10 mV more hyperpolarized than that of the somatic g_{Na}. In our models the voltage dependency of the IS g_{Na} was further shifted to the hyperpolarizing direction by 5 mV for the S- and FR-type and by 6 mV for the FF-type motoneurones. The density of the maximum conductance (g_{max}) was set to 120, 240, and 200 mS/cm^2 for axon, initial segment, and soma compartments, respectively, in all three models.

2) $g_{K(DR)}$: The delayed rectifier potassium conductance was included in the axon, initial segment, and soma compartments. The state variable for this channel was taken from Traub (1977), with an activation of IS $g_{K(DR)}$ also 10 mV more hyperpolarized from

the somatic $g_{K(DR)}$. The values of g_{max} were set to 40, 110, and 35 ms/cm^2 for axon, IS, and soma compartment, respectively in all three models.

3) $g_{K(A)}$: The A-current was included in the soma compartment. Parameters for this conductance were based on previous reports (Safronov and Vogel, 1995). In our models, the voltage dependency of both activation and inactivation curves was positively shifted by 10 mV in order to match the recordings of fast A-current from guinea pig trigeminal motoneurones (Chandler et al., 1994). The g_{max} was set to 5.5 mS/cm^2 for all three models, roughly based on the report by Safronov and Vogel (1995).

4) g_h: The h-current was included in the soma compartment. The state variable for h-current was based on Binder (1996). The g_{max} was set to 6, 6, and 4 mS/cm^2 for S-, FR-, and FF-type model motoneurones, respectively. These settings, along with leak current, resulted in an appropriate input resistance in the models.

5) g_{Ca_T}: The T-type calcium conductance was included in the soma compartment with parameters based on Tegner el al (1997). However, the voltage dependency of the state variables (both activation and inactivation) was positively shifted by 20 mV to approximate the recordings from neonatal rat hypoglossal motoneurones (Umemiya and Berger 1994; Viana et al., 1993) and mouse motoneurones (Mynlieff and Beam 1992). The g_{max} was set to 4 mS/cm^2 for all three models.

6) g_{Ca_N}: The N-type calcium conductance was included in the soma and proximal dendrite compartments with parameters from Booth et al (1997). In our models a 10 mV shift in the depolarizing direction was made for the voltage dependency of the conductance in order to make this channel high-voltage activated (HVA). The g_{max} was set to 12 and 1.5 mS/cm^2 for the soma and proximal dendrite compartments, respectively,

in all three types of the model motoneurones. Current from this channel was used to gate the AHP conductance ($g_{K(AHP)}$).

7) g_{Ca_L}: The L-type calcium conductance was included in the soma and proximal dendrite compartments with parameters from Booth et al (1997). The voltage activation was positively shifted by 10 mV to make the channel relatively high-voltage activated and to approximate the behaviours of L-type calcium channels in rat hippocampal CA3 pyramidal neurones (Avery and Johnston 1996). The activation of L-type calcium channels in spinal cat motoneurones was about 10 - 30 mV positive to the resting membrane potential (Schwindt and Crill 1980). The g_{max} was set to 2 mS/cm^2 for the soma and 0.33 mS/cm^2 for the proximal dendrite compartment in all three models.

8) $g_{K(AHP)}$: The AHP conductance was included in the soma and proximal dendrite compartments. This conductance was dependent on the intracellular calcium concentration, which was determined by activation of g_{Ca_N}. Parameters for this channel were based on Traub et al (1991). The rate constants were adjusted to generate a small time constant, which reduced accumulation of AHP current and produced an appropriate repetitive firing behaviour and f-I relationship. The g_{max} was set to 8, 10, and 18 mS/cm^2 for the soma, and 3, 6, and 6 mS/cm^2 for the proximal dendrite compartment for the S-, FR-, and FF-types of model motoneurones, respectively.

9) g_{leak}: The leak current was included in the soma and proximal dendrite compartments. It was a potassium conductance, having an effect on input resistance and resting membrane potential. The g_{max} was set to 0.35, 0.6 and 0.9 ms/cm^2 for the soma, and 0.3, 0.6 and 1.5 ms/cm^2 for the proximal dendrite compartment for the S-, FR-, and

FF-types of model motoneurones, respectively. These settings resulted in an appropriate input resistance and resting membrane potential.

10) g_{NaP}: The persistent sodium conductance was included in the initial segment and soma compartments. g_{NaP} activated about 10 mV negative to the fast g_{Na} with a magnitude ~1% of the fast I_{Na} (Crill 1996). Parameters for g_{NaP} in our model were modified from the somatic g_{Na}. The inactivation of state variables was removed, and the activation voltage was negatively shifted by 10 mV. The g_{max} was set to 12 mS/cm^2 (~5% of IS g_{Na}) for IS compartment and 3 mS/cm^2 (~1.5% of somatic g_{Na}) for soma compartment in all three models.

Cable equations

The simulations were done in the GENESIS environment (Bower and Beeman, 1998) on Pentium PCs running the Linux operating system (http://www.redhat.com). The time step for all the simulations was set to 0.05 ms. Three variations of a five compartment single cell models (Fig. 1A) were built. In general, the cable equation for compartment k (=2, 3, or 4) can be written as

$$C_K \frac{dV_k}{dt} = g_{k-1,k}(V_{k-1} - V_k) + g_{k+1,k}(V_{k+1} - V_k) - I_{ionic,k} + I_{injected,k} \qquad (1)$$

where, V_{k-1} , V_k, and V_{k+1} are membrane potentials of the compartments k-1, k, and k+1; $g_{k-1,k}$ and $g_{k,k+1}$ are conductances between the compartments k-1 and k and compartments k and k+1; C_k is the capacitance of the compartment k; $I_{injected,k}$ is the injected current to the compartment k, and $I_{ionic,k}$ is the ionic current of the compartment k. For the soma compartment $I_{ionic,k}$ is written as

$$I_{ionic,soma} = g_{Na} m^3 h (V_m - E_{Na}) + g_{K(DR)} n^4 (V_m - E_K) + g_{K(AHP)} q\ (V_m - E_K) \qquad (2)$$

$$+ g_{K(A)} m_A^4 h_A (V_m - E_K) + g_{leak} (V_m - E_K) + g_h m_h (V_m - E_h)$$

$$+ g_{Ca\_L} m_L (V_m - E_{Ca}) + g_{Ca\_T} m_T^3 h_T (V_m - E_{Ca})$$

$$+ g_{Ca\_N} m_N^2 h_N (V_m - E_{Ca})$$

where, g_{Na}, is the maximum conductance for fast Na^+ channel; $g_{k(DR)}$, delayed rectifier K^+; $g_{k(AHP)}$, Ca^{++}-dependent K^+ ; $g_{k(A)}$, A-currents; g_{leak} , leak currents; g_h, h-current; g_{Ca_T}, T-type Ca^{++}, g_{Ca_N}, N-type Ca^{++}, and g_{Ca_L}, L-type Ca^{++}. E_{Na}, E_K, E_{Ca} *and* E_h are equilibrium potentials for Na^+, K^+, Ca^{++} & h currents and equal to 55 mV, -75 mV, 80 mV and -55 mV respectively. Letters *m, h, n* and *q* (with or without subscripts) are membrane state variables that are defined by the Hodgkin-Huxley type equation:

$$\frac{dX}{dt} = \alpha(1 - X) - \beta X \qquad (3)$$

where steady-state value $X_\infty = \alpha/(\alpha+\beta)$ and time constant $\tau = 1/(\alpha+\beta)$.

The intracellular calcium concentration $[Ca^{++}]_{in}$ in the soma and dendrite compartments satisfy the following equation (Traub et al., 1991)

$$\frac{d[Ca^{++}]_{in}}{dt} = BI_{Ca} - \frac{[Ca^{++}]_{in}}{\tau_{Ca}} \qquad (4)$$

where B is a scaling constant in arbitrary units and set to -17.402 in the soma compartment and -10.769 in the dendrite compartment. τ_{Ca} is a time constant, the rate of decay of $[Ca^{++}]_{in}$. It is set to 13.33 ms for both soma and dendrite compartments. I_{Ca} is equivalent to the N-type Ca^{++} current.

The passive parameters of the models are shown in Table 1, rate constants in Table 2, and the membrane properties of the resultant model motoneurones in Table 3.

Figure 1

Table 2

Electrophysiological behaviour of the models

The self-imposed criteria that the model had to meet to be accepted as a suitable representation of a spinal motoneurone were:

1. An input resistance, a membrane time constant, AHP, and rheobase comparable to those reported for a cat lumbar motoneuron;
2. An initial segment (IS) spike that is separable from the somatodendritic spike (SD spike);
3. A realistic frequency-current (f-I) relationship;
4. A Vth within the range of the experimental data.

To achieve different membrane properties for each type of model motoneurone, the voltage dependency of the IS g_{Na}, the g_{max} of somatic and dendritic $g_{K(AHP)}$ & g_{leak}, and the g_{max} of somatic g_h were altered. The target values defining different cell types were taken from adult cat motoneurones (Hochman and McCrea 1994b and c; Krawitz et al 2001). These included input resistance, rheobase current, time constant, AHP duration and amplitude, AP height, and Vth. The resting membrane potential (Em) and AP width of the models are resultant values (see Table 3).

Some of the resulting biophysical properties of the model motoneurones are illustrated in Figure 1. Fig. 1B (dashed line) shows an antidromic action potential (IS/SD spike) elicited by injecting a pulse of current (15 nA, 1 ms) into the axon compartment. Hyperpolarization of soma by injecting a -2 nA current into the soma compartment blocked the SD potion of this action potential leaving the smaller IS spike (solid line). The f-I relationships are illustrated in Fig. 1C, and the characteristics of the AHPs are

shown in Fig. 1D. The response to a -2 nA, 100 ms duration current pulse injected in the soma compartment is shown in Fig. 1E.

To be consistent with the experimental data, Vth of an action potential was defined as the membrane potential at which $dV/dt \geq 10mV/ms$ (Brownstone et al 1992 and Krawitz et al 2001). This membrane potential was then used as the reference value to calculate the height of the action potential, which was considered to be the voltage difference between the Vth and the peak value of the AP. The width of the AP was defined as the time interval between the depolarization and the repolarization of the membrane potentials equal to the Vth. Table 3 shows the resulting parameter values from these simulations.

Our recent experimental data (n=38, Krawitz et al. 2001) reported a mean value of absolute voltage threshold of -44.1±9.3 mV, and firing could be evoked by a mean depolarization of 22.6±9.0 mV from resting membrane potential (-66.8±6.2 mV). The absolute Vth for the models are -47.2 mV for the S-type, -46.7 mV for the FR type, and -49.0 mV for the FF-type. About 20 mV of depolarization is needed above resting membrane potentials (S-type: -65 mV; FR-type: -67 mV; and FF-type: -70 mV) to reach the spike threshold. This is within the range of values reported in the literature (Krawitz et al., 2001; Pinter et al., 1983; Gustafsson and Pinter, 1984).

Table 3

The repetitive firing evoked by low intensity current injection in the models was similar to that reported for real motoneurones (e.g. Kernell 1965). The slope of the secondary range of the f-I relation produced by the models did not perfectly match that of

cat lumbar motoneurones, which should be within the range of 3 to 8 Hz/nA (Kernell, 1965). The present models produced a relative high firing frequency in response to high current injections (see f-I curves above the dashed line in Fig. 1C). To avoid this affecting the reliability of our simulation results, the currents injected into the model cells for all simulations were maintained within the primary range of the f-I curves. In addition, the AP width generated by our models in the control condition (Table 3) was about 1 ms larger than the experimental data. This did not influence analysis of simulation results since we were primarily interested in the changes in AP width between simulated control and locomotor conditions.

Constraints for computer simulation of Vth hyperpolarization

To be considered as a plausible mechanism underlying Vth hyperpolarization, the simulation results had to meet some constraints. This modeling study was based on our recent data (Krawitz et al., 2001) that Vth is hyperpolarized by a mean value of 8.0±5.5 mV (n=38) during fictive locomotion. The three cases in which Vth was hyperpolarized more than 19 mV (Fig. 2D) were ignored, and a mean value of 6.2±3.9 mV (n=35) of Vth hyperpolarization was set as a target value for simulations. About 50% of the cells displayed a Vth hyperpolarization of 3 - 9 mV (Figure 2D). This range was used as the boundary within which the simulation results had to fall to be considered a possible mechanism. Data from nine motoneurons in the Krawitz et al (2001) study were re-analysed to determine changes in spike size and shape width during fictive locomotion to provide target data for simulations. During fictive locomotion AP height increased by a mean value of 2.6±6 mV (ranging from -1.6 to 17.3 mV) and AP width by 0.5±0.6 ms

(from -0.1 to 1.6 ms). We set less than 3 mV as a desirable change in AP height (ΔH) with an upper boundary of ≤ 10 mV and less than 0.5 ms for change in AP width (ΔW) with upper boundary of ≤ 1.2 ms. Thus we were most interested in those simulations where 1) ΔVth ≥ 3.0 mV; 2) ΔH ≤ 10 mV; and 3) ΔW ≤ 1.2 ms.

Results

Effect of synaptic inputs on Vth. Motoneurones receive excitatory and inhibitory synaptic inputs from locomotor networks during fictive locomotion. These alternating synaptic inputs result in membrane potential oscillations, termed locomotor drive potentials (LDPs). In order to test if the Vth hyperpolarization might be induced directly by excitatory synaptic inputs, we previously measured the Vth in both excitatory (depolarizing) and inhibitory (hyperpolarizing) phases of the LDPs (Krawitz et al., 2001). We analyzed additional eight cells to more rigorously exam this issue. The Vth during the excitatory component of the LDP was measured from the spike train induced by MLR stimulation, and the Vth during the inhibitory component of the LDP was measured from the spike train elicited by a single pulse with the minimum amount of current (5-25 nA, 0.2 s) required for repetitive firing. Experimental results from eight cat lumbar motoneurones showed that all motoneurones displayed hyperpolarization of Vth in both the excitatory phase (mean 6.8±5 mV) and the inhibitory phase (mean 6.6±5 mV) of the LDPs. Three of the eight motoneurones exhibited a more hyperpolarized Vth by a mean value of 6.0±7 mV in the inhibitory phase than that in the excitatory phase, while four of them displayed a more hyperpolarized Vth in the excitatory inhibitory phase (mean 4.8±5

mV) than that in the inhibitory phase. One motoneurone showed no difference (only 0.1 mV) in Vth between the two phases.

These experimental results show that the observed hyperpolarization of spike threshold induced by fictive locomotion is not directly linked to the periodic synaptic excitation during the fictive step cycle. If this were true the Vth measured in the inhibitory phase of the LDPs would have been always more depolarized than the Vth measured in the excitatory phase. Instead, these new experimental results show a modulation of Vth throughout fictive locomotion and confirm our previous conclusion that the Vth hyperpolarization was state-dependent (Krawitz et al., 2001).

Figure 2 illustrates experimental data forming the basis of the simulations in this study. During the resting (or control) condition repetitive firing of the motoneurone was evoked by a triangular shaped current injection (Fig. 2A). The Vth for the first spike was -27.4 mV. During fictive locomotion, Vth hyperpolarization was observed in all spikes, and the Vth of the first spike was -34.6 mV (Fig. 2B). Action potentials occurring in the two conditions were averaged and overlaid in Fig. 2C to compare the action potential shape and size in the two conditions. Note the small increase in spike height (3.7 mV) and width (0.3 ms) as the Vth hyperpolarized by 7.2 mV during locomotion (solid trace). The example in Fig. 2 is representative of the experimental finding that while there is a significant hyperpolarization of Vth, the size and shape of the action potential are little changed. The distribution of Vth hyperpolarization from 38 motoneurones (Krawitz et al., 2001) is shown in Fig. 2D.

Figure 2

A series of computer simulations were done with the objective of identifying ionic currents likely responsible for mediating the hyperpolarization of Vth that occurs during fictive locomotion. The protocol for these simulations was to inject a triangular-shaped current ramp into the model motoneurones that started from a value of -2 nA and rose to a peak amplitude of 15 - 30 nA with a total duration of 5 sec. Responses in the "control" condition were then recorded using model neurones with the conductances outlined in Table 2 and parameters as described in Method. Response during "locomotion" were those in which conductance were altered as described in left column of Table 4. The resulting effects on Vth, AP shape, and rheobase current were measured. The results are shown in Table 4. For simplicity, all illustrations in this paper were taken from the S-type model motoneurone.

Influence of somatic currents on Vth

Reducing AHP current. Previous experimental results have shown that the amplitude of the post-spike afterhyperpolarization (AHP) in spinal motoneurones is decreased during locomotion by 18-59% (Brownstone et al., 1992). The current underlying the AHP is mediated by an apamin sensitive, Ca^{2+}-activated K^+ channel that may account for 20% of the resting input conductance of the cell (Krnjevic et al., 1978; Zhang and Krnjevic, 1987, 1988) and is sensitive to modulation by various neurotransmitters (Sah, 1996). We used the motoneurone models to test whether a reduction in the conductance of the $I_{K(AHP)}$ could account for both the reduced AHP and the hyperpolarization of Vth observed in the locomotor state (Figure 3).

A triangular ramp of current (bottom panels in Fig. 3A and B) was injected into the soma compartment of the S-type model cell to induce repetitive firing under two conditions: control (Fig. 3A) and 50% reduction of $g_{K(AHP)}$ (Fig. 3B). Voltage threshold for each spike is plotted as a dot in the middle panels in Fig. 3A and B, and the averaged spikes taken from Fig. 3A and B are overlapped in Fig. 3C. The mean value of Vth was -47.2±0.3 mV in control (dashed line in the middle panel of Fig. 3A) and this changed by less than 0.3 mV in the test condition. The simulation results illustrate that a 25 % reduction in the amplitude of the AHP produced by decreasing $I_{K(AHP)}$ is unlikely to be the mechanism responsible for hyperpolarizing Vth during fictive locomotion.

Figure 3

Increasing Sodium Current. Changes in somatic sodium conductance hyperpolarized Vth to some extent. Equal shifts of the activation and inactivation curves of somatic sodium conductance resulted in large increases in the height of the action potential (not shown). In order to maintain the size and shape of the action potential within boundaries, an unequal shift of the activation and inactivation curves was required. Fig. 4A (left panel) illustrates the effect of shifting the activation curve (m) by 4 mV and the inactivation curve (h) by 6mV in the hyperpolarizing direction. This shift produced a smaller product of hm^3 with peak activation occurring about 5 mV more hyperpolarized than control (right panel, Fig. 4A). Shifting the voltage dependence of the somatic sodium conductance to the left reduced the Vth to -50.3 mV, a 3.1 mV hyperpolarization with respect to control Vth (Fig. 4B2) and produced an action potential that was 1 mV smaller

and 0.7 ms wider. The inset shows the averaged spikes from the control (dashed line) and test condition (solid line) superimposed.

Figure 4

In the second test condition (Fig. 4C) the maximum somatic sodium conductance (g_{Na}) was increased by 100%. This resulted in a mean Vth of -49.3 mV, i.e. a 2.1 mV hyperpolarization with respect to control but also a 13 mV increase in the action potential amplitude and a 2.3 ms increase in width along with the generation of a double spike (inset in Fig. 4C1). This produced a relatively small hyperpolarization of the Vth which was outside the simulation boundaries for changes in height and width.

Altering Other Currents. The effects of modulation of other somatic currents and the associated effects on Vth are summarized in Table 4. Aside from changes in sodium (g_{Na}) or delayed rectifier ($g_{K(DR)}$) conductances, changes in other somatic currents had limited effects on the Vth although in many cases the current threshold of the models was altered (see right column of Table 4).

Table 4

Influence of initial segment currents on Vth

The effects of changing the I_{Na} and $I_{K(DR)}$ currents in the initial segment are shown in Figure 5. Response to the same triangular current injection used in Fig. 3 & 4 are shown in the top panels, and the corresponding Vth for each spike is shown as a dot in the middle panels. The averaged spikes from each condition (dark lines) are overlapped on the averaged spike of control (dashed line spikes) and shown in the bottom panels.

Figure 5A shows that a 50% increase in maximal conductance of the I_{Na} produced a 5.5 mV hyperpolarization of Vth, with an 8 mV increase in amplitude and little increase (0.7 ms) in width of the action potential. Similar to the somatic case, a hyperpolarization of Vth could also be produced by shifting the state variables of the IS g_{Na} in the hyperpolarizing direction. Fig. 5B shows an equal shift in the activation and inactivation voltages of the IS g_{Na} to the left by 3 mV produced a 5.6 mV hyperpolarization of Vth with a 7 mV increase in the AP height and a 1.2 ms increase in the AP width.

Unlike the change in somatic $g_{K(DR)}$, a 70% decrease in the maximum conductance of $g_{K(DR)}$ in the initial segment produced a 3.1 mV hyperpolarization of Vth with a 5.3 mV increase in amplitude of the action potential and a little increase (0.5 ms) in the AP width (Fig. 5C). A similar result could be also produced by positively shifting the state variable n of the IS $g_{K(DR)}$ by 5 mV (Fig. 5D).

Figure 5

Combining changes in initial segment and somatic currents

The effect of altering both initial segment and somatic I_{Na} & $I_{K(DR)}$ on Vth are summarized in Table 4. In general, a combined modulation of both IS and somatic g_{Na} or $g_{K(DR)}$ does not significantly lower Vth much more than modulating the IS g_{Na} or $g_{K(DR)}$ alone. These results suggest a dominant role of initial segmental conductances, the sodium conductance in particular, in modulating the Vth.

The results of a combined modulation of g_{Na} and $g_{K(DR)}$ in both the IS and soma are shown in the bottom two rows in Table 4. The Vth was hyperpolarized by 4.5 mV when IS & somatic g_{Na} was increased by 30% and the IS & somatic $g_{K(DR)}$ was reduced

by 30%. This resulted in a 12.0 mV increase in AP height and a 3.2 ms increase in AP width (double spike). With a relatively small increase in AP height (6.4 mV) and width (3.2 ms, double spike), a 6.2 mV Vth hyperpolarization could be also produced by a 2 mV shift of the IS & somatic g_{Na} state variables (m and h) to the left and a 2 mV shift of the IS & somatic $g_{k(DR)}$ state variable (n) to the right.

Effect of persistent sodium current on Vth

In addition to examining the effect of the rapidly inactivating, low-voltage activated sodium current (I_{Na}), a persistent sodium current (I_{NaP}) was incorporated into the model. Compared to the fast I_{Na}, the I_{NaP} had a smaller effect on Vth for the same amount of conductance modulation (either enhancing the maximum conductance or shifting the voltage dependency to the left). Addition of the g_{NaP} to both the IS and soma compartments hyperpolarized the Vth by 1.7 mV with small changes in AP height (4.1 mV) and width (1.0 ms) (Fig. 6A, middle trace). Increasing the IS g_{NaP} by 150%, in an attempt to lower the Vth further, resulted in a 2.9 mV hyperpolarization of Vth, a 6.9 mV increase in AP height, and a 1.3 ms increase in AP width. A 3.2 mV Vth hyperpolarization could be produced by negatively shifting the voltage activation of the IS g_{NaP} by 5 mV, but this also caused a 6.6 mV increase in AP height and a 1.6 ms increase in AP width (Fig. 6B).

Compared to the IS g_{NaP}, modulation of somatic g_{NaP} had a smaller effect on Vth but a larger effect on AP size and shape. A 150% increase in the somatic g_{NaP} resulted in a 2.2 mV hyperpolarization of Vth and a significant distortion of the shape of the action potential and (Fig. 6C). The Vth could be hyperpolarized to the same amount by a 5 mV

left-shift of the activation voltage of the somatic g_{NaP} leaving a large change (double spike) in shape of the spike (Fig. 6D).

Enhancing both the IS and somatic g_{NaP} did not lower Vth significantly more than modulating the IS g_{NaP} alone but resulted in a relatively larger increase in spike size and width. The Vth could be hyperpolarized by 3.2 mV by either increasing the IS & somatic g_{NaP} by 150% or negatively shifting the activation voltage of the IS & somatic g_{NaP} by 5 mV (not illustrated, see results in Table 4). Both modulations caused a large increase in spike width and more than a 7 mV increase in spike height.

Figure 6

Discussion

Simulation results suggest that the selective modulation of sodium and/or delayed-rectifier channels in the initial segment are candidate ionic mechanisms for hyperpolarization of Vth that occurs in adult cat spinal motoneurones during fictive locomotion.

Mechanisms unlikely contributing to Vth hyperpolarization during locomotion.

Excluded Ionic Mechanisms. Seven of the ionic conductances ($g_{K(AHP)}$, $g_{K(A)}$, g_h, g_{CaT}, g_{CaL}, g_{CaN}, and g_{leak}) included in the models had no effect on the Vth when the effects of neuromodulators were simulated by changing the maximum conductance through these channels (Table 4). Initially we anticipated that currents such as $g_{K(A)}$, g_h, and g_{Ca_T} which are active at subthreshold membrane potentials, would have an important role in

determining Vth. Simulations show, however, that compared to the fast sodium current these conductances have little effect on Vth either because their activation time constants are relatively long or because the induced currents are relatively small. In general increasing these conductances had little or no effect on current threshold (right column, Table 4). Other mechanisms excluded because of their small effect on Vth (< 3.0 mV) or large effect on the action potential amplitude or width were: (1) increasing the maximum conductance of somatic g_{Na}; (2) decreasing the maximum conductance of the somatic $g_{K(DR)}$; (3) shifting the voltage dependency of the somatic $g_{K(DR)}$ to the right; and (4) increasing the somatic g_{NaP}.

Effect of rate of change of membrane potential on Vth. Spike threshold in cat spinal motoneurones can be hyperpolarized by a rapid membrane depolarization produced by a current pulse in both anaesthetised (Powers and Binder 1996) and decerebrate cats (Krawitz et al., 2001). The mechanism underlying this type of Vth hyperpolarization was recently investigated using a single cell model (Dai et al., 2000). The simulation results suggested that Vth hyperpolarization produced by membrane potential oscillation could be due to a quicker activation of the fast sodium conductance, which induces a relatively large amount of I_{Na} in the subthreshold range of the membrane potential and thus results in a lowering of the Vth. It is important to note that only the first spike in a train shows a reduced Vth due to these rapid depolarizations. In contrast in both the present simulations (Fig. 5) and during fictive locomotion (Krawitz et al. 2001) all spikes display a lowered Vth. Furthermore, the extent of Vth hyperpolarization induced by a rapid depolarization is smaller (mean 3.8 mV, Powers and Binder 1996; 2.5 in Krawitz et al, 2001) than that

observed during fictive locomotion (mean 8.0 mV, Krawitz et al, 2001). These observations argue against the rhythmic changes in motoneurone membrane potential *per se* being primarily responsible for threshold lowering during locomotion. Instead it is more likely that Vth lowering during locomotion results from the actions of as yet unknown neuromodulatory mechanisms acting on motoneurone membrane currents.

Possible mechanisms for mediating Vth hyperpolarization.

Simulations show that Vth can be hyperpolarized by modulations of g_{Na} or $g_{K(DR)}$ that either change maximum channel conductance or shift the voltage dependency of channel opening and closing (i.e. alter the state variables). Of these putative mechanisms, enhancing initial segment g_{Na} plays a dominant role in hyperpolarizing the Vth (~6 mV) while at the same time producing only small increases in spike height (< 8 mV) and width (<1 ms). In contrast increasing somatic g_{Na} by shifting the voltage dependency (i.e. more channels open at a hyperpolarized membrane potential) produces only a relatively small amount of Vth hyperpolarization (< 3.5 mV) while increasing somatic g_{Na} increases action potential height more than 15 mV. The four conductance changes found to hyperpolarize the Vth to an extent approaching that occurring during locomotion while maintaining the action potential within acceptable limits were: 1) increasing the initial segment maximum conductance of g_{Na}; 2) shifting the initial segmental g_{Na} voltage dependency in the hyperpolarizing direction; 3) reducing the initial segment maximum conductance of $g_{K(DR)}$; and 4) shifting the initial segment $g_{K(DR)}$ voltage dependency in the depolarizing direction. The first two increase the absolute amount of sodium current in the subthreshold range while the other two produce a

relative increase in the inward current by reducing the outward $I_{K(DR)}$. All four changes increase the net inward current at subthreshold membrane potentials and thus hyperpolarize Vth.

The I_{NaP} in cat motoneurones activates quickly and at more hyperpolarized membrane potentials than the fast sodium current. Thus it could contribute to subthreshold inward currents even though it is estimated to make up only 1% of the fast sodium current (Crill 1996). Our simulations suggest, however, that increasing I_{NaP} alone is unlikely responsible for Vth lowering during fictive locomotion since it greatly affects action potential shape with only modest reductions in Vth. The present simulations did not explore the possibility that changes in this conductance during locomotion might affect other aspects of motoneurone behaviour such as the f-I gain during rhythmic firing (Lee and Heckman 2001). In brainstem motoneurones I_{NaP} appears important in mediating bistable membrane behaviours and evoking plateau potentials in guinea pig trigeminal motoneurones (Hsiao et al. 1998), and regulating firing rate in guinea pig facial motoneurones (Nishimura et al., 1989). Also relevant in this regard is the report that the activation of I_{NaP} can be shifted in the hyperpolarizing direction by activation of protein kinase C in neocortical neurones (Astman et al., 1998).

Modulation of sodium channels

The earliest intracellular studies suggested that the initial segment was the site of action potential initiation in cat motoneurones. Activation of fast Na^+ channels in the initial segment produces large inward currents (30 - 80 nA, Barrett & Crill 1980) that would readily lead to action potential initiation since they are well above the current

threshold for cat spinal motoneurones (2-40 nA, see Hochman and McCrea 1994). Simulations summarized in Table 4 suggest a potentially important role for modulation of initial segment sodium currents in lowering Vth during locomotion. The potential contribution of changes in somatic g_{Na} to decreasing Vth (Table 4) may be an overestimate since the simulations assumed a similar density of Na^+ channels in the soma and initial segment. In cultured spinal neurons and retina ganglion cells the density of Na^+ channels in the soma is much lower than in the initial segment (Catterall, 1981; Wollner and Catterall, 1986). This results in about 80% of the inactivating Na^+ current in dorsal horn neurones coming from the initial segment/axon (see Safronov, 1999).

There is mounting evidence that the sodium current is a target for modulation by neurotransmitters. Modulation of sodium channels has been shown to control the input-output relations in neostriatal cells and to regulate firing patterns of pyramidal neurones (see Cantrell and Catterall 2001). The modification of voltage_dependent activation and inactivation of sodium channels has been reported for extracellular toxin binding, suggesting that voltage dependency may be amenable to modulation (Cestèle et al., 1998; and Catterall, 1992). A recent study (Azouz and Gray, 2000) in cat visual cortical neurons suggested that an increased availability of sodium channels is responsible for a lowering of voltage threshold which enhances the sensitivity of cortical neurones to synchronous synaptic inputs. These studies raise the possibility that the Na^+ channel is a potential target for modulation during activity in several places in the nervous system (Cantrell and Catterall 2001).

The Vth of spinal motoneurones consistently decreases during brainstem-evoked fictive locomotion without large alterations in action potential shape (Krawitz et al 2001).

Present simulations using realistic models of the threshold behaviour of adult cat spinal motoneurones, show that increasing activity of the Na^+ or reducing activity of the delayed rectifier K+ channels during locomotion can also reduce motoneurone Vth without producing large changes in the action potential. Similar effects can be achieved by shifting the voltage dependency (m & h) of g_{Na} in the hyperpolarizing direction or shifting the voltage dependency (n) of $g_{K(DR)}$ in the depolarizing direction. Previous studies on the fast potassium conductance (delayed rectifier) showed that its activation in cat spinal motoneurones could induce a large (~30 nA) outward current when the membrane potential was brought 20 mV positive to the resting potential (Barrett et al., 1980). Thus a reduction of this current during locomotion could result in an increase in the relative amount of inward current and hence reduce Vth. Neuromodulators acting on Na^+ or K^+ channels located in the initial segment would seem to be the most effective for threshold reduction.

In both the present simulations and experimental results (Krawitz et al 2001) the hyperpolarization of Vth reduces both the current and the amount of membrane potential depolarization required to reach threshold. Such locomotor-state dependent changes could substantially facilitate motoneurone recruitment during locomotion (Dai et al., 1999; Krawitz et al 2001). The challenge is to find potential neuromodulatory substances that may be released with the onset of locomotion and contribute to threshold reduction.

Conclusions

The state-dependent hyperpolarization of Vth during fictive locomotion will increase motoneurone excitability and is suspected to play an important role in

motoneurone recruitment during locomotion (Dai et al., 1999). Our simulation results suggest that the mechanisms producing this dynamic change in the biophysical properties of spinal motoneurones may be a receptor-activated modulation of the Na^+ and/or delayed rectifier K^+ channels. Furthermore, the simulations suggest that the most effective modulation of Vth will occur if the receptor-activated modulation is targeted within the initial segment. These predictions are amenable to testing in future experiments.

Tables

Table 1. Structural measurements of the motoneurone models and their cable parameters.

MN type	diameter (μm)	length (μm)	R_M (Ωcm^2)	R_A (Ωcm)	C_M ($\mu F/cm^2$)
S-type					
Axon	10	400	7000	20	1.0
Initial segment	6	100	7000	20	1.0
Soma	10	360	7000	20	1.0
Proximal dendrite	40	500	7000	60	1.0
Distal dendrite	30	400	7000	60	1.0
FR-type					
Axon	10	400	5000	20	1.0
Initial segment	6	100	5000	20	1.0
Soma	10	360	5000	20	1.0
Proximal dendrite	40	700	5000	60	1.0
Distal dendrite	30	500	5000	60	1.0
FF-type					
Axon	10	400	4000	20	1.0
Initial segment	6	100	4000	20	1.0
Soma	10	360	4000	20	1.0
Proximal dendrite	40	700	4000	60	1.0
Distal dendrite	30	500	4000	60	1.0

Table 2. Rate constants in Hodgkin-Huxley equations.

Conductance	Compartment	Forward (α)	Backward (β)
g_{Na}	Initial segment (IS)		
	S- & FR- type:	$\alpha_m = \frac{0.4(5-V)}{\exp(\frac{5-V}{5})-1}$	$\beta_m = \frac{0.4(V-30)}{\exp(\frac{V-30}{5})-1}$
		$\alpha_h = 0.28\exp(\frac{25-V}{20})$	$\beta_h = \frac{4}{\exp(\frac{25-V}{10})+1}$
	FF-type:	$\alpha_m = \frac{0.4(4-V)}{\exp(\frac{4-V}{5})-1}$	$\beta_m = \frac{0.4(V-29)}{\exp(\frac{V-29}{5})-1}$
		$\alpha_h = 0.28\exp(\frac{24-V}{20})$	$\beta_h = \frac{4}{\exp(\frac{24-V}{10})+1}$
	Axon and soma	$\alpha_m = \frac{0.4(17.5-V)}{\exp(\frac{17.5-V}{5})-1}$	$\beta_m = \frac{0.4(V-45)}{\exp(\frac{V-45}{5})-1}$
		$\alpha_h = 0.28\exp(\frac{25-V}{20})$	$\beta_h = \frac{4}{\exp(\frac{40-V}{10})+1}$
g_{NaP}	IS and soma	$\alpha_m = \frac{0.4(7.5-V)}{\exp(\frac{7.5-V}{5})-1}$	$\beta_m = \frac{0.4(V-35)}{\exp(\frac{V-35}{5})-1}$
$g_{k(DR)}$	IS	$\alpha_n = \frac{0.02(10-V)}{\exp(\frac{10-V}{10})-1}$	$\beta_n = 0.25\exp(\frac{-V}{80})$
	Axon and soma	$\alpha_n = \frac{0.02(20-V)}{\exp(\frac{20-V}{10})-1}$	$\beta_n = 0.25\exp(\frac{10-V}{80})$
$g_{k(A)}$	soma	$\alpha_{m_A} = \frac{0.032(V+54)}{1-\exp(\frac{V+54}{-6})}$	$\beta_{m_A} = \frac{0.203}{\exp(\frac{V+30}{24})}$
		$\alpha_{h_A} = \frac{0.05}{1+\exp(\frac{V+76}{10})}$	$\beta_{h_A} = \frac{0.05}{1+\exp(\frac{V+76}{-10})}$
g_h	Soma	$\alpha_{m_h} = \frac{0.06}{1+\exp(\frac{V+75}{5.3})}$	$\beta_{m_h} = \frac{0.06}{1+\exp(\frac{V+75}{-5.3})}$
g_{Ca_T}	Soma	$\alpha_{m_T} = \frac{0.02(V+38)}{1-\exp(\frac{V+38}{-4.5})}$	$\beta_{m_T} = \frac{-0.05(V+41)}{1-\exp(\frac{V+41}{4.5})}$
		$\alpha_{h_T} = \frac{-0.0001(V+43)}{1-\exp(\frac{V+43}{7.8})}$	$\beta_{h_T} = \frac{0.03}{1+\exp(\frac{V+41}{-4.8})}$
g_{Ca_N}	Soma and dendrite	$\alpha_{m_N} = \frac{0.25}{1+\exp(\frac{V+20}{-5})}$	$\beta_{m_N} = \frac{0.25}{1+\exp(\frac{V+20}{5})}$
		$\alpha_{h_N} = \frac{0.025}{1+\exp(\frac{V+35}{5})}$	$\beta_{h_N} = \frac{0.025}{1+\exp(\frac{V+35}{-5})}$
g_{Ca_L}	Soma and dendrite	$\alpha_{m_L} = \frac{0.025}{1+\exp(\frac{V+30}{-7})}$	$\beta_{m_L} = \frac{0.025}{1+\exp(\frac{V+30}{7})}$
$g_{k(AHP)}$	Soma	$\alpha_q = 10^{-3}[Ca^{2+}]_{in}$	$\beta_q = 0.04$
	Dendrite	$\alpha_q = 10^{-4}[Ca^{2+}]_{in}$	$\beta_q = 0.04$

Table 3. Membrane properties of three motoneuron types produced by the models.

Properties of model cell	S-type model cell	FR-type model cell	FF-type model cell
Rin (MΩ) *	1.6 (1.77±0.7)	1.0 (0.91±0.2)	0.6 (0.62±0.1)
Rheobase (nA) *	6.0 (4.3±2.5)	13.0 (11.6±3.1)	23.0 (19.7±5.1)
τ_m (ms) *	7.0 (7.0±2.0)	5.0 (5.1±1.1)	4.0 (4.4±0.9)
AHP duration (ms) *	100 (110.5±31.5)	85.0 (81.9±17.1)	80.0 (79.5±21.4)
AHP amplitude (mV) *	4.0 (4.8±2.0)	3.0 (3.1±1.1)	2.0 (2.3±0.9)
AP Height (mV) †	67.0 (58.5±9.7)	62.4 (58.5±9.7)	68.0 (58.5±9.7)
AP Width (ms) †	3.7 (2.2±0.4)	3.4 (2.2±0.4)	3.3 (2.2±0.4)
Vth (mV) †	-47.2 (-44.1±9.3)	-46.7 (-44.1±9.3)	-49.0 (-44.1±9.3)
Resting Em (mV) †	-65.0 (-66.8±6.2)	-67.0 (-66.8±6.2)	-70.0 (-66.8±6.2)

Notes: (1) Unbracketed values are the results from simulation in the three types of model cells. (2) Rin was measured from membrane hyperpolarization produced by long pulse (-2nA, 100 ms) current injection into the soma compartment. Vth, AP height and width were measured from averaged spikes elicited by a ramp of current injected into the soma compartment. AHP duration and amplitude were measured from a single SD-spike evoked by an antidromic short pulse (1 msec) to the axon compartment. (3) Values in brackets are means (±SD) of measurements obtained experimentally in adult cat motoneurones (*: Hochman and McCrea 1994c; †: Krawitz et el 2001). (4) The method used to measure AP height and Vth in this paper was different from that used in Hochman and McCrea (1994a, b and c). This resulted in different values of the AP height and Vth in Table 3 from those in Hochman and McCrea.

Table 4. Effects of changes in ionic currents on threshold properties of the models.

Conductance	Change in g_{max}	ΔVth (mV)				ΔH (mV)				ΔW (ms)				ΔIr (nA)			
		S	FR	FF	Mean	S	FR	FF	Mean	S	FR	FF	Mean	S	FR	FF	Mean
Experimental values		-	-	-	**-6.2**	-	-	-	**3.0**	-	-	-	**0.5**	-	-	-	**N/A**
Initial Segment																	
g_{Na}	shift m & h by -3 mV	-5.6	-5.7	-5.2	**-5.5**	7.0	9.3	3.0	**6.4**	1.2	1.3	0.5	**1.0**	-4.0	-7.0	-9.0	**-6.7**
	increased by 50%	-5.5	-5.3	-5.0	**-5.3**	8.0	9.0	7.0	**8.0**	0.7	0.9	0.7	**0.8**	-2.0	-4.0	-6.0	**-4.0**
$g_{K(DR)}$	shift n by 5 mV	-3.0	-3.5	-3.0	**-3.2**	4.2	4.7	3.0	**4.0**	0.3	0.7	0.0	**0.3**	-2.0	-2.0	-2.0	**-2.0**
	reduced by 70%	-3.1	-3.7	-3.0	**-3.3**	5.3	7.0	5.0	**5.8**	0.5	0.9	0.0	**0.5**	-2.0	-2.0	-2.0	**-2.0**
g_{NaP}	added to IS and soma	-1.7	-1.8	-1.5	**-1.7**	4.1	6.2	5.2	**5.2**	1.0	0.9	0.3	**0.7**	0.0	0.0	0.0	**0.0**
	increased by 150%	-2.9	-3.4	-3.0	**-3.1**	6.9	9.5	7.7	**8.0**	1.3	1.2	0.6	**1.0**	-1.0	-1.0	-1.0	**-1.0**
	shift m by -5 mV	-3.2	-3.4	-3.0	**-3.2**	6.6	8.5	6.2	**7.1**	1.6	1.3	0.5	**1.1**	-1.0	-1.0	0.0	**-0.7**
Soma																	
g_{Na}	shift m by -4 & h by –6 mV	-3.1	-3.7	-3.0	**-3.3**	-1.0	0.0	-1.2	**-0.7**	0.7	0.5	0.0	**0.4**	-1.0	-1.0	-1.0	**-1.0**
	increased by 100%	-2.0	-1.5	-1.5	**-1.7**	13.0	18.0	16.0	**15.7**	2.3*	0.4	0.0	**0.9**	-1.0	-1.0	-1.0	**-1.0**
$g_{K(DR)}$	shift n by 5 mV	-2.3	-3.0	-2.0	**-2.4**	3.1	6.2	4.0	**4.4**	1.3	1.4	0.5	**1.1**	-1.0	-2.0	-1.0	**-1.3**
	reduced by 50%	-1.5	-1.0	-1.0	**-1.2**	1.6	2.6	2.0	**2.1**	2.6*	1.2	1.0	**1.6**	0.0	0.0	0.0	**0.0**
$g_{K(AHP)}$	reduced by 50%	0.0	0.0	0.0	**0.0**	0.0	0.0	0.0	**0.0**	0.0	0.0	0.0	**0.0**	0.0	0.0	0.0	**0.0**
$g_{K(A)}$	reduced by 50%	0.0	0.0	0.0	**0.0**	0.0	0.0	0.0	**0.0**	0.0	0.0	0.0	**0.0**	0.0	0.0	0.0	**0.0**
g_h	increased by 50%	0.0	0.0	0.0	**0.0**	0.0	0.0	0.0	**0.0**	0.0	0.0	0.0	**0.0**	0.0	0.0	0.0	**0.0**
g_{CaT}	increased by 100%	0.0	0.0	0.0	**0.0**	0.0	0.0	0.0	**0.0**	0.0	0.0	0.0	**0.0**	-1.0	-1.0	-1.0	**-1.0**
g_{CaL}	increased by 100%	0.0	0.0	0.0	**0.0**	0.0	0.0	0.0	**0.0**	0.0	0.0	0.0	**0.0**	-1.0	-1.0	-1.0	**-1.0**
g_{CaN}	increased by 100%	0.0	0.0	0.0	**0.0**	0.0	0.0	0.0	**0.0**	0.0	0.0	0.0	**0.0**	0.0	0.0	0.0	**0.0**
g_{Leak}	increased by 100%	0.0	0.0	0.0	**0.0**	0.0	0.0	0.0	**0.0**	0.0	0.0	0.0	**0.0**	2.0	2.0	3.0	**2.3**
g_{NaP}	increased by 150%	-2.2	-2.5	-1.9	**-2.2**	7.7	8.9	8.4	**8.3**	4.1	3.2	2.3	**3.2**	-1.0	-1.0	-1.0	**-1.0**
	shift m by -5 mV	-2.2	-2.4	-1.7	**-2.1**	5.7	7.5	5.9	**6.4**	3.6*	1.4	0.4	**1.8**	-1.0	-1.0	0.0	**-0.7**
Combination of Initial Segment and Soma																	
g_{Na}	shift m by -3 & h by -5 mV	-4.8	-5.3	-4.8	**-5.0**	0.0	0.7	0.0	**0.2**	1.1	0.8	0.4	**0.8**	-2.0	-5.0	-4.0	**-3.7**
	shift m & h by -2 mV	-4.8	-5.3	-4.4	**-4.8**	2.5	7.4	5.5	**5.1**	1.2	1.0	0.4	**0.9**	-1.0	-3.0	-4.0	**-2.7**
	increased by 50%	-5.4	-5.7	-5.1	**-5.4**	15.6	19.4	17.0	**17.3**	1.4	1.3	0.5	**1.1**	-1.0	-3.0	-4.0	**-2.7**
$g_{K(DR)}$	shift n by 5 mV	-3.5	-4.0	-3.0	**-3.5**	4.3	8.0	5.6	**6.0**	2.0	1.5	0.0	**1.2**	-1.0	-3.0	-3.0	**-2.3**
	reduced by 50%	-2.5	-3.1	-2.2	**-2.6**	3.0	7.0	4.6	**4.9**	3.0*	1.9	0.3	**1.7**	-1.0	-2.0	-2.0	**-1.7**
g_{NaP}	increased by 150%	-3.2	-3.1	-3.1	**-3.1**	10.1	11.5	10.1	**10.6**	5.0*	3.9*	1.7	**3.5**	-1.0	-1.0	-1.0	**-1.0**
	shift m by -5 mV	-3.2	-3.4	-3.0	**-3.2**	7.8	9.0	7.2	**8.0**	3.7*	1.7	0.5	**1.9**	-2.0	-2.0	-1.0	**-1.7**
g_{Na} $g_{K(DR)}$	increased by 30% and reduced by 30%	-4.5	-5.2	-4.3	**-4.7**	12.0	16.0	13.0	**13.7**	3.2*	1.8	0.4	**1.8**	-1.0	-3.0	-3.0	**-2.3**
g_{Na} $g_{K(DR)}$	shift m & h by -2 mV and shift n by 2 mV	-6.2	-5.6	-4.3	**-5.4**	6.4	7.4	3.3	**5.7**	3.2*	3.0*	0.6	**2.3**	-4.0	-5.0	-5.0	**-4.7**

Notes: 1) Changes less than 1 mV in membrane potential or 0.3 ms in AP width or 1 nA in rheobase with respect to control were assigned to 0. 2) g_{max} : the maximum conductance. 3) m and h: state variables of sodium conductance; n: state variable of potassium conductance (delayed rectifier). 4) g_{NaP}: persistent sodium current, which was added to the models to test its effect on Vth. The simulation results for other conductances were collected in the control models without including g_{NaP}. 5) symbol Δ: changes in Vth, AP height (H), AP width (W), or rheobase (Ir). *: AP width is measured from double spike as shown in Fig. 4C.

Figure Legends

Figure 1. Single cell models and initial properties. **A**. Three types of single cell models (S, FR and FF) with five compartments were built that retained the macro structure of cat lumbar motoneurones important for the generation of anti- and orthodromic action potentials. **B**. Overlap of the IS/SD and IS spikes produced by the S-type model motoneurone. The amplitude of the IS/SD spike is ~67mV and the IS spike ~30mV. **C**. Frequency-current (f-I) relations produced by step current injection into the soma compartments of the three types of model cell (S, FR and FF). The frequency was calculated by dividing the number of spikes by the duration (500 ms) of each step current. The slopes of the primary range for the three models are 3.4, 1.8 and 3.6 Hz/nA respectively (below the horizontal dashed line), and the slopes of the secondary range are 12, 13, and 11 Hz/nA (above the dashed line). **D**. Enlarged IS/SD spikes taken from the antidromic single spikes produced by the three types of the model cell. Spikes were overlapped on the alignment of their resting membrane potentials. The afterhyperpolarization (AHP) durations are 100, 85, and 80 ms for the S-, FR- and FF-type models respectively, and the amplitudes of the AHP are 4, 3, and 2 mV respectively. **E.** Passive responses of the models to an injection of -2 nA current into the soma compartments. The voltage trajectories are aligned on the resting membrane potentials. The membrane hyperpolarizations produced by a -2 nA current injection were -3.2 mV for the S-type model cell, -2.0 mV for the FR-type, and -1.2 mV for the FF-type.

Figure 2. Intracellular recording from a cat lumbar motoneurone (Krawitz et al 2001). Spikes were evoked by injecting triangular currents (not shown) into the motoneurone before (panel **A**) and during fictive locomotion (panel **B**). The averaged

spikes made from the firing in panels A and B respectively were overlapped in panel **C** to show the differences in voltage threshold (Vth), AP height, and AP width between control (dashed line) and fictive locomotion (dark line). In this example, the mean Vth, averaged spike height, and averaged spike width were -27.4 mV, 52.2 mV, and 2.0 ms respectively in control and -34.4 mV, 55.9 mV, and 2.3 ms respectively during fictive locomotion. The motoneurone showed a 7.2 mV hyperpolarization in Vth, 3.7 mV increase in AP height, and 0.3 ms increase in AP width during fictive locomotion. Voltage calibration bar for panels A and B is shown in panel A. The measurement of Vth and action potential amplitude and width is described in method. The distribution of Vth hyperpolarization from 38 motoneurones (Krawitz et al., 2001) is shown in Panel **D**. 16% of the cells displayed a Vth hyperpolarization of 1 - 3 mV, 47% of the cells within 3 - 9 mV, 29% of the cells within 9 - 12 mV, and 8% of the cells over 12 mV.

Figure 3. Reducing $I_{K(AHP)}$ does not affect Vth. Triangular currents (15 nA, 5 Sec, starting from -2 nA; shown in the bottom panels in A and B) were injected into the soma compartment of the S-type model cell to make the cell fire in two conditions (A and B). Each dot in the middle panels of A and B is the Vth for the corresponding spike in the top panels. **A.** In control, the mean Vth was -47.2±0.3 mV (dashed lines in top and middle panels in A and B). **B.** A decrease in the maximum conductance of the $I_{K(AHP)}$ by 50% resulted in a reduction in the amplitude of the AHP by ~25% (reducing ~1.0 mV) with little hyperpolarization (< 0.3 mV) of Vth (dark line in the middle panel of B) and no changes in spike height or width. **C.** The first four spikes from A and B were averaged and then overlapped. The dashed line is for the averaged control spike, and the dark line for the averaged spike where $g_{K(AHP)}$ was reduced by 50%.

Figure 4. Altering somatic I_{Na} alters Vth. The S-type model cell was made to fire under two conditions (B and C) by injecting triangular current (the same as that used in Fig. 3) into the soma compartment. Vth for each spike shown in panels B1 and C1 was plotted as a dot in B2, and C2 respectively. The first four spikes in each condition were averaged and then overlapped on the averaged spike of control taken from Fig. 3C (insets in B1 and C1, dashed-line spike for control). The dashed line crossing panels B1 and C1 represents the resting membrane potential of -65 mV, and the dashed line crossing panels B2 and C2 represents the mean value of the Vth of -47.2 mV for the S-type model cell in the control condition. **A.** Curves of the state variable m & h were shifted to the hyperpolarizing direction by 4 & 6 mV respectively (left panel). This resulted in a left-ward shift of product of hm^3 (right panel). Dashed lines stand for control and dark lines for shifted curves. **B.** Vth could be hyperpolarized by unevenly shifting the state variables of g_{Na} (shown in panel A) with small changes in spike height and width. **C.** Increasing the somatic max g_{Na} resulted in a large increase in spike height and width.

Figure 5. Hyperpolarization of Vth could be produced by increasing the initial segment (IS) I_{Na} or decreasing the IS $I_{K(DR)}$. Triangular currents (as used in Fig. 3 & 4) were injected into the soma compartment of the S-type model cell to make the cell repetitively fire in four conditions (A, B, C and D). Vth for each spike shown in A1, B1, C1 and D1 are plotted in A2, B2, C2 and D2, and the average of the first four spikes in each condition is superimposed on the control spike (dashed line) in A3, B3, C3 and D3. The dashed line crossing the top panels represents the resting membrane potential of -65 mV, and the dashed lines crossing the middle and bottom panels represent the mean value of the Vth of -47.2 mV for the S-type model cell measured in control. **A.** Increasing the

max IS g_{Na} hyperpolarized the Vth by 5.5 mV with small increases in AP height (8.0 mV) and width (0.7 ms). **B**. Shifting the IS g_{Na} state variables m and h to the hyperpolarizing direction lowered the Vth by 5.6 mV and resulted in a 7.0 mV increase in AP height and 1.2 ms increase in AP width. **C**. Reducing the max IS $g_{K(DR)}$ produced a hyperpolarization of the Vth by 3.1 mV and caused a small increase in AP height (5.3 mV) and width (0.5 ms). **D.** Shifting the state variable of IS $g_{K(DR)}$ to the depolarizing direction hyperpolarized the Vth by 3.0 mV with little increase in AP height (4.2 mV) and width (0.3 ms).

Figure 6. Altering g_{NaP} affects Vth and spike shape. Repetitive firing of the S-type model cell was evoked by a triangular current injection as shown in Fig. 3. Averaged spikes (dark line) from each condition (A-D) are superimposed on the control spike (dashed line). The dashed-straight line crossing panels A-D represents the mean value of Vth (-47.2 mV) measured in control. **A**. Addition of g_{NaP} to both the initial segment compartment with g_{NaP}= 12 mS/cm^2 (~5% of IS g_{Na}) and soma compartment with g_{NaP}= 6 mS/cm^2 (~1.5% of somatic g_{Na}) hyperpolarized the Vth by 1.7 mV and resulted in a 4.1 mV increase in AP height and 1.0 ms increase in width (middle trace). A 2.9 mV hyperpolarization of Vth could be produced by increasing the IS g_{NaP} by 150%. **B.** Negatively shifting the activation curve of the IS g_{NaP} by 5 mV hyperpolarized Vth by 3.2 mV and increased the spike height and width. **C**. Increasing the somatic g_{NaP} by 150% hyperpolarized the Vth by 2.2 mV with a 7.7 mV increase in AP height and 4.1 ms increase in AP width. **D.** Shifting the activation voltage of somatic g_{NaP} to the left by 5 mV hyperpolarized the Vth by 2.2 mV and resulted in a double spike with a 5.7 mV increase in the AP height and a 3.6 ms increase in AP width.

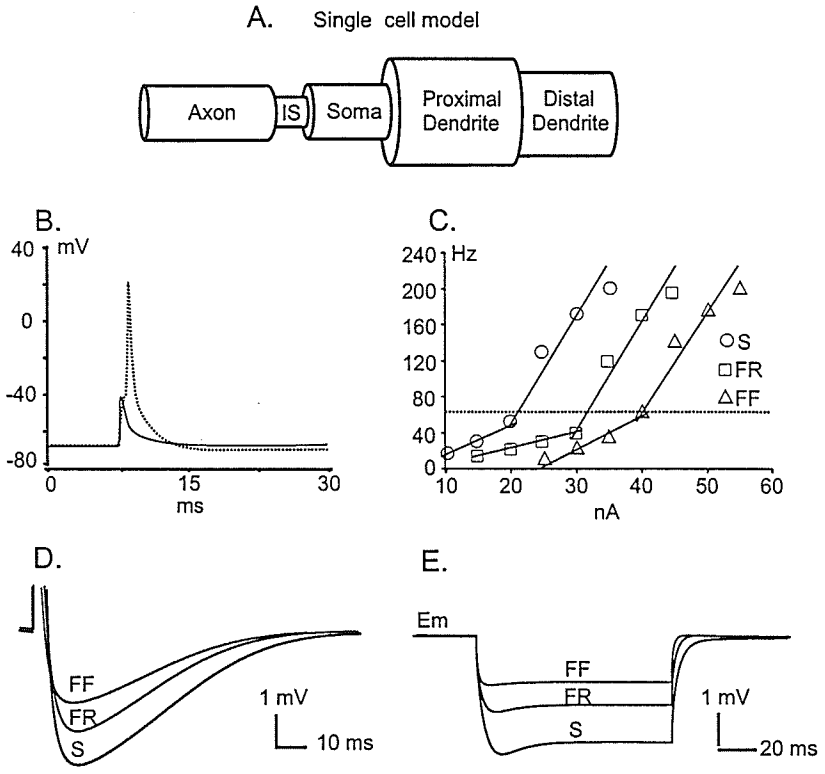

Section I: Figure 1

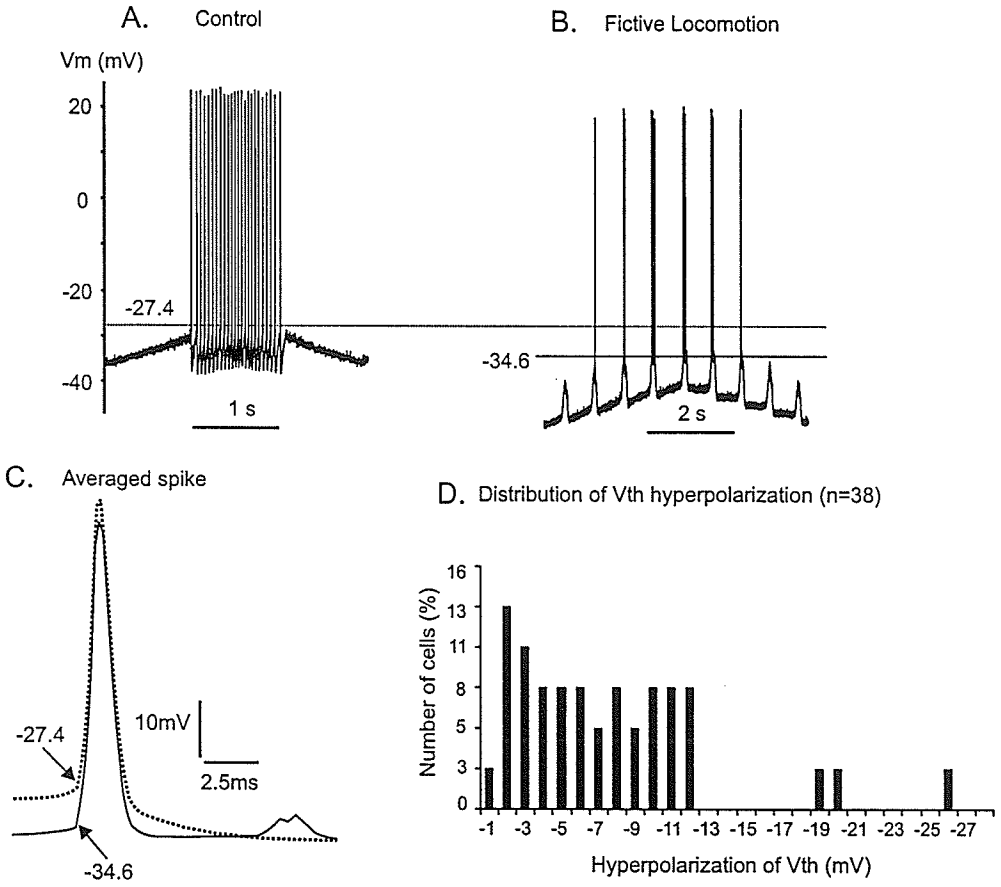

Section I: Figure 2

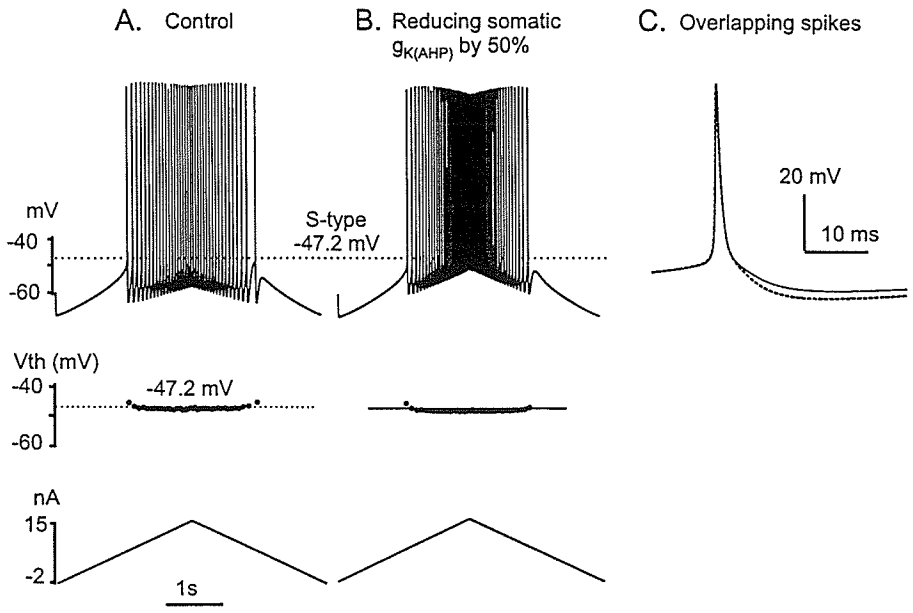

Section I: Figure 3

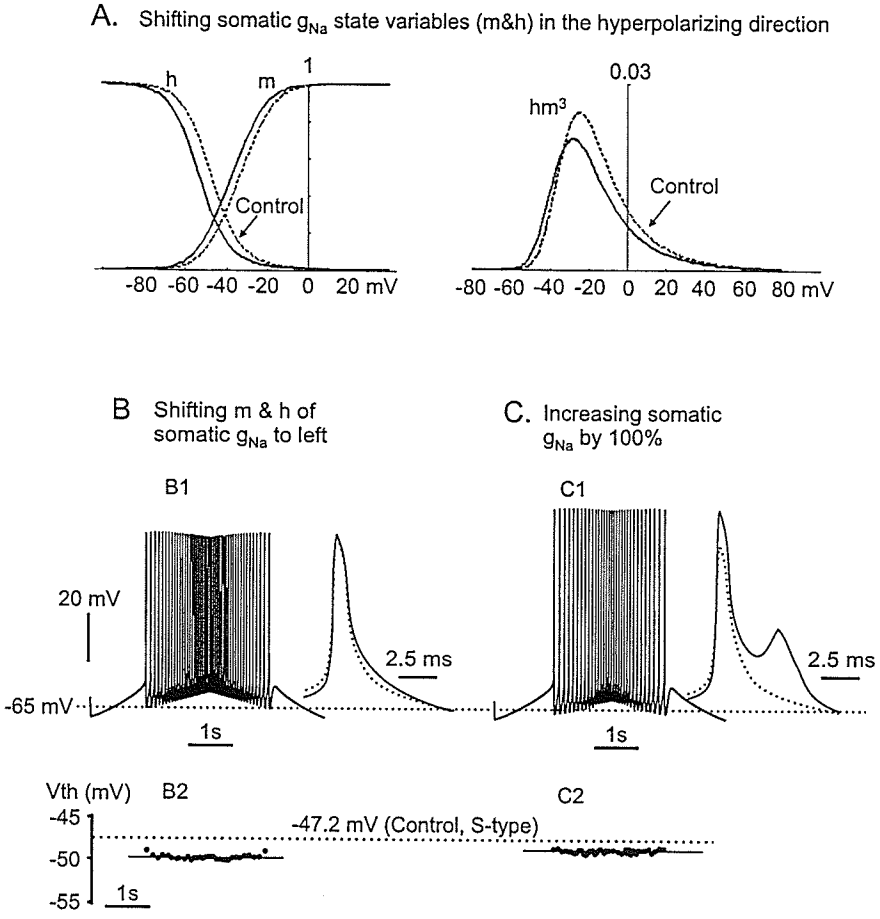

Section I: Figure 4

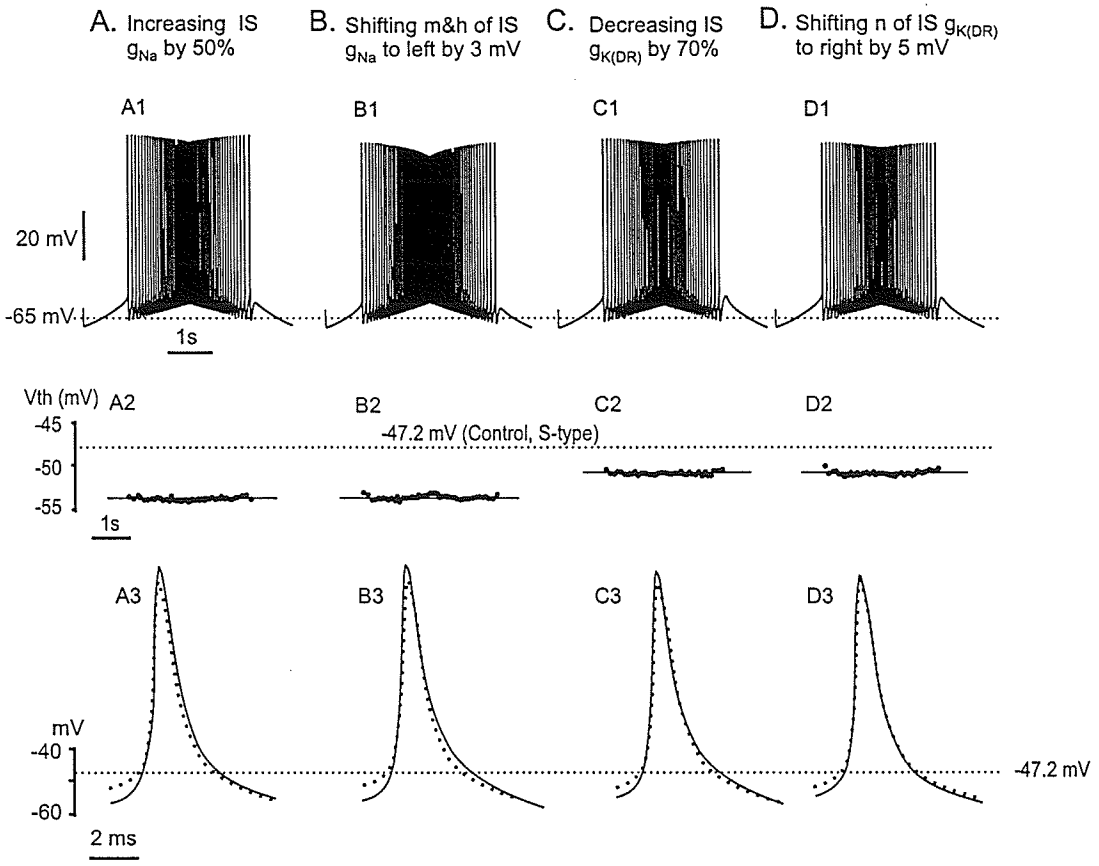

Section I: Figure 5

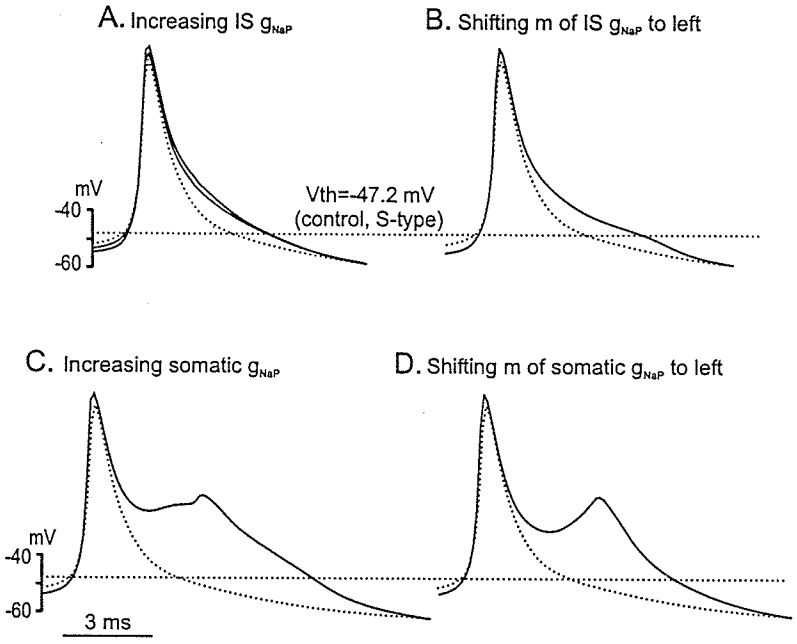

Section I: Figure 6

Section II

Effects of voltage trajectory on action potential voltage threshold in simulations of cat spinal motoneurones

YUE DAI, KELVIN E. JONES, BRENT FEDIRCHUK,

LARRY M. JORDAN

Department of Physiology,

University of Manitoba,

Winnipeg, MB, R3E 3J7, Canada

Abstract

A single cell neuronal model based on cat experimental results was used to investigate the effect of membrane trajectory on voltage threshold (Vth) for action potential generation. Previous results suggested that hyperpolarization of Vth could be produced by a rapid membrane depolarization, but this effect is limited to the first spike in a train. This study shows that rapid current injections hyperpolarize Vth because they are more effective in activating the sodium current underlying spiking. The hyperpolarization of Vth induced by rapid membrane depolarization becomes less effective in altering Vth when other mechanisms of enhancing the fast sodium current underlying action potentials are activated.

1. Introduction

During fictive locomotion evoked by stimulation of the midbrain locomotor region (MLR) in decerebrate cats, motoneurones receive alternating excitatory and inhibitory inputs from the central pattern generator (CPG). These inputs produce rhythmic oscillations of membrane potential termed locomotor drive potentials (LDPs, Jordan 1983). If the neuron is recruited during locomotion, it fires action potentials on the depolarized portion of the LDP. Compared to the resting condition, cat lumbar motoneurones undergo various changes in excitability during fictive locomotion. Recently Krawitz et al. (2000) showed that the voltage threshold (Vth) for action potential generation becomes hyperpolarized during fictive locomotion.

The effects of a rapid membrane potential depolarization on Vth were examined in our recent study (Krawitz et al., 2000). Current pulses (15 nA and 500 ms) were injected into the motoneurones at rest to produce very rapid membrane depolarizations. The results showed that the Vth for action potential generation could be hyperpolarized by a rapid membrane depolarization produced by the injection of a rapid current pulse at rest. But the Vth hyperpolarization produced by the current pulses was restricted to the first spikes of the train and was small compared to the amount of the Vth hyperpolarization seen during locomotion. The present study utilizes a single cell computer model combining the cat experimental results to examine the mechanisms by which the membrane potential trajectory can affect Vth. This study will help us to better understand how the Vth is modulated during fictive locomotion. Part of the data has been previously published (Figs 1,5 and 6 in Dai et al., 2000; Figs 2 and 4 in Krawitz et al., 2001).

2. Methods

Cat experiment

The surgical procedures and data collection methods have been described in Section 1. For details please see previous publications (Brownstone et al., 1992; Krawitz et al., 2000).

Computer model

A single cell model with five compartments (axon, initial segment (IS), soma, proximal dendrite and distal dendrite) was built using GENESIS software. The model was similar to those built in Section 1. The same cable equations and dynamic equations for active conductances described in Section I (Method) were used to build this model. The structural, passive, and active parameters including rate constants are shown in Table 1 - 3 in this section.

The model included a fast sodium current (I_{Na}) and a delayed rectifier potassium current ($I_{K(DR)}$) in the axon, initial segment and soma compartments. Additional currents included in the soma compartment were a calcium-dependent potassium current ($I_{K(AHP)}$), a fast transient potassium current ($I_{K(A)}$), a hyperpolarization activated current (I_h) and three classes of voltage activated calcium currents (L-Type: $I_{Ca(L)}$, N-Type: $I_{Ca(N)}$, and T-type: $I_{Ca(T)}$). The proximal dendritic compartment included $I_{K(AHP)}$, $I_{Ca(N)}$ and $I_{Ca(L)}$. No active conductance was included in the distal dendrite compartment. The input resistance of the model cell = 2.0 MΩ; membrane time constant = 4 ms; and the rheobase current = 11 nA. Resting membrane potential = -60 mV. The time step for simulation was = 0.05 ms. The simulations were done on Pentium PCs running the Linux operating system.

Figure 1A illustrates a schematic of the single cell model. Repetitive firing of the model cell was evoked by injection of a triangular current to the soma compartment (starting from -5nA with peak of 30nA and duration of 1s, not shown) as shown in panel B. The mean value of Vth is -35.8 ± 0.7 mV. The F-I relation produced by step current injections is shown in panel C.

Figure 1

Tables 1 - 3

3. Results

Result from cat experiments

In order to produce the rapid membrane depolarizations in rest state we injected current pulses superimposed on triangular current to motoneurones. Recordings were made from 9 antidromically identified motoneurones, and each motoneurone's Vth was measured in three conditions: 1) during control firing using a triangular current injection; 2) during fictive locomotion using triangular current injection; and 3) control using simultaneous pulse and triangular current injection. The Vth of action potentials is measured at the membrane potential at which the $dV/dt \geq 10mV/ms$ (Brownstone et al., 1992 and Krawitz et al., 2000). The results from one cell with a resting membrane potential of -55 mV are illustrated in Figure 2. In each condition the intracellularly recorded membrane potential is shown in the top panels, current injection in the middle, and action potential Vth for each of the spikes in the bottom. The average Vth during fictive locomotion (condition 2, Fig. 2B) was -34.4 mV, and this value was significantly more hyperpolarized with respect to the average value of -27.2 mV in condition 1 (Fig. 2A; $p < 0.001$ Student's paired *t* test). This result is consistent with previously reported experimental results (Krawitz et al., 2000).

Figure 2

However, there is a major difference in the rates of depolarization between conditions 1 and 2 due to rhythmic membrane potential fluctuations associated with locomotion (locomotor drive potentials, LDPs). The possibility that hyperpolarization of Vth in the locomotion condition was due to the rapid rates of depolarization associated with LDPs was investigated. Current pulses (10 nA, 300 ms duration) were delivered to produce membrane depolarizations with the amplitude, duration and frequency similar to the LDPs (Fig 2C). A triangular current injection was superimposed on the ongoing current pulse train, and the Vth for action potentials in this condition were measured. The average Vth was -27.8 mV and was not significantly different from the average Vth in condition 1 even though the rate of depolarization produced by the current square waves was much greater than the rate of depolarization produced by the LDPs. However, a significant difference remained between the average values in conditions 2 and 3.

It is obvious from Fig 2 that, during conditions 2 and 3, the first spikes in each train of action potentials (circled) had lower voltage thresholds than the remaining spikes. A comparison of the average voltage thresholds of the first spikes revealed that this subset of the data also showed significant hyperpolarization during the locomotion condition. In general, there was no difference in the average Vth of spikes in the two control conditions. In contrast, the Vth for an action potential during fictive locomotion was always hyperpolarized more than either of the two control conditions. The results from 9 motoneurone recordings were summarized in Table 4&5 and Figure 3. These results show that membrane potential oscillations produced by either square pulses at rest (condition 3) or LDPs during fictive locomotion (condition 2) could cause alteration in

voltage threshold. However, such Vth alteration caused by LDPs is limited to a range of less than 3 mV.

Tables 4&5

Figure 3

These results suggest that the phenomenon of hyperpolarization of Vth that accompanies the onset of locomotion could not be produced by the increased rate of depolarization produced by the LDPs. This position was strengthened by the data presented in Figure 4 where the Vth for a medial gastrocnemius (MG) motoneurone was measured in three different conditions. In the control condition (Fig. 4A) a train of current pulses (15 nA, 250 ms duration) was applied to produce the rapid membrane depolarizations similar to the LDPs. The resulting mean Vth was -66.4 mV. Fig. 4B illustrates the firing behaviour and Vth of the motoneurone during the initial phase of locomotion in which the LDPs were not very well developed. In this condition the average Vth was -75.8 mV, a difference of 9.4 mV compared to control (Fig. 4A). In Fig. 4C the Vth was measured from the same motoneurone during well-developed locomotion in which the motoneurone received much stronger inhibitory input from the CPG in the antagonist phase of the step cycle. This resulted in a sharp and increased amplitude of the LDPs. During this condition the average Vth was -74.6 mV, which was not significantly different from that during the locomotion condition in which the LDPs were not very well developed. Thus, irrespective of a well-developed LDP and the resultant increase in the rate of depolarization, the Vth for action potentials in spinal motoneurones was significantly hyperpolarized upon the transition to the fictive locomotion state.

Figure 4

Results from the computer model

In order to examine the possible mechanisms by which a rapid change in membrane potential produces the Vth hyperpolarization, we injected triangular currents with varying slopes into the soma compartment of the model. Figure 5 shows these simulation results. In panels A and B the somatic membrane potentials were shown in the top panels, the net membrane currents (Im) in the middle, and the injected triangular currents in the bottom.

Figure 5

Figure 5A shows that a single spike was evoked by injecting a triangular current (starting at –5 nA with peak 15 nA and duration 125 ms) into the soma compartment. The slope of the ramp current was 0.33 nA/ms (bottom panel in A). The Vth for this spike was -42.0 mV (top panel in A), and the peak membrane current (Im) underlying the spike was -126 nA (middle panel in A). Increasing the slope of the ramp current to 0.66 nA/ms (bottom panel in B) evoked three spikes in the model cell (top panel in B). The Vth for the first spike was -43.4 mV, ~1.5 mV lower than that in panel A. The peak Im for this spike was -140 nA (middle panel in B), 14 nA larger than that in A. The Vth for the remaining two spikes were -40.2 mV and -39.9 mV respectively, which were relatively depolarized compared with the first spike. The Im corresponding to these two spikes were also smaller than that for the first spike. These results suggest that steeper slopes of the ramp current produce a larger peak Im and a lower Vth for the first spike initiation. A systematic series of simulations were done and the results are summarized in Figure 5C. These results show that increasing the slope of the ramp current results in an increase in the peak Im. This increased Im would in turn cause a lowering of Vth.

In regard to spike initiation, the major component of the Im at the rising phase of

the spike was mainly from the fast sodium current (I_{Na}). Therefore, the hyperpolarization of Vth produced by a rapid membrane depolarization is likely due to a rapid activation of the I_{Na}, which was relatively limited to the first spike of the train. In contrast, slower depolarizations would cause relatively greater accommodation and be relatively less effective in activating the I_{Na} underlying the action potential.

The relationship between the enhanced activation of the fast sodium current by rapid membrane depolarization and the Vth hyperpolarization during fictive locomotion was further explored in Figure 6. Panels A and B illustrate conditions where conductances of the initial segment compartment have been modified to produce Vth effects which we have previously postulated to be analogous to that observed during fictive locomotion (Dai et al., 2001, i.e. Section I). In panel A the max g_{Na} was increased by 100% and in panel B the delayed rectifier potassium conductance (max $g_{K(DR)}$) was decreased by 70%. Panel C shows the control response, without modification of the model's properties. In each condition the membrane potential is shown in top the panel, current injection in the middle, and action potential Vth in the bottom. The Vth was plotted as dot corresponding to each spike in the top panel. The circled dot represents Vth of the first spike in each spike train. Current pulses (middle panels: 15 nA and 500 ms) superimposed on triangular current (starting at -10 nA with peak 15nA and duration 10s) were used to produce rapid membrane depolarizations similar to a procedure used in our cat experiments (Krawitz et al., 2000).

Figure 6

A rapid membrane depolarization produced hyperpolarization of the Vth when comparing the first spikes to subsequent spikes in the train. The difference was 1.7 mV in panel A, 1.5 mV in panel B, and 5.2 mV in panel C while the mean values of Vth for the

first spikes (dashed lines) were –44.7, –42.6, and –41.4 mV and those for the subsequent spikes (dark lines) were -43.0, -41.1 and -36.2 mV respectively. These results indicated that the effect of rapid membrane depolarizations on Vth was smaller in simulated fictive locomotion (A and B) than that in control (C). The hyperpolarization of the Vth produced by the rapid depolarization was restricted to the first spike in the spike train.

On the other hand, the mean value of Vth for all spikes was hyperpolarized by 7.7 mV in panel A (mean -43.5 mV), 5.6 mV in panel B (mean -41.4 mV), and 1.8 mV in panel C (mean -37.6 mV) compared to the mean value of the Vth (-35.8 mV) measured under triangular current injection in control (Figure 1B). The amount of Vth hyperpolarization produced by the rapid membrane depolarization in control (panel C) is much smaller than the amount of Vth hyperpolarization produced by a modulation of IS g_{Na} (panel A) or IS $g_{K(DR)}$ (panel B). This result suggests that the hyperpolarization of Vth seen during fictive locomotion is not dependent on the rapid membrane depolarization.

The simulation results suggest that the hyperpolarization of Vth induced by rapid membrane depolarization is less effective in altering Vth during fictive locomotion when other mechanisms of enhancing the sodium conductance underlying action potentials (either directly through modification of the sodium conductance, or indirectly by modification of the delayed rectifier conductance) are activated. The fact that the two mechanisms of altering Vth: 1) rapid membrane depolarization and 2) modulation of conductance properties seem to not be additive provides further evidence that neuronal Vth is likely more affected by modulation of neuronal conductances rather than being determined by the trajectory of the membrane potential.

4. Conclusion

These simulation results compliment experimental observations that the Vth for action potential generation can be hyperpolarized by a rapid membrane depolarization. However, Vth hyperpolarization produced in this way was limited to only the first spike in the spike train, and the amount of the Vth hyperpolarization was small. These limitations are likely due to the kinetics of the fast sodium channel. The hyperpolarization of Vth induced by rapid membrane depolarization seems less effective in altering Vth when other mechanisms of enhancing the fast sodium current underlying action potentials are activated.

Table 1. Structural measurements of the motoneurone models and their cable parameters.

Compartment	Diameter (μm)	Length (μm)	RM (Ωm^2)	RA (Ω m)	CM (Farads/m^2)
Axon	10	400	0.4	0.2	0.01
Initial segment	6	100	0.4	0.2	0.01
Soma	10	360	0.4	0.2	0.01
Proximal dendrite	40	500	0.4	0.5	0.01
Distal dendrite	30	400	0.4	0.5	0.01

Table 2. Distribution and density of ionic currents in the models.

	Density of the Maximum Conductance (S/m^2)								
Compartment	g_{Na}	$g_{K(DR)}$	$g_{K(AHP)}$	$g_{K(A)}$	g_{Ca_N}	g_{Ca_L}	g_{Ca_T}	g_h	g_{leak}
Axon	1200	400	0	0	0	0	0	0	0
Initial segment	2100	1400	0	0	0	0	0	0	0
Soma	2000	350	80	55	120	20	40	60	0.5
Proximal dendrite	0	0	13	0	3.0	3.3	0	0	0.5
Distal dendrite	None								

Table 3. Rate constants in Hodgkin-Huxley equations.

Conductance	Compartment	Forward (α)	Backward (β)
g_{Na}	Initial segment (I.S.)		
		$\alpha_m = \frac{0.4(5-V)}{\exp(\frac{5-V}{5})-1}$	$\beta_m = \frac{0.4(V-30)}{\exp(\frac{V-30}{5})-1}$
		$\alpha_h = 0.28\exp(\frac{25-V}{20})$	$\beta_h = \frac{4}{\exp(\frac{25-V}{10})+1}$
	Axon and soma	$\alpha_m = \frac{0.4(17.5-V)}{\exp(\frac{17.5-V}{5})-1}$	$\beta_m = \frac{0.4(V-45)}{\exp(\frac{V-45}{5})-1}$
		$\alpha_h = 0.28\exp(\frac{25-V}{20})$	$\beta_h = \frac{4}{\exp(\frac{40-V}{10})+1}$
$g_{k(DR)}$	I.S	$\alpha_n = \frac{0.02(10-V)}{\exp(\frac{10-V}{10})-1}$	$\beta_n = 0.25\exp(\frac{-V}{80})$
	Axon and soma	$\alpha_n = \frac{0.02(20-V)}{\exp(\frac{20-V}{10})-1}$	$\beta_n = 0.25\exp(\frac{10-V}{80})$
$g_{k(A)}$	soma	$\alpha_{m_A} = \frac{1.408+0.032V}{1-\exp(\frac{V+44}{-6})}$	$\beta_{m_A} = \frac{0.203}{\exp(\frac{V+20}{24})}$
		$\alpha_{h_A} = \frac{0.05}{1+\exp(\frac{V+66}{10})}$	$\beta_{h_A} = \frac{0.05}{1+\exp(\frac{V+66}{-10})}$
g_h	Soma	$\alpha_{m_h} = \frac{0.02}{1+\exp(\frac{V+75}{5.3})}$	$\beta_{m_h} = \frac{0.02}{1+\exp(\frac{V+75}{-5.3})}$
g_{Ca_T}	Soma	$\alpha_{m_T} = \frac{0.02(V+58)}{1-\exp(\frac{V+58}{-4.5})}$	$\beta_{m_T} = \frac{-0.05(V+61)}{1-\exp(\frac{V+61}{4.5})}$
		$\alpha_{h_T} = \frac{-0.0001(V+63)}{1-\exp(\frac{V+63}{7.8})}$	$\beta_{h_T} = \frac{0.03}{1+\exp(\frac{V+61}{-4.8})}$
g_{Ca_N}	Soma and dendrite	$\alpha_{m_N} = \frac{0.25}{1+\exp(\frac{V+20}{-5})}$	$\beta_{m_N} = \frac{0.25}{1+\exp(\frac{V+20}{5})}$
		$\alpha_{h_N} = \frac{0.025}{1+\exp(\frac{V+35}{5})}$	$\beta_{h_N} = \frac{0.025}{1+\exp(\frac{V+35}{-5})}$
g_{Ca_L}	Soma and dendrite	$\alpha_{m_L} = \frac{0.025}{1+\exp(\frac{V+30}{-7})}$	$\beta_{m_L} = \frac{0.025}{1+\exp(\frac{V+30}{7})}$
$g_{k(AHP)}$	Soma	$\alpha_q = 10^{-3}[Ca^{2+}]_{in}$	$\beta_q = 0.04$
	Dendrite	$\alpha_q = 10^{-4}[Ca^{2+}]_{in}$	$\beta_q = 0.04$

Table 4. Voltage thresholds measured from nine cat lumbar motoneurones

	V_{th} at Rest (mV)				**V_{th} During Locomotion (mV)**	
	Ramp Injection (condition 1)		**Ramp + Pulses Injection** (condition 3)		**Ramp Injection** (condition 2)	
Cell No.	**(0) All spikes**	**(1) 1st spikes**	**(2) All spikes**	**(3) 1st spikes**	**(4) All spikes**	**(5) 1st spikes**
1. Extensor	-39.29±0.87	-38.52	-41.35±2.05	-44.73±2.05	-42.80±2.14	-45.67±0.76
2. Extensor	-38.91±1.04	-40.66	-37.75±10.3	-47.36±6.09	-45.43±2.25	-47.86±1.57
3. CP	-35.60±0.92	-36.98	-34.52±7.46	-42.29±4.14	-47.10±1.76	-48.54±0.96
4. FDHL	-44.66±2.04	-47.64	-46.05±3.05	-48.14±1.81	-59.63±6.25	-63.52±6.26
5. PB	-51.00±0.67	-51.6	-51.27±1.45	-53.6±1.04	-52.21±1.04	-54.0±1.16
6. SmAB	-27.21±0.88	-26.3	-27.80±2.65	-32.50±1.23	-34.38±2.0	-36.13±1.46
7. Flexor	-48.01±0.89	-48.2	-47.66±1.65	-49.76±0.64	-51.87±2.78	-55.08±0.98
8. Extensor	-37.52±0.96	-37.8	-37.96±1.75	-43.75±0.35	-43.54±2.85	-46.75±2.18
9. SmAB	-48.45±1.90	-49.50	-47.11±1.57	-51.50±0.0	-67.32±3.20	-69.81±2.09
Mean	**-41.20±7.55**	**-41.90±8.07**	**-41.27±7.48**	**-45.96±6.24**	**-49.36±9.77**	**-51.92±10.07**

Table 5. Results calculated from Table 4.

Cell No.	Hyperpolarization of Voltage Threshold (mV)				
	Rest	Locomotion	Locomotion - Rest		
	1st spikes (3) – (2)	1st spikes (5) – (4)	All Spikes (4) –(0)	All Spikes (4) –(2)	1st spikes (5) –(1)
1. Extensor	-3.38	-2.86	-3.51	-1.45	-7.15
2. Extensor	-9.62	-2.43	-6.52	-7.68	-7.2
3. CP	-7.77	-1.14	-11.5	-12.6	-11.56
4. FDHL	-2.09	-3.88	-14.97	-13.58	-15.87
5. PB	-2.36	-1.81	-1.21	-0.94	-2.4
6. SmAB	-4.70	-1.75	-7.17	-6.58	-9.83
7. Flexor	-2.09	-3.21	-3.86	-4.21	-6.88
8. Extensor	-5.78	-3.21	-6.02	-5.58	-8.95
9. SmAB	-4.38	-2.48	-18.87	-20.21	-20.36
Mean	**-4.6±2.6 (↓)**	**-2.5±0.8 (↓)**	**-8.1±5.8 (↓)**	**-8.1±6.3 (↓)**	**-10.0±5.3 (↓)**

Figure Legends

Figure 1: Single cell model and initial properties. **A.** A single cell model with five compartments was built that retained morphological features of motoneurones important for the generation of anti- and orthodromic action potentials. The input resistance of the model cell R_{in}=2.0MΩ; membrane time constant t_m=4ms; and the rheobase current I_{rhe}=11nA. **B.** Repetitive firing of the model cell was evoked by injecting a triangular current (starting from -5nA with peak 30 nA and duration 1s, not shown) to the soma compartment. The mean value of the voltage threshold was -35.8±0.7mV (dark line). **C.** Frequency-current (F-I) relation produced by step current injections into the soma compartment. The slope of the primary range is 1.1 Hz/nA, and the slope of the secondary range is 11 Hz/nA. The frequency was calculated by dividing the number of spikes by the duration (500 ms) of each step current. (Modified from Dai et al., 2000)

Figure 2: Intracellular recording from a cat lumbar motoneurone. The motoneurone was made to fire under three conditions (A-C): 1) control state using triangular current injection; 2) locomotion state with triangular current injection; and 3) control state with repetitive current pulses superimposed on triangular current injection. The repetitive current pulses in condition 3 (C2) were used to produce rapid membrane depolarizations (C1) similar to the locomotor drive potentials (B1). Voltage threshold of an action potential is measured at the membrane potential at which the dV/dt ≥ 10mV/ms (Brownstone et al., 1992; Krawitz et al., 2000). Each dot shown in A3, B3 and C3 represents the voltage threshold for each spike shown in A1, B1 and C1 respectively. The current injections were shown in A2, B2 and C2. The circled dots represent the voltage

thresholds of the first spikes in each spike train that was produced by the LDPs during locomotion (B) or by triangular current (A) or current pulses superimposed on triangular current (C) at rest. Dark lines in A3, B3 and C3 stand for the mean values of the voltage thresholds for all spikes. **A.** At rest (condition 1), a triangular current injection made the motoneurone firing with an averaged voltage threshold of -27.2±0.9 mV (dark line in A3). **B.** During fictive locomotion (condition 2) the neurone fired at a lower voltage threshold (mean -34.4±2.0 mV for all spikes, dark line in B3) under a similar current injection to the condition 1. The mean value of the voltage threshold for the first spikes was -36.1±1.4 mV. **C.** At rest (condition 3), the neurone was made to fire under the injection of current pulses superimposed on triangular current. The mean value of voltage threshold for all spikes was -27.8±2.6 mV (dark line in C3) and that for the first spikes was -32.5±1.2 mV. (Modified from Krawitz et al., 2001)

Figure 3: Voltage threshold (Vth) measured from nine motoneurones (see Table 4). Open bars: Vth measured at rest with condition 1 (triangular current injection); dark bars: Vth measured during fictive locomotion (condition 2); and grey bars: Vth measured at rest with condition 3 (triangular current injection superimposed by square current pulses).

Figure 4: Intracellular recording from a cat lumbar motoneurone. An intracellular recording was made at rest (A) and during fictive locomotion (B and C). Voltage thresholds for each spike in A1, B1, and C1 were measured and plotted as dots in A2, B2 and C2 respectively. The circled dots represent the value of the first spike thresholds in each spike train. Dark lines represent the mean values of the voltage threshold for all spikes. **A.** At rest, a long pulse current of 15 nA and 200 ms was injected into this medial

gastrocnemius (MG) motoneurone to produce a quick membrane depolarization (A1) to the amount equivalent to the depolarization produced by the LDPs during fictive locomotion (C1). The motoneurone was made to fire with an averaged voltage threshold of -66.4±1.7 mV (A2 dark line). The mean value of the voltage threshold for the first spikes was -69.9±0.1 mV. **B.** The neurone fired in the initial phase of fictive locomotion. The mean values of voltage threshold were -75.8±1.3 mV for all spikes (B2 dark line) and -76.3±0.5 for the first spikes. **C.** The neurone made firing during a well-developed fictive locomotion. The voltage threshold for all spikes was -74.6±1.9 mV (C2 dark line) and that for the first spikes was -76.6±0.6 mV. There was no current injection in conditions B and C. (From Krawitz et al., 2001)

Figure 5: Faster rates of current injection are more effective at activating action potentials. **A.** A triangular current (bottom panel: starting at -5nA with peak 15nA and duration 125ms) was injected into the soma compartment. The slope of the ramp was 0.33 nA/ms. Peak membrane current (Im) underlying the action potential was -126nA (middle panel), and the Vth of the spike was -42.0mV (top panel). **B.** Doubling the slope of the ramp current to 0.66nA/ms (bottom panel: starting at -5nA with peak 35nA and duration 125ms) increased the peak Im for the first spike to -140nA (middle panel) and hyperpolarized the Vth of the first spike to -43.4 mV (top panel). Vth for the remaining two spikes were -40.2 mV and -39.0 mV respectively. **C.** Upper panel: relation between the slope of the injected ramp current and the peak Im underlying the first spike. Lower panel: relation between the slope of the ramp current and the Vth for the first spike. (From Dai et al., 2000)

Figure 6: Effects of rapid membrane depolarizations on voltage threshold (Vth). The membrane potential is shown in the top panel, current injection in the middle, and voltage threshold in the bottom. In all three panels current pulses (15 nA, 500 ms) were superimposed on triangular current (starting at -10 nA with peak 15 nA and duration 10 s) and injected into the soma compartment to produce rapid membrane depolarizations. The fictive locomotion state was simulated by increasing initial segment (IS) sodium conductance (max g_{Na}) by 100% (panel A) or by reducing the IS delayed rectified (max $g_{K(DR)}$) by 70% (panel B). Each dot shown in the bottom panels represents the Vth for each spike shown in the top panels respectively. The circled dots represent the Vth of the first spikes in each spike train. Dashed lines represent the mean values of Vth for the first spikes from all spike trains while the dark lines represent the mean values of the Vth for the subsequent spikes. **A.** The fictive locomotion state was simulated by increasing IS max g_{Na} by 100%. The mean value of the Vth for all spikes was -43.5±1.4 mV. The mean values of the Vth for the first and subsequent spikes were -44.7±0.8 mV (dashed line) and -43.0±0.7 mV (dark line) respectively. **B.** The fictive locomotion state could be also simulated by reducing the IS max $g_{K(DR)}$ by 70%. The mean value of Vth for all spikes was -41.4±1.2 mV while the mean values of the Vth for the first and subsequent spikes were -42.6±0.7 mV (dashed line) and -41.1±0.4 mV (dark line) respectively. **C.** Repetitive firing was evoked by the same current injection as used in A and B. Conductances of the model cell were not modified. The mean values of Vth were -37.6±3.0 mV for all spikes, -41.4±1.6 mV for the first spikes (dashed line), and -36.2±0.6 mV for the subsequent spikes (dark line). (From Dai et al., 2001).

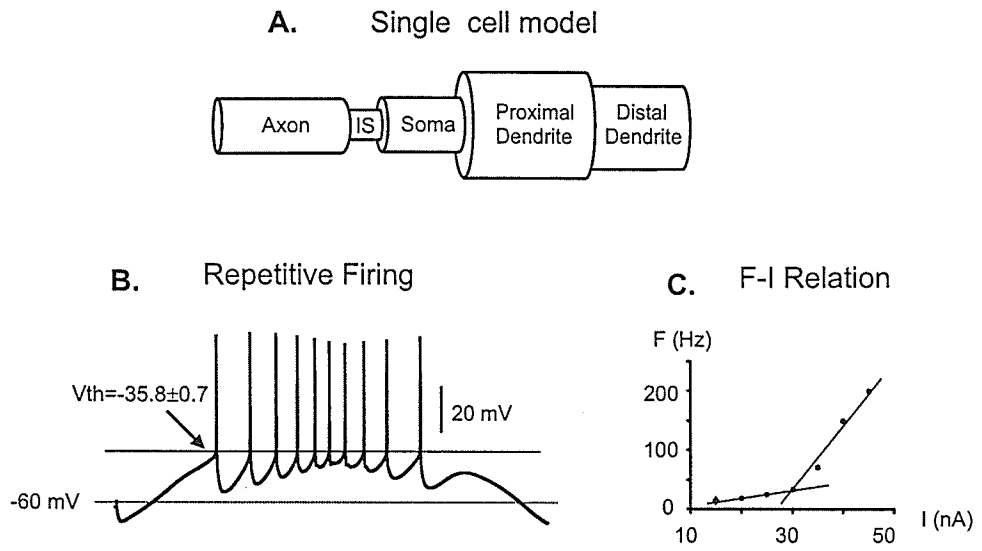

Section II: Figure 1

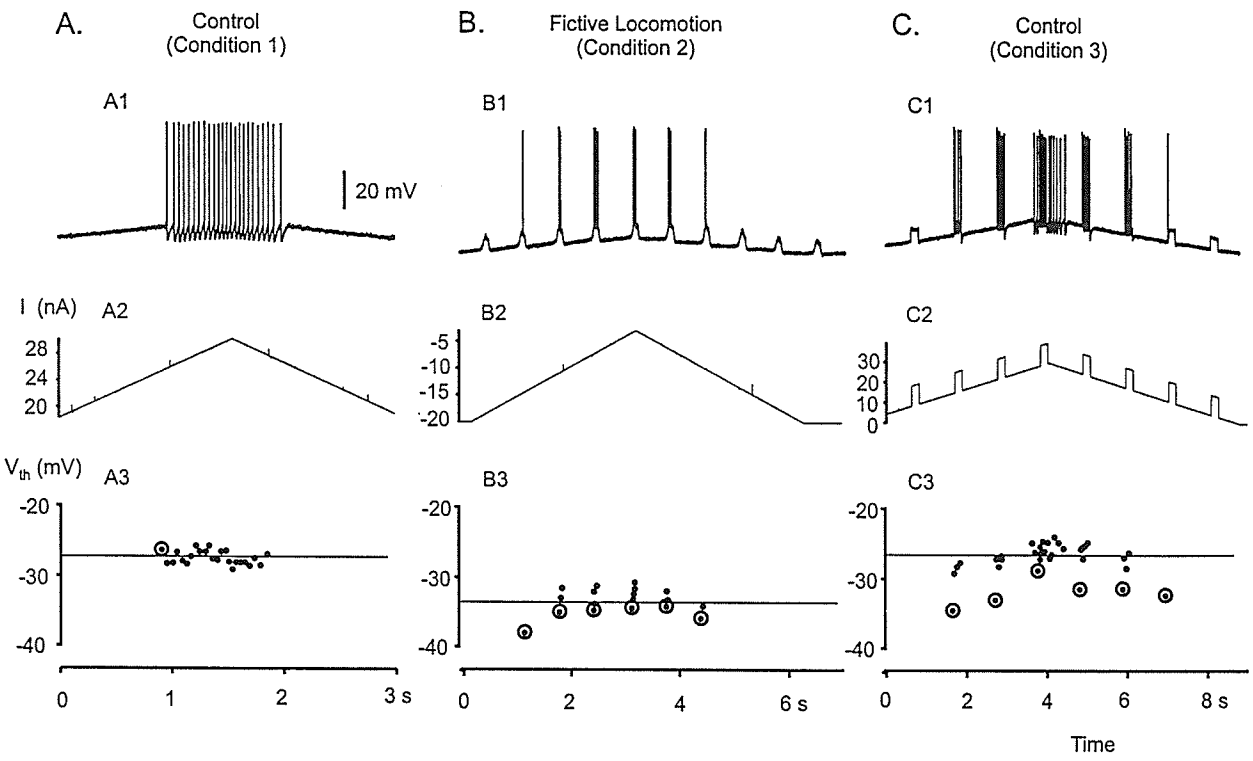

Section II: Figure 2

Vth measured from 9 cat lumbar motoneurones

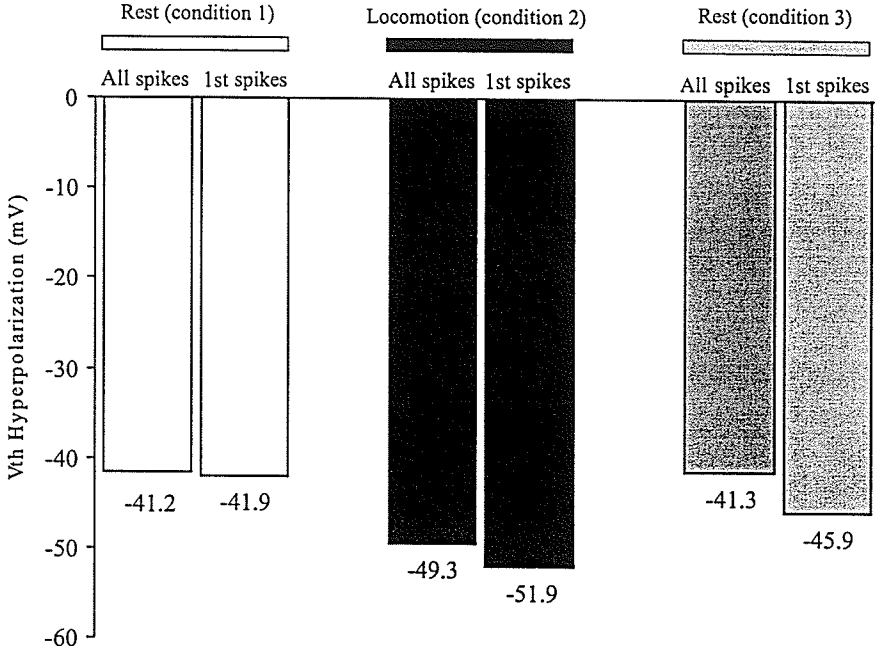

Section II: Figure 3

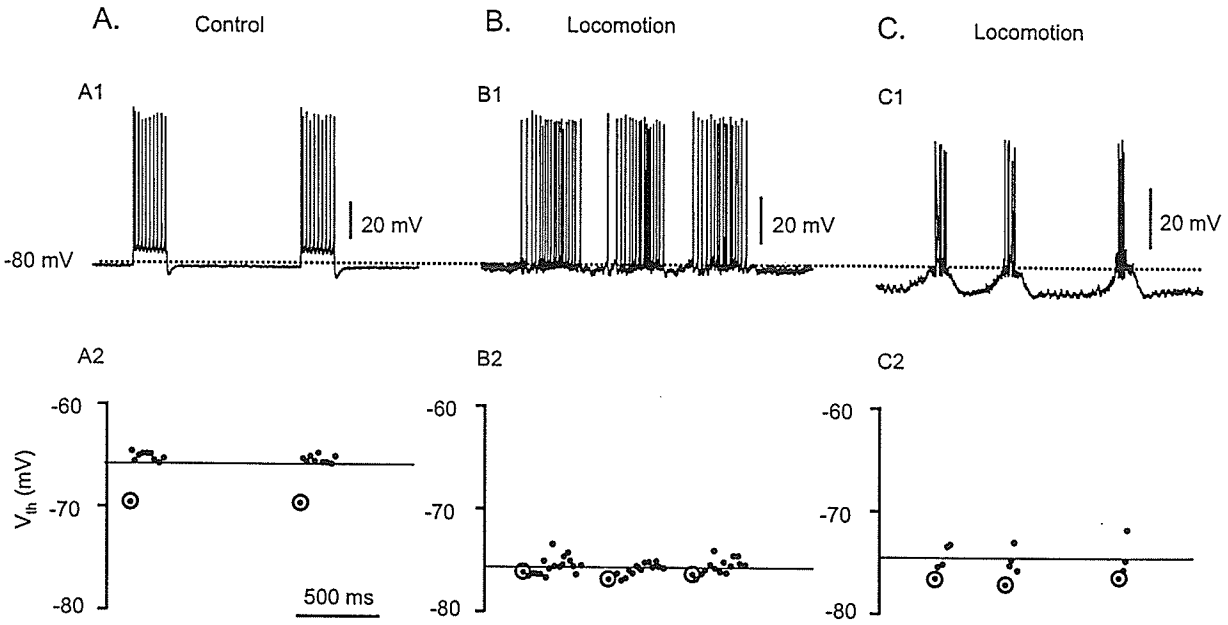

Section II: Figure 4

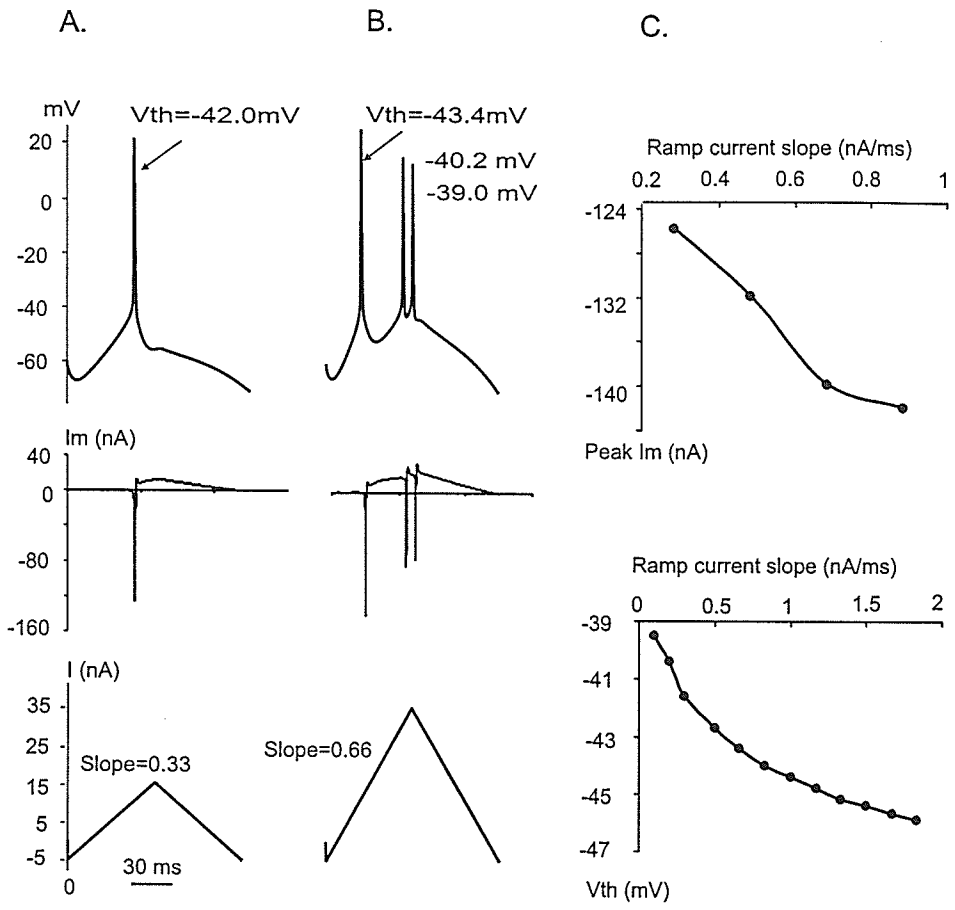

Section II: Figure 5

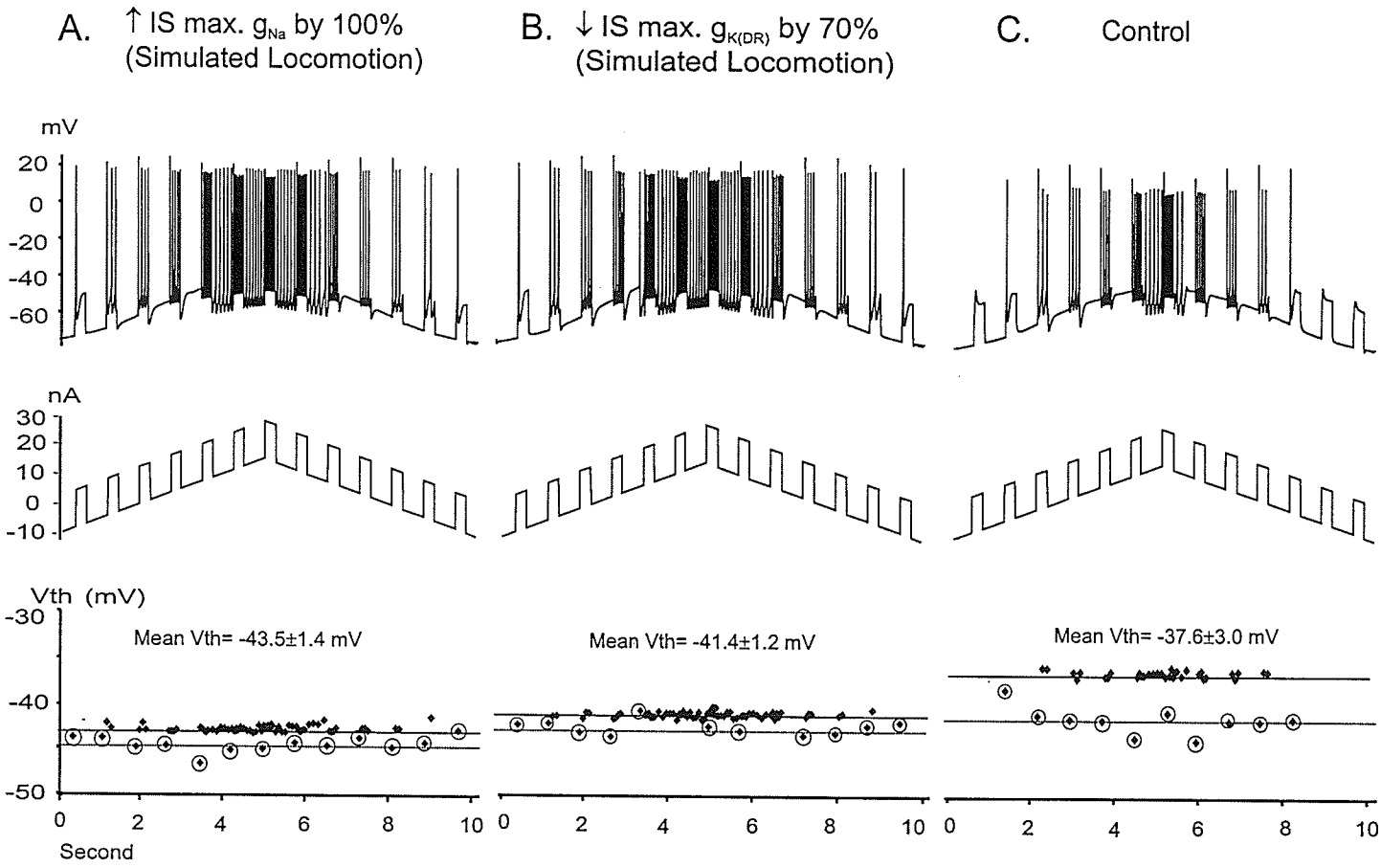

Section II: Figure 6

Section III

Motoneurone threshold hyperpolarization: alteration of population output predicted by a large-scale simulation

Y. Dai[1], D. Bashor[2], B. Fedirchuk[1], and L.M. Jordan[1].

[1]Dept.of Physiology,

University of Manitoba,

Winnipeg R3E 3J7, CANADA;

[2]Dept.of Biology,

The University of North Carolina at Charlotte,

Charlotte, NC 28223, USA

Abstract

Krawitz et al (1997) showed that the voltage threshold (V_{th}) for action potentials in cat motoneurones is hyperpolarized (-6.3 ± 3.9 mV) during fictive locomotion. Computer simulation (Dai et al, 1998) using a Hodgkin-Huxley type model with three compartments (initial segment, soma and dendrite) suggested that modulation of sodium and/or potassium conductances in the initial segment is a possible mechanism for producing the hyperpolarization of V_{th}. However, the impact of V_{th} hyperpolarization of motoneurones on the output of the entire motoneuronal pool is unknown.

A large-scale population model constructed from single-point neurons (Bashor, 1998) was used to investigate the population-level effects when the V_{th} for action potentials in motoneurones was hyperpolarized. Simulation results showed that without V_{th} hyperpolarization, a low intensity synaptic input recruited ~17% of S-type cells and ~1% of the F-type cells, whereas a high intensity input recruited ~80% of S-type cells and ~65% of F-type cells. When V_{th} was hyperpolarized by 7mV, a low intensity input recruited ~40% of S-type cells and ~45% of F-type cells, and a high intensity input recruited more than 90% of cells for both S- and F-type pools. Therefore, recruitment of the F-type motoneuronal pool was relatively more sensitive to the modest hyperpolarization of V_{th}, but in each case the S-type motoneurone pool contributes more recruited cells. The change of V_{th} produced only a small change in firing frequencies for both S- and F- type motoneurones in response to either low- or high-intensity inputs. These simulation results suggest that hyperpolarization of the V_{th} of motoneurones enhances the output of the motoneuronal pool primarily through increased recruitment. Perhaps this serves to minimize the central drive required to produce a behaviour.

Introduction

A recent study (Krawitz et al, 2001) showed that the voltage threshold (Vth) for the action potential in cat lumbar motoneurones was hyperpolarized during fictive locomotion induced by stimulation of the mesencephalic locomotor region (MLR). The mean value of Vth hyperpolarization was 6.3 mV (S.D. 3.9) compared to the threshold at rest. Computer simulation (Section I) using a single cell model with three compartments (initial segment, soma and dendrite) suggested that a modulation of the sodium channel or potassium channel or both in the initial segment could be the possible mechanisms producing the hyperpolarization of the voltage threshold during fictive locomotion. However, the impact of Vth hyperpolarization of motoneurones on the output of the entire motoneuronal pool is still unknown. The purpose of this study is to use a large-scale computer model to investigate the contributions made by each individual motoneurone to the output of the whole population when voltage threshold for action potential generation in each neuron is hyperpolarized.

Method

A large-scale model constructed from single point neurons was used to investigate the population-level effects when the V_{th} for action potentials in motoneurones was hyperpolarized. Details of the model construction are described in a previous publication (Bashor, 1998). In brief, the model was built with point neurones that were described by an equivalent-circuit algorithm of the potential across a unit-area membrane. The properties of the neurone are determined by six parameters: (1) B, a dimensionless intensity parameter that sets and size of the AHP; (2) TGK, the decay time constant of the

AHP following a spike; (3) C, a fractional intensity parameter for determining refractoriness following a spike; (4) TTH, time constance of accommodation; (5) TMEM, membrane time constance; and (6) TH0, initial voltage threshold. Cell input is the sum of synaptic conductances of each cell or terminal delivering input to that cell. Each cell in a source population had the possibility of contacting any cell population in the target population. Three different synaptic types were possible for connecting cells in a source population to a target. Cell populations were driven by fiber populations. Each of the number of terminals (NT) from a cell or fiber to the receiving population had the same strength of the output synapses (STR), and a random number seed was used to choose the target cells. All conduction times from source to target were 1 ms. (see Bashor 1998 for details).

The point neurone used in this section is very different from the HH-type single neurone in sections I and II. However, an aproximate relationship could be established between the parameters of these two types of neurones based on their output behaviour, i.e. the generation of action potentials. The parameters B and TGK in point neurone are equivalent to the AHP conductance ($g_{K(AHP)}$) in the HH-type neurone, while the TMEM in point neurone is equivalent to the membrane time constance (τ_m) which is equal to the product of $R_M C_M$ in the HH-type neurone. Change in parameter TH0 in the point neurone can be approached by altering the sodium conductance (g_{Na}) in the HH-type neurone, while setting of the parameters C and THH in the point neurone are equivalent to the alteration of the inactivation of g_{Na}, i.e. the setting of inactivation state variable h and time constance $\tau_h=1/(\alpha_h+\beta_h)$.

Two types of point neuron (S- and F-type) were built based on membrane properties of cat lumbar motoneurones. In the point neuron model, the voltage threshold (TH) for spike generation is a function of the membrane potential (E) and can be controlled by three parameters: initial threshold (TH0), accommodation sensitivity (C, ranging from 0 to 1), and time constant for accommodation (TTH). Both C and TTH have little effect on the voltage threshold for repetitive firing of the neuron. Therefore, hyperpolarization of voltage threshold is mimicked by reducing the value of TH0 in this study.

Definition of S- and F-type Point Neurons

Two types of motoneurone model (S- and F-type) were defined by adjusting a set of parameters (C, TTH, B, TGK, EK, TD and TH0) which determined the single point neuron's properties based on the cat lumbar motoneurone properties (Eccles, 1957b, Zengel et al., 1985, Gustafsson et al., 1984b). In general, an S-type motoneurone has a larger AHP duration, lower rheobase current intensity, higher input resistance, and lower voltage threshold compared to the F-type motoneurone. Table 1 shows the definition of the S- and F-types of point motoneurone and their properties. Single spikes produced by injections of rheobase current to the S- and F-type point neurons are shown in Figure 1A, and the F-I relations for both type neurons are shown in Figure 1B.

Table 1

Figure 1

Two types (S and F) of large-scale motoneurone population were constructed from the above-defined S- and F-type point neuron. Each population contains 100 cells

with identical properties as shown in Table 1 and receives excitatory synaptic input from the same source (Figure 2). The strength of the synaptic input is altered by adjusting the number of terminals (NT) from the excitatory fibers to the motoneurone pools (For details of the model construction, see Bashor, 1998).

Figure 2

Normalization of Voltage Threshold Measured from Cat Experiments

Recent experimental data (Krawitz et al., 2001) showed that the mean value of voltage threshold measured in control (V_{th_c}) was -44.1 mV (n=38) and that the mean value of the voltage threshold during fictive locomotion (V_{th_l}) was -52.0 mV. Hyperpolarization of the threshold during fictive locomotion was about -8.0 mV (V_{th} = V_{th_l} - V_{th_c}= -7.9). The resting membrane potential (Em) was -66.7 mV on average. The voltage difference (V_{th0}) between V_{th_c} and Em was ~22 mV (i.e. V_{th0}= V_{th_c} - Em = 22.6 mV). We called V_{th0} the initial voltage threshold in order to establish a relation corresponding to TH0 used in the point neuron model. If we normalize the V_{th0}, then each 1% of the V_{th0} is equal to 0.22 mV voltage threshold, whereas each 1mV of the voltage threshold corresponds to 4.5% of the V_{th0}. Hyperpolarization of voltage threshold by 8.0 mV is equivalent to 36% reduction of the V_{th0}. For simplicity, therefore, the physiological range of the Vth hyperpolarization observed during fictive locomotion is simulated by ~40% reduction of the initial voltage threshold (TH0) in the model.

Based on the above normalization we can establish a relation of voltage thresholds between the experimental and modeling data (Table 2).

Table 2

Definition of the Low- and High-Intensity of Stimulation and Synaptic Input

For clarity we give some definitions of the terms used in this modeling study.

(1) A minimum amount of stimulation current (SC) which makes the S-type point neuron repetitively to fire is defined as *the low-intensity stimulation* (SC=17), and the resultant firing frequency is defined as the *minimum firing frequency of the S-type point neuron* (f=12 Hz).

(2) A minimum amount of stimulation current (SC) which makes the F-type point neuron repetitively to fire is defined as *the high-intensity stimulation* (SC=24), and the resultant firing frequency is defined as the *minimum firing frequency of the F-type point neuron* (f= 15 Hz).

(3) The strength of synaptic input, which drives the S-type motoneurone pool to fire at the average frequency approximately equal to the *minimum firing frequency of the S-type point neuron,* is defined as the *low-intensity synaptic input* (NT=3).

(4) The strength of synaptic input, which drives the F-type motoneurone pool to fire at the average frequency approximately equal to the *minimum firing frequency of the F-type point neuron*, is defined as the *high-intensity synaptic input* (NT=9).

The strength of synaptic input can be determined by several parameters in this large-scale model. We use the number of terminals (NT) from the excitatory fibers to the motoneurone pools to adjust the synaptic drive potential in current simulation.

Simulation Procedure

The simulation was done in two conditions: low-intensity synaptic input (NT=3) and high-intensity synaptic input (NT=9). Both the S- and F-type motoneurone pools

received the same synaptic inputs from the excitatory fibers with a duration of 300 ms (Figure 2). The initial voltage threshold (TH0) for spike generation in point neurons that constructed the S- and F-type motoneurone pools was reduced successively to mimic the hyperpolarization of voltage threshold (Table 2). Simulation data was collected and later analyzed using the analyses tool developed by Bashor (1998).

Results

Figure 1A shows single spikes evoked by injections of rheobase current to the point neuron models. An S-type point neuron generates a single spike with AHP duration of ~120 ms, rheobase current intensity of 13, and initial voltage threshold (TH0) of 10 mV while a F-type point neuron produces a single spike with AHP duration of ~80 ms, rheobase of 21, and TH0 of 17 mV. The F-I relations produced by the two types of the point neuron are plotted in Figure 1B1 (filled circle for S-type and open circle for F-type). A 40% reduction of TH0, which corresponds to ~8 mV hyperpolarization of voltage threshold in cat lumbar motoneurones observed during fictive locomotion, shifts the F-I relations to the left (Fig. 1B2).

The relation of firing frequency and voltage threshold produced by the two types of point neuron is shown in Figure 3. Figure 3A shows that with low-intensity stimulation (SC=17) the reduction of voltage threshold resulted in an increase in firing frequency in both S- and F-type point neurons. However, the firing frequency of the F-type point neuron is more sensitive to the hyperpolarization of voltage threshold than the S-type, especially when the hyperpolarization of Vth $\leq$ 40%, where the F-type point neuron was

almost inactivated. A 40% hyperpolarization of Vth made both types of neuron to fire at the same frequency of 16 Hz (gray bar in the figure).

Hyperpolarization of Vth also caused an increased firing frequency in both types of point neuron with high-intensity stimulation (SC=24, Fig. 3B). In this case, both types of neuron were firing in the control condition (i.e. 0% reduction of Vth), and the F-type point neuron always fired at a higher frequency than the S-type fired in response to the successive reduction of Vth. In general, the firing activity of the F-type point neuron is more sensitive to the hyperpolarization of the Vth than the S-type.

Figure 3

The effect of Vth hyperpolarization on the motoneurone pools is similar to that on the single point neurons. Figure 4A shows that with low-intensity synaptic input (NT=3) hyperpolarization of Vth in each point neuron that constructed the motoneurone pools increased the mean firing frequency in both S- and F-type motoneurone pools. A 40% hyperpolarization of Vth made both types of pool to fire at the same averaged frequency of 13 Hz (gray bar in the figure). A further reduction of Vth caused the F-type pool to fire at a higher frequency than the S-type. However, the firing frequency of the F-type pool is lower than the S-type pool when the Vth hyperpolarization $\leq$ 40%. In general, the firing activity of the F-type pool is more sensitive than that of the S-type pool in response to the hyperpolarization of Vth. Hyperpolarization of Vth also caused an increase in number of recruited cells in both S- and F-type pools. Figure 4B shows that with low-intensity synaptic input (NT=3) the number of recruited cells caused by the Vth hyperpolarization is larger in F-type pool than in S-type pool although the absolute number of recruited

cells in the F-type pool is less than that in the S-type pool when Vth hyperpolarization ≤ 40%.

Figure 4

Results in Figure 4 suggest that under the condition of low-intensity synaptic input, Vth hyperpolarization resulted in an increased output of both S- and F-type motoneurone pools through either increasing the firing frequency of the pools or increasing the number of recruited motoneurones. In either case, the F-type motoneurone pool displayed a higher sensitivity to the changes in Vth than the S-type pool. This conclusion was further confirmed in the condition of the high-intensity synaptic input (NT=9). Figure 5 shows that with high-intensity synaptic input hyperpolarization of Vth caused an increase in both firing frequency and number of recruited cells in both S- and F-type motoneurone pools. The F-type pool fired at a higher frequency than the S-type pool (Fig. 5A). Although the number of recruited motoneurones in S-type pool was larger than in F-type pool, the amount of recruited motoneurones in S-type pool was smaller than in F-type pool (Fig. 5B). This is because with high-intensity synaptic input the S-type motoneurones have been recruited by ~83% before Vth is hyperpolarized, therefore it is easy for S-type pool to get saturated in recruitment in response to the Vth hyperpolarization. Figure 5 shows that a 40% hyperpolarization of Vth resulted in a 3 Hz increase in firing frequency in F-type pool and 2 Hz in S-type pool and recruited more than 90% of motoneurones in both S- and F-type pools.

Figure 5

Hyperpolarization of voltage threshold also increases the number of cells active per millisecond. Figure 6 shows that the number of population cell firings per millisecond is increased when voltage threshold is recursively reduced from 0% (control, bottom traces) to 80% (top traces) with either low-intensity or high-intensity synaptic inputs.

Figure 6

The primary simulation results are shown in both Table 3 and Figure 7.

Table 3

Figure 7

Discussion

A possible mechanism for increasing the output of the spinal motor system

Simulation results show that hyperpolarization of voltage threshold could increase the output of motor system through increasing either the mean firing frequency of the motoneurone pools or the number of recruited motoneurones or both. In both low- and high-intensity synaptic inputs a 40% reduction of voltage threshold, which corresponds to ~8 mV hyperpolarization of Vth in cat lumbar motoneurone during fictive locomotion, caused a small increase in firing frequency ($\leq$ 3 Hz) in both S- and F-types of motoneurone pool. With the same amount of Vth hyperpolarization, however, a low-intensity synaptic input recruited more than 40% of both S- and F-type motoneurones while a high-intensity synaptic input recruited more than 90% of both types of motoneurone. These results suggest that the spinal motor system would be more sensitive to recruitment of motoneurones than to the increment of firing frequency in response to the Vth hyperpolarization. The Vth hyperpolarization would enhance system output without a need to increase the excitatory synaptic input to the motoneurone pools during

locomotion. This mechanism would be different from that of reduction of afterhyperpolarization (AHP) that was observed during fictive locomotion (Brownstone et al., 1992) and expected to have an effect on the increment of the motor system output through increasing the mean firing frequency of the motoneurone pools.

Voltage threshold hyperpolarization facilitates recruitment of motoneurones

In the 1960s, Elwood Henneman proposed the "size principle" based on the observation that motoneurones are recruited by synaptic action in a fixed order reflecting the conduction velocity and the diameter of the their axons. Because the size of the cell body varies with the diameter of its axon, the smallest cells are recruited first by the weakest inputs for their lowest threshold for synaptic activation. This order of recruitment is called the size principle.

Motoneurone recruitment is mainly determined by three factors (Heckman and Binder, 1990, 1993; Pinter 1990): (1) intrinsic current threshold of the motoneurone. (2) strength of synaptic input to the motoneurone; and (3) degree of randomness inherent in either the motoneurone threshold or its share of the synaptic input (i.e. the variation between the first and second factors). Studies (Fleshman et al., 1981; Zengel et al., 1985) have shown that motoneurones are systematically different in current threshold. This difference is the principle factor underlying orderly recruitment of motoneurones, and is referred to as the "size principle" (Henneman et al 1965). Motoneurones requiring small synaptic currents for firing are recruited before those requiring larger currents.

Simulation results show that, in general, hyperpolarization of voltage threshold for action potential generation within motoneurone pools does not change the orderly

recruitment of motoneurones but changes the sensitivity of the pools to the synaptic inputs. F-type motoneurone pools become more sensitive than S-type to the synaptic inputs when voltage threshold is hyperpolarized by an amount comparable to the experimental observations. This result suggests that hyperpolarization of voltage threshold could be a strategy used by spinal motor system to enhance the force generation without increasing synaptic input.

Deviations from orderly recruitment has been reported in previous studies in both human and animals (e.g. Riek and Bawa, 1992; Cope and Clark, 1991). This phenomenon is also observed in our simulations. Figure 4B in Section III shows that with low-intensity synaptic inputs, recruitment of the F-type motoneurone pool becomes larger than that of the S-type pool when voltage threshold is hyperpolarized more than 8 mV (i.e. > 40% of hyperpolarization of Vth), suggesting a potential mechanism responsible for deviation from the predictions of the size principle in recruitment of motoneurones. These simulation results suggest that voltage threshold could be considered an additional factor which influences or even determines the motoneurone recruitment.

Conclusion

Simulation results show that recruitment of the F-type motoneuronal pool is relatively more sensitive to modest hyperpolarization of Vth and that the S-type motoneurone pool contributes more recruited cells. The change of Vth produces only a small change in firing frequencies for both S- and F- type motoneurons. These results suggest that hyperpolarization of the Vth of motoneurones enhances the output of the

motoneuronal pool primarily through increased recruitment. Perhaps this serves to minimize the central drive required to produce behaviour.

Abbreviation

SC : Stimulation current.

NT : Number of terminals.

C : Sensitivity to accommodation (range, 0 - 1).

TD : Membrane time constant.

TTH : Time constant of accommodation.

TH0 : Baseline voltage threshold (initial Vth, mV)

B : Sensitivity of potassium conductance to spike; sets size of AHP.

TGK : Decay time constant of potassium conductance recovery following spike.

EK : Potassium equilibrium potential (-10 mV).

Irhe : Rheobase current intensity.

MN : Motoneurone.

V_{th0} : Initial value of voltage threshold (= 22 mV) for cat lumbar motoneurones with respect to the resting membrane potential.

Table 1. The S- and F-type single point neurons.

Neuron	C	TTH (ms)	B	TGK (ms)	EK (mV)	TD (ms)	TH0 (mV)	Irhe	AHP (ms)	Vth (mV)
S-type	0.4	20	800	20	-10	5.0	10	13	120	12
F-type	0.3	20	700	13	-10	5.0	17	21	80	19

Table 2. Successive reduction of the initial thresholds (V_{th0} and TH0) by percentage.

	Successive reduction of V_{th0} and TH0 by percentage										
% :	0	10	20	30	40	50	60	70	80	90	100
Cat MN V_{th0} (mV)	22	19.8	17.6	15.4	13.2	11.0	8.8	6.6	4.4	2.2	0
S-type TH0 (mV)	12	10.8	9.6	8.4	7.2	6.0	4.8	3.6	2.4	1.2	0
F-type TH0 (mV)	19	17. 1	15.2	13.3	11.4	9.5	7.6	5.7	3.8	2.9	0

Table 3. Primary simulation results.

	Control		Vth hyperpolarization by 40% (~8 mV)	
	Low-Intensity Synaptic Input	High-Intensity Synaptic Input	Low-Intensity Synaptic Input	High-Intensity Synaptic Input
Recruitment of S-type motoneurone pool (%)	17	83	45	96
Recruitment of F-type motoneurone pool (%)	1	65	40	96
Frequency of S-type motoneurone pool (Hz)	12	13	13	15
Frequency of F-type motoneurone pool (Hz)	10	15	13	18

Figure Legends

Figure 1. Two types of single point neuron. The S- and F-type point neurons are defined by adjusting a set of parameters (Table 1) based on the membrane properties of cat lumbar motoneurones. **A1.** A single spike is elicited by injection of rheobase current to the S-type point neuron which produces the afterhyperpolarization (AHP) duration of ~120 ms, baseline of voltage threshold of 10 mV (TH0), and rheobase current intensity of 13. **A2.** The rheobase current is injected into the F-type point neuron to produce a single spike with AHP duration of ~80 ms, TH0 of 21 mV, and rheobase current intensity of 21. **B1.** The relations of firing frequency and current (F-I) are produced by injecting step current to the two types of neuron. The minimum current that makes the S-type point neuron fire repetitively is defined as the low-intensity stimulation current (SC=17) while the minimum current that drives the F-type point neuron repetitive firing is defined as the high-intensity stimulation current (SC=24). **B2.** Reduction of voltage threshold (Vth) by 40%, which corresponds to a ~8 mV hyperpolarization of Vth in cat lumbar motoneurones, shifts the F-I relations of both types of neuron to the left (filled circle for S-type and open circle for F-type).

Figure 2. Large-scale population model. A large-scale model is constructed from the single point neurons. The model contains two types of motoneurone pools (S-type in left side and F-type in right side). Each pool contains 100 point neurons with identical membrane properties. Both pools receive the excitatory synaptic input from the same source. The synaptic strength is adjusted by altering the number of terminals (NT) of the excitatory fibers projecting to the motoneurone pools. A low-intensity synaptic input is

generated by setting NT=3 while a high-intensity synaptic input is produced by setting NT=9. See text for the definition of the low- and high-intensity of synaptic input.

Figure 3. The effect of voltage threshold hyperpolarization (Vth) on the output of single point neurons. The firing frequencies are plotted versus the voltage threshold which is reduced successively with low- and high-intensity stimulation applied to the S- and F-type point neurons. Hyperpolarization of Vth causes an increase in firing frequency in both S- (filled circle) and F-type (open circle) point neurons. A 40% reduction of Vth in the models is equivalent to an ~8 mV hyperpolarization of Vth in cat lumbar motoneurones (gray bars in A and B). **A.** A low-intensity stimulation (SC=17) is applied to the S- and F-type models with successive reduction of voltage threshold. **B.** A high-intensity stimulation (SC=24) is given to the S- and F-type point neurons when Vth is successively hyperpolarized.

Figure 4. The effect of voltage threshold hyperpolarization on the output of motoneurone pools in the condition of low-intensity synaptic input. With low-intensity synaptic input hyperpolarization of Vth causes a small increase in firing frequencies and a relatively large increase in number of recruited cells in both S- and F-type motoneuronee pools. **A.** The mean firing frequencies of the S- and F-type pools are plotted versus the reduction of voltage threshold. **B.** The number of firing cells (i.e. the number of cells recruited) is plotted versus the reduction of voltage threshold. The S- and F-type motoneurone pools are composed of 100 point neurons respectively. The filled circle represents the S-type pool and open circle represents the F-type. A 40% reduction of Vth in the models (gray

bars in A and B) corresponds to ~8 mV hyperpolarization of Vth in cat lumbar motoneurones.

Figure 5. The effect of voltage threshold hyperpolarization on the output of motoneurone pools with high-intensity synaptic input. Hyperpolarization of Vth causes an increase in both firing frequencies and recruitment numbers in both S- and F-type motoneurone pools. **A.** The mean firing frequencies of the S- and F-type pools are plotted versus the reduction of voltage threshold. **B.** The number of firing cells (i.e. the number of cells recruited) is plotted versus the reduction of voltage threshold. The S- and F-type motoneurone pools are composed of 100 point neurons. The filled circles represent the S-type pool and open circles represent the F-type. A 40% hyperpolarization of Vth in the models (gray bars in A and B) corresponds to ~8 mV hyperpolarization of Vth in cat lumbar motoneurones.

Figure 6. Hyperpolarization of voltage threshold increases population cell firings. A 100-point moving average of the number of active cells (population cell firings) at each millisecond is plotted in panels **A**, **B**, **C**, and **D**. The voltage threshold (TH0) is recursively reduced from 0% (control, bottom traces) to 80% (top traces) with low-intensity (**A** and **B**) and high-intensity (**C** and **D**) synaptic inputs, and the number of active cells in both S-type (**A** and **C**) and F-type (**B** and **D**) motoneurone pools are increased with the reduction of TH0.

Figure 7. Results from table 3 are plotted in this figure. Panel **A**, hyperpolarization of voltage threshold increases the recruitment of motoneurone pools (both S- and F-type) with low- and high-intensity synaptic inputs. Panel **B**, hyperpolarization of voltage threshold increases the mean firing frequency of the motoneurone pools with the same synaptic input conditions. Gray bars: control, and ark bars: hyperpolarization of voltage threshold by 40% which corresponds to ~8 mV hyperpolarization of Vth in cat lumbar motoneurones.

A. Two types of single point neuron

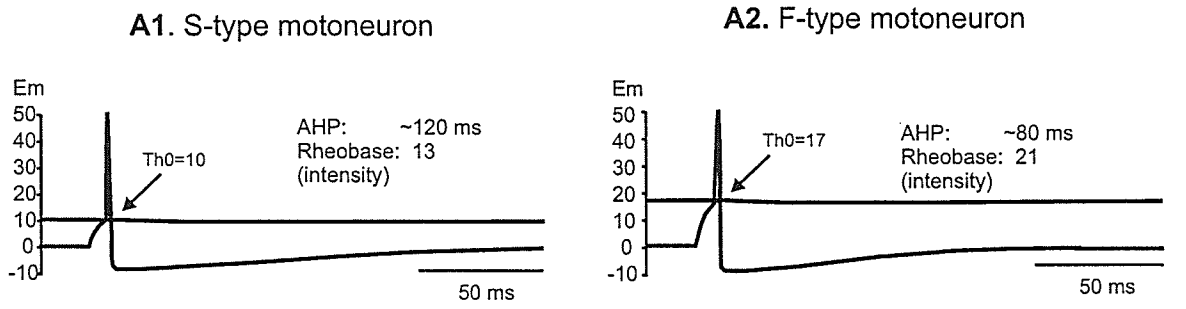

B. F-I relation (S- and F-type)

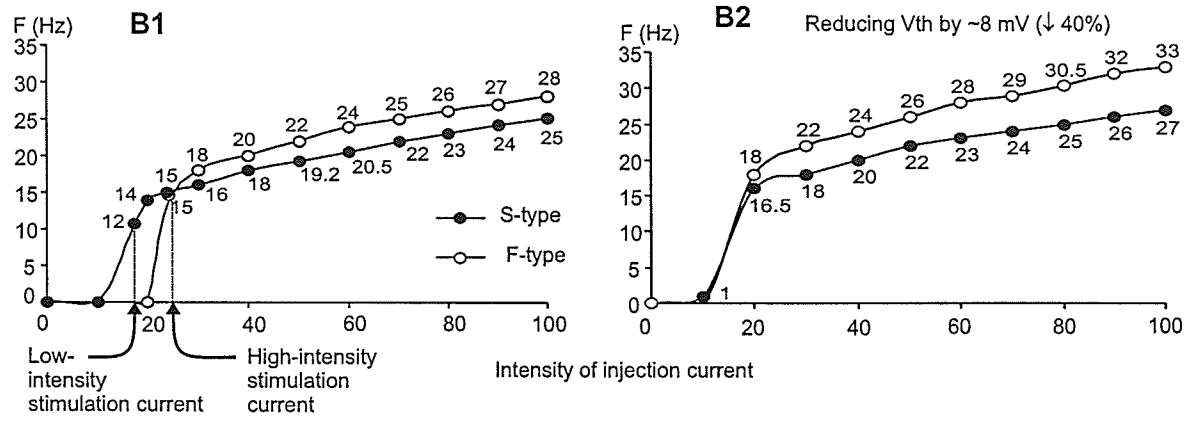

Large-scale population model

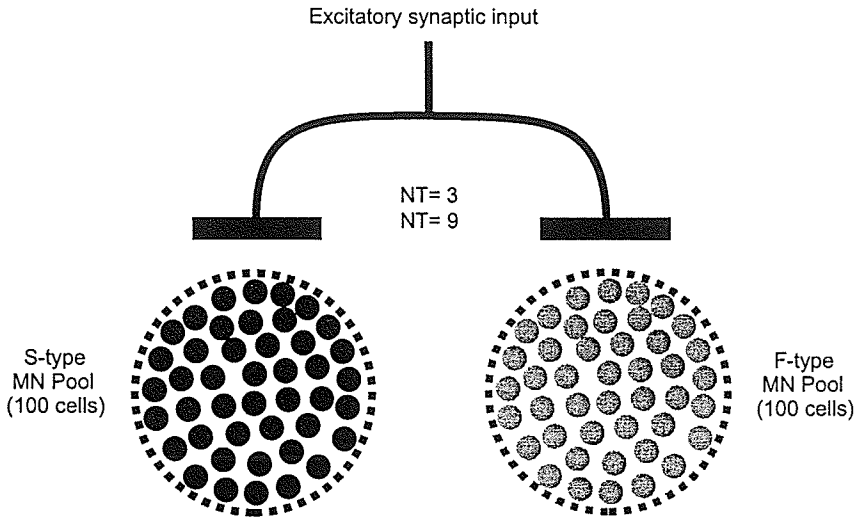

NT= 3: Low intensity synaptic input
NT= 9: High intensity synaptic input

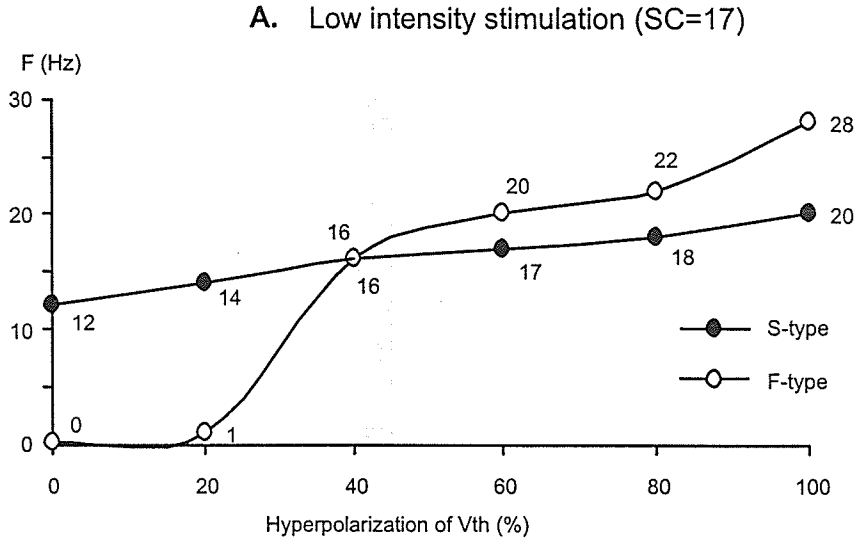

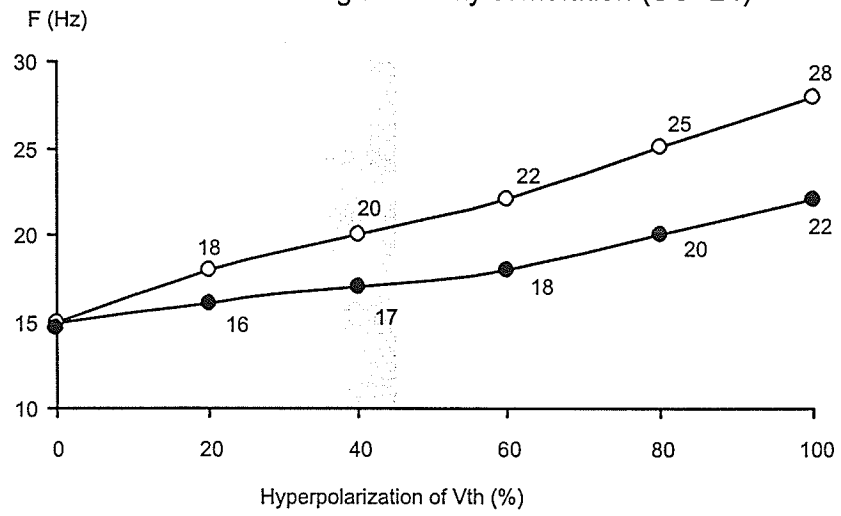

Section III: Figure 3

Effect of Vth hyperpolarization on population output

Low-intensity synaptic input (NT=3)

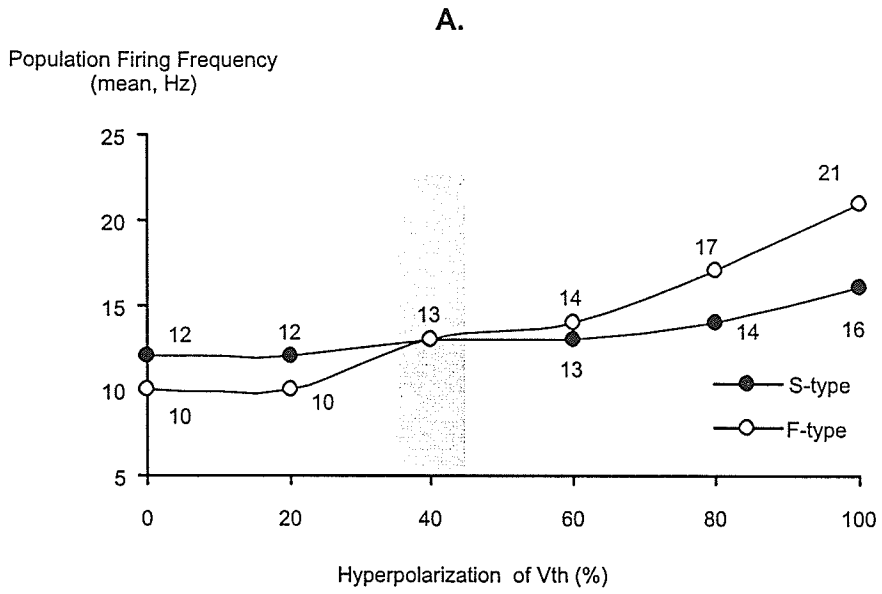

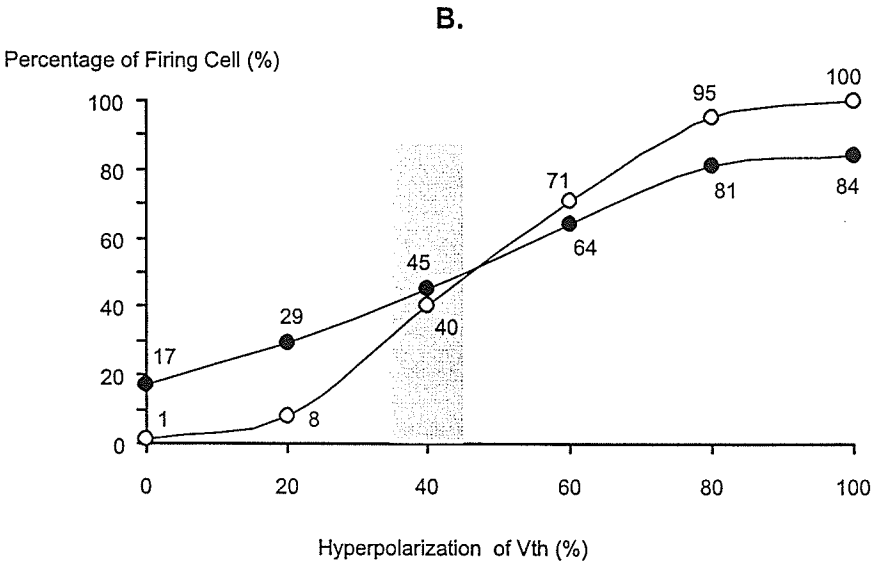

Section III: Figure 4

Effect of Vth hyperpolarization on population output

High-intensity synaptic input (NT=9)

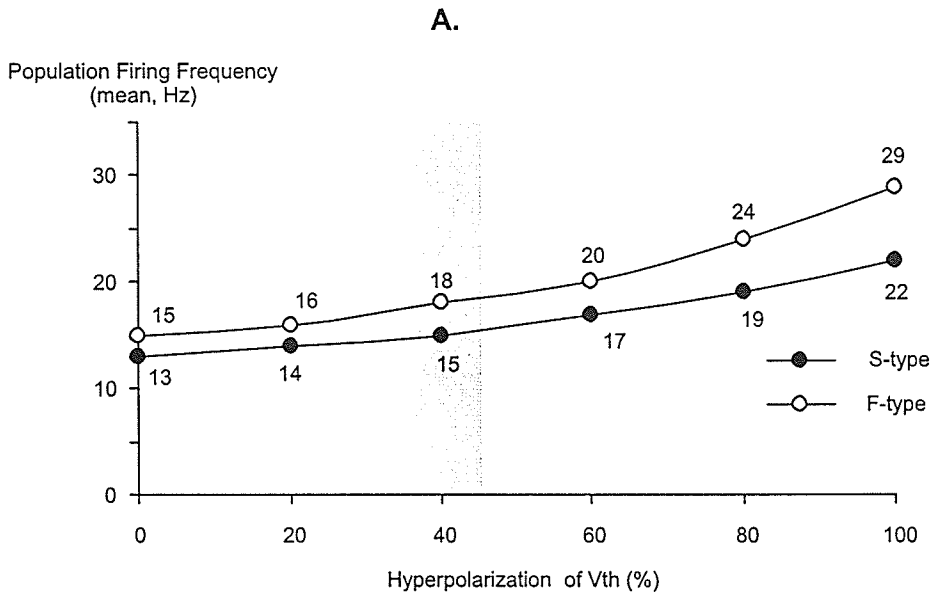

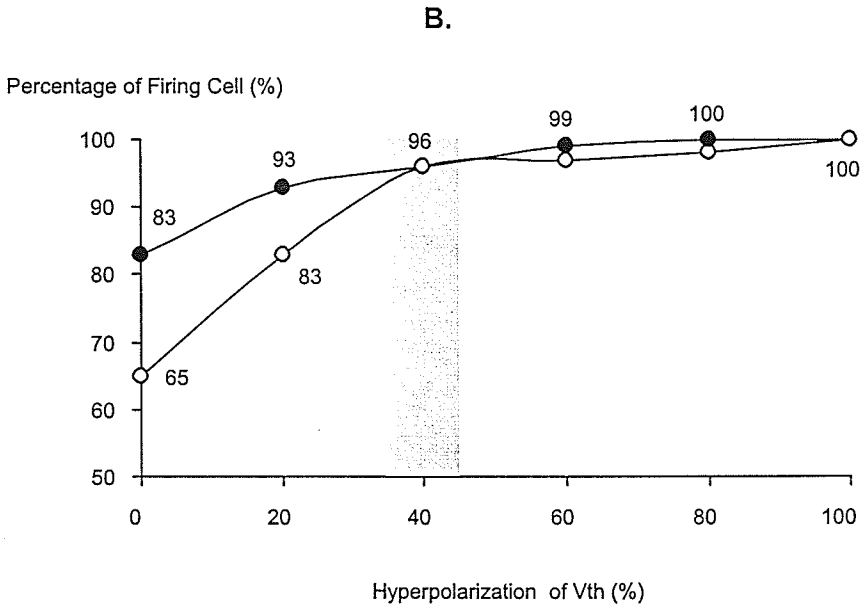

Section III: Figure 5

Hyperpolarization of voltage threshold increases the number of active cells

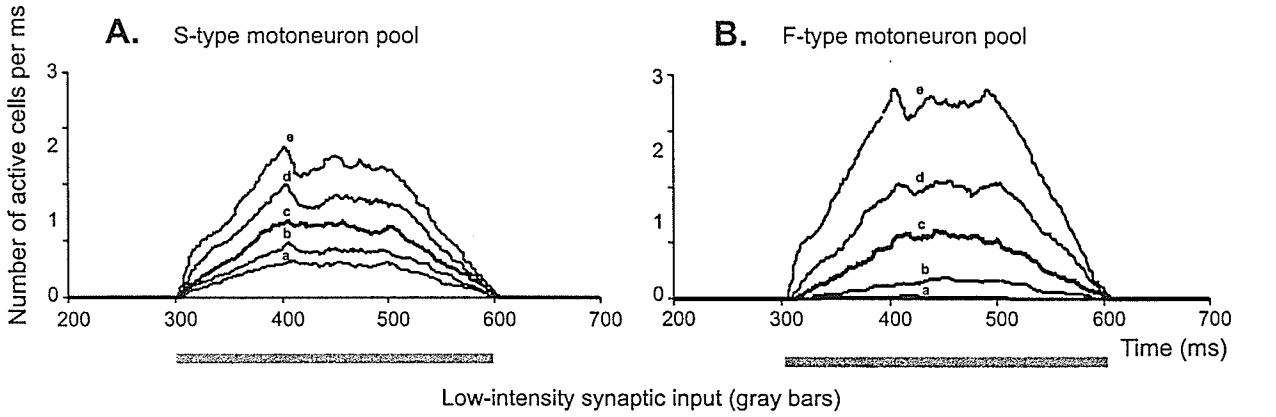

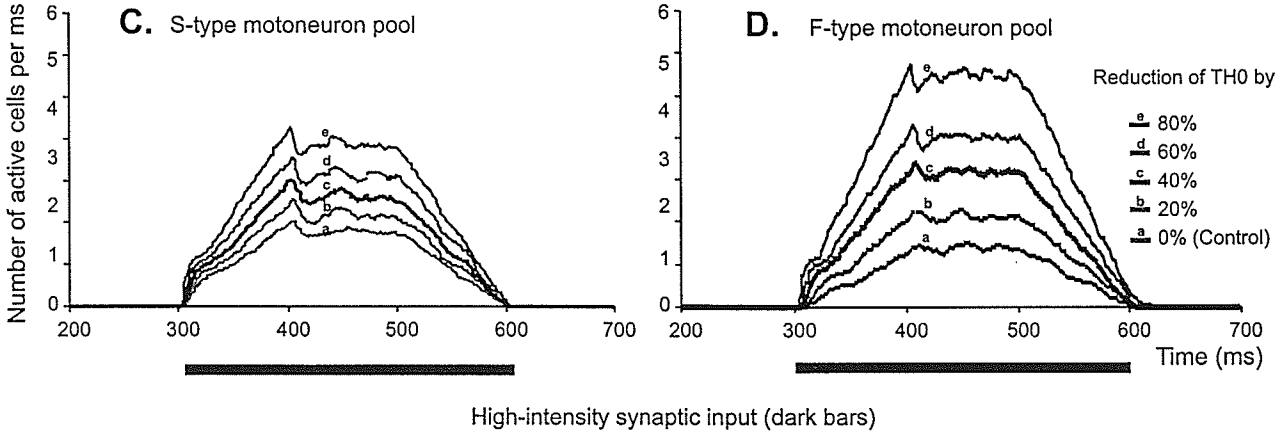

A. Motoneurone Recruitment

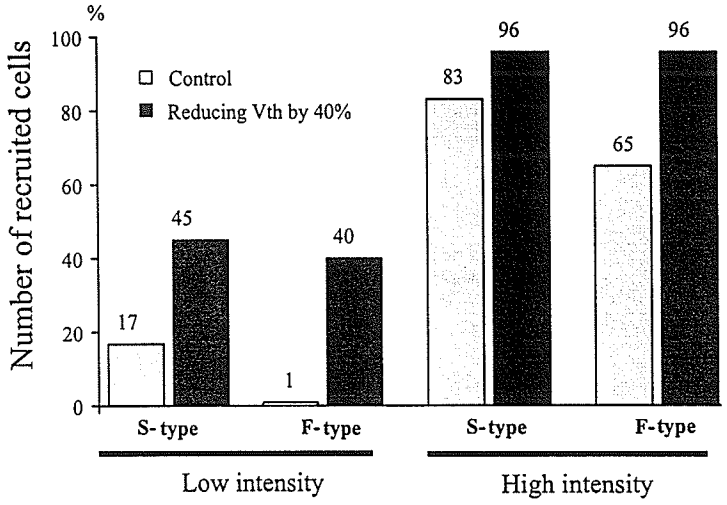

B. Mean Firing Frequency of Motoneurone Pools

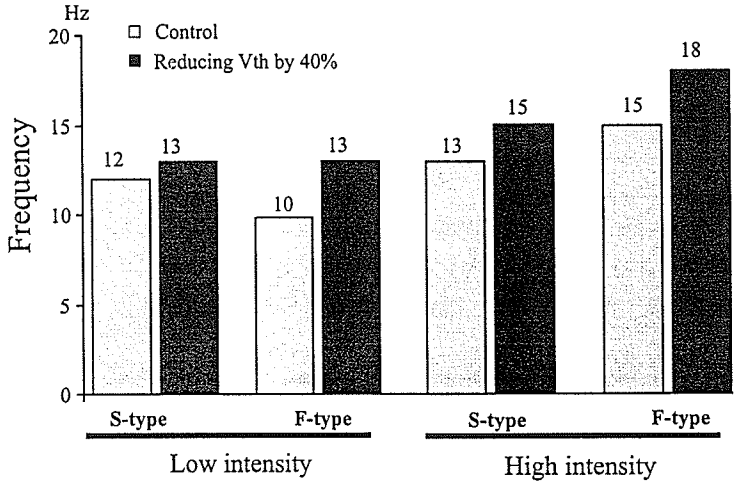

General Discussion

A modeling and experimental study of voltage threshold hyperpolarization induced by fictive locomotion has been presented in the above three sections. In this section, some additional information is added as supplemental material as well as a general review of the above three sections.

Measurement of electrical properties of motoneurones

The single cell model for the three types of cat spinal motoneurones was based on the passive and active properties of the motoneurones. The properties we chose for our models are somewhat arbitrary. But this does not constitute a serious flaw in our present study of Vth for action potential generation, as the main conclusion of this study are not likely to be affected by the exact starting values of these properties. A brief description of measurement of some passive membrane properties of the motoneurones is given in this section.

There are three parameters that are essential to computational models, namely R_M, C_M, and R_A. The R_M can be derived from $G_M=G_P/A_P$, where G_p is patch conductance and A_P is patch area (see Rall et al. 1992 for review.). However, A_P is difficult to measure. A better way is to estimate the time constant (τ) of the membrane patch which is independent of membrane area. Then $R_M = \tau / C_M$, where C_M is generally assumed to be 1.0 $\mu F/cm^2$. R_M can be also deduced from an input resistance of a branched neuron, which is estimated by dividing the input conductance by the total membrane surface. But this estimation neglects the cable properties of dendrites and soma shunting caused by microelectrode penetration, resulting in an underestimation (a low value) of R_M. This erroneously low estimate of R_M causes an overestimate of C_M ($=\tau/R_M$) two to five times

larger than 1.0 μF/cm^2 (Rall et al., 1992). Rall et al (1992) developed some equations for evaluating R_M to avoid this error by simply assuming that R_M nonuniformity is present only as a difference between the soma and a uniform dendritic membrane or that R_M increases continuously with dendritic distance away from soma. The cytoplasmic resistivity R_A is difficult to measure directly. The reported value of R_A for mammalian neurons is 70±15 Ωcm (Barrett, J.N. and Crill, W.E. (1974), and a 43 Ωcm of R_A value is estimated in cat spinal motoneurones (Clements and Redman 1989).

Measurement of time constant (τ) is relatively easy. There are many ways to do it, including the graphic peeling, nonlinear regression, transform method, and optimization method (see Rall et al., 1992 for review). As a practical matter, a measurement of time constant is made from transient records using the graphic peeling. In general, a decay of membrane potential following a transient perturbation induced by a current step can be described by a sum of exponential decays: $V = \sum_{k=0}^{\infty} C_k e^{-t/\tau_k}$, where coefficients C_k are constants and τ_k are equalizing time constants satisfying $\tau_k > \tau_{k+1} (k = 0,1,2,...)$. τ_0 is the slowest time constant which can be peeled from the faster decaying portion of the transient using semilogarithmic plotting if the values of t is sufficient large that faster decaying terms of $\sum_{k=0}^{\infty} C_k e^{-t/\tau_k}$ are negligibly small compared with τ_0. The same method can be used to peel τ_1 from the peeled V (Rall 1969).

The values of equalizing time constants are dependent on the electrotonic length (L) of the cylinder or neurone. For a cylinder with both ends sealed, the values of the equalizing time constants are given by $\tau_k = \tau_0/(1+(k\pi/L)^2)$, where, k=1,2, ... (Rall 1969). Based on this equation and the above estimation of τ_0 and τ_1 the electrotonic length (L)

can be estimated by $L=\pi(\tau_0/\tau_1-1)^{1/2}$. The peeling method applied to many neuron types has showed that L ranges between 0.3-2λ (λ is space constant), suggesting that dendrites are electrically rather compact from the viewpoint of soma.

Motoneurone behaviour modified by changes in membrane properties during fictive locomotion.

As mentioned in the general introduction of this thesis, motoneurones display changes in excitability during fictive locomotion. These changes include a reduction of input resistance; a reduction of AHP; hyperpolarization of voltage threshold, changes in f-I relation; and voltage-dependent excitation. The changes in motoneuronal excitability are important in modifying the motoneurone behaviour during locomotion.

Reduction of AHP. In general, the repetitive firing behaviour of motoneurones could be regulated by modulation of AHP. A reduction of AHP results in an increase in firing frequency or increase in slope of the motoneurone firing frequency/current (F/I) relation. But this seems not true during fictive locomotion. The lack of relationship between the frequency of firing and the current injected during fictive locomotion suggested that the AHP might not be involved in the regulation repetitive firing (Brownstone et al., 1992). Brownstone showed that the motoneurone did not fire repetitively in response to the net excitatory synaptic current during fictive locomotion. This result suggests that the capacity of the nervous system to alter the responsiveness of its motoneurones to synaptic currents could provide it with the ability to exercise a high degree of control over its motor output.

Hyperpolarization of Vth. Simulation results in Section I show that Vth hyperpolarization is always accompanied by a reduction of rheobase current. This result is consistent with experimental observations that in many cases less current was required to inject into the motoneurones to evoke repetitive firing during fictive locomotion. Both simulation and experiment results suggest that the Vth hyperpolarization along with a reduction of rheobase current would enhance the motoneuronal excitability and tend to counter the decrease in excitability resulted from the reduction of input resistance. Furthermore, as predicted in Section III, this enhanced excitability would facilitate the recruitment of motoneurones since less depolarization from either central or reflex pathways would be required to recruit motoneurones (Krawitz et al., 2001). Our recent modeling studies show that modulation of the IS sodium conductance (either shifting the voltage dependency to the left or increasing the maximum conductance), which hyperpolarized the Vth, could reduce the slope of the F/I curve and shift the F/I curve to the left. Therefore, the reduction of slope of the F/I curve observed during fictive locomotion (Brownstone et al., 1992; Fedirchuk et al., 1998) could partly result from the hyperpolarization of Vth. The increased neuronal excitability via voltage threshold hyperpolarization is thought to synchronize synaptic inputs leading to rapid rates of depolarization in cortical neurones (Azouz and Gray, 2000). Similarly, hyperpolarization of voltage threshold in motoneurones could be also considered a quick facilitation of control from descending system to motoneurones and an effective enhancement of motor system output without increasing driving force for walking.

Voltage-dependent excitation. Brownstone et al (1994) suggested that the voltage dependent excitation of motoneurones during fictive locomotion could result from

activation of the L-type calcium channels and/or the NMDA channels that produce the plateau potentials. This prediction was supported by our recent computer simulation (Dai et al., 2000). The voltage dependent excitation makes a major contribution to the output (repetitive firing) of the motoneurones and makes the motoneurones proceeding from a state of quiescence to one of firing repetitively with a rate sufficient to cause appropriate muscle contraction (Brownstone et al., 1994). The plateau potential provides an important amplification mechanism: the enhancement of the response to brief synaptic inputs both in intensity and duration. The efficacy of different synaptic inputs converging onto the motoneurone pool might be changed as a consequence of motoneurone properties (Kiehn 1991). A recent study by Bennett el al (1998) showed that the threshold for activation of plateau potential in cat spinal motoneurones could be lowered by synaptic excitation evoked by stretching the muscle or stimulating the nerves and that the plateau potentials with the low-threshold activation would be important in securing an effective recruitment to frequencies that produce significant force generation. In general, the voltage dependent excitation of the motoneurones observed during fictive locomotion could enhance the motoneuronal excitability and make the motoneurones directly recruited to higher, more efficient firing frequencies.

Reduction of input resistance. In contrast to the reduction of AHP, the hyperpolarization of Vth, and the voltage dependent excitation of motoneurones, reduction of input resistance reduced the motoneuronal excitability. The function of this change in motoneuronal excitability during locomotion is unknown. Our recent modeling studies show that reducing the input resistant could shift the F/I curve to the right and reduce the slope of the F/I curve. Therefore, the reduction of F/I slope observed during fictive

locomotion could be partly due to the reduction of input resistance, which might balance the increased excitability of the motoneurones and make the motoneurones more tolerant to the synaptic inputs and more controllable to the motor system during locomotion.

The above changes in membrane properties of motoneurones observed during fictive locomotion suggest that although the output of spinal motor system is regulated by the central pattern generator and modulated by descending and afferent inputs, motoneurones might use their active membrane properties to participate in shaping and timing the final motor output.

Physiological basis of sodium conductance modulation

Simulation results suggest that modulation of sodium channels in initial segment, through either shifting the voltage-dependent activation of the channels in the hyperpolarizing direction or increasing the maximum conductance of the channels, could be a possible mechanism underlying the hyperpolarization of voltage threshold during fictive locomotion. Now a question arises: what might be the physiological basis for the above modulations of sodium conductance ?

It is well known that sodium channels are composed of a α subunit of 260 kDa and two auxiliary subunits $\beta 1$ of 36 kDa and $\beta 2$ of 33 kDa (see Catterall, 1992 and Cestèle, 1998 for reviews). The α subunit is composed of four repeat domains. Each of the domains has six transmembrane segments (S1-S6) and one membrane reentrant segment. The voltage sensors are located in the S4 segment that contains 4~8 positively charged residues. Under the influence of an electric field the charged residues can move outward to initiate the voltage-dependent activation of sodium channels. The inactivation of sodium channels is mediated by the intracellular loop connecting domains III and IV.

The sites of cAMP-dependent phosphorylation are located in the intracellular loop connecting domains I and II.

Shifting the voltage-dependent activation of sodium channels to the hyperpolarizing direction suggests that the voltage sensors of sodium channels may become more sensitive to electric field during locomotion. Therefore, the sodium channels would be able to open at a lower membrane potential and this increase in the subthreshold sodium current would give rise to a hyperpolarization of voltage threshold for action potential generation. Evidences of shifting voltage dependency of sodium channels have been previously reported (e.g. Cestèle et al., 1998; Purkerson et al., 1999; Astman et al., 1998).

On the other hand, the sodium conductance may not be completely (100%) available for activation at rest; a certain percentage of the channels would keep inactivated in normal state of firing. Therefore, increasing the maximum conductance of the sodium channels suggests that during fictive locomotion some unknown factors may cause an increased availability of the sodium channels for activation thus increases the sodium peak current and produces the hyperpolarization of voltage threshold.

5-HT modulation of motoneuronal excitability

Hyperpolarization of voltage threshold is one of the changes in motoneuronal excitability observed during fictive locomotion. Mechanisms underlying these changes in membrane property are still unknown. In general, motoneurone excitability can be influenced by many factors including (a) anatomic structure (size of the neurone); (b) afferent and segmental inputs; (c) intrinsic properties; and (d) neuronal modulators. As

mentioned at the beginning of this thesis (General Introduction), the anatomic structure and afferent input are not likely the reasons that cause the hyperpolarization of voltage threshold during fictive locomotion because this phenomenon is observed regardless of motoneurone type and in the absence of afferent inputs. Therefore, as the computer models predicted, the most plausible mechanism would be transmitter modulation of motoneuronal excitability.

Many neurotransmitters have effects on motoneurone excitability. These transmitters include serotonin, glutamate, γ-Aminobutyric acid (GABA), glycine, norepinephrine & epinephrine, dopamine, acetylcholine (Ach), adenosine triphosphate (ATP), adenosine, thyrotropin-releasing hormone (TRH), neurokinins, arginine vasopressin & oxytocin, and other neuropeptides. Transmitter actions at ionotropic receptors usually induce or reduce the localized membrane currents while actions at metabotropic receptors initiate second messenger cascades that have various effects including altering channel or receptor function (Rekling et al, 2000).

5-HT is a well known neuromodulator of spinal motoneurones. The 5-HT neurons originate in the medullary raphe nuclei and the reticular formation. The distribution of 5-HT and NE in the spinal cord of the rat, rabbit, and cat is similar for both amines, with highest levels found in the lateral and ventral horns. The 5-HT content is 2 to 5 times as great as the amount of NE in each area.

Although there is no experimental support of 5-HT modulation of fast sodium conductance in mammalian motoneurones, studies (Azmitia, et al., 1996; Kheck et. al., 1995) have shown that 5-HT_{1A} receptors are densely located in axon hillock, diffusely in soma, and absently in dendrite, suggesting that 5-HT signaling may have effect on action

potential generation via 5-HT_{1A} receptor. A study (Hsiao et al., 1998) of serotonin-induced bistable membrane behaviours in guinea pig trigeminal motoneurones (TMNs) suggests that 5-HT enhances the bistable membrane behaviours in TMNs that are mediated by L-type Ca^{2+} and persistent Na^{+} currents. A recent study (Hochman & Schmidt, 1998) in the *in vitro* neonatal rat spinal cord shows that motoneurones display a hyperpolarization of Vth and an increase of action potential width after bath application of 5-HT and NMDA during repetitive firing evoked by step currents (see Fig. 2, Hochman & Schmidt 1998). Release of 5-HT has been also detected during locomotion in the neonatal rat brainstem-spinal cord preparation (Fyda et al., 1999; Gerin and Privat, 1998; Schmidt and Jordan, 2000). In general, the dominant effect of the serotonergic raphe system on the enhancement of spinal and cranial motoneurone excitability is mediated by activation of I_h, reduction of specific potassium conductances, uncovering of L-type Ca^{2+} currents, reduction of spike AHP amplitudes, and an increase in membrane input resistance (Rekling et al., 2000). The effect of 5-HT on spike initiation remains to be tested. The following table lists the 5-HT modulation of some ionic conductances in mammalian motoneurones.

Effect of 5-HT on ionic conductances in mammalian motoneurones.

Conductance	Motoneurone	Animal	Receptor	Effect	Reference
g_{NaP}	Spinal Phrenic Hypoglossal Facial Trigeminal	Guinea Pig	5-HT	+	84
g_{K_leck}	Spinal Phrenic Hypoglossal Facial	Rat	5-HT_2	-	101,102,103,134
	Trigeminal	Guinea Pig	5-HT_2	-	83,84
$g_h/g_{IR}/g_{exc}$	Spinal	Neonatal rat	5-HT_{1A}, 5-HT_2	+	157
		Cat	5-HT	+	172
	Phrenic Hypoglossal	Neonatal rat	5-HT_{1C}, 5-HT_2	+	106
	Facial	Adult & neonatal rat	5-HT, 5-HT_2	+	101,102, 103,104 134,166,167
	Trigeminal	Guinea Pig	5-HT_2	+	83, 84
g_{Ca_HVA}	Spinal Phrenic				
N- & P-type	Hypoglossal Facial	Neonatal rat	5-HT_{1A}	-	14
L-type	Trigeminal	Guinea Pig	5-HT	+	84
g_{Ca_LHA}	Spinal Phrenic Hypoglossal Facial Trigeminal	Neonatal rat	5-HT	+	16

g_{NaP}: persistent sodium conductance; g_{K_leak}: leak (potassium) conductance; g_h: h-current conductance; g_{IR}: inward rectifier conductance; g_{exc}: an excitatory conductance induced by 5-HT, activation of this conductance depolarizes motoneurones. It could be produced by g_h, g_{IR} or reduction of the g_{K_leck} or some other unknown conductances; g_{Ca_HVA}: high voltage activated calcium conductance; g_{Ca_LHA}: low voltage activated calcium conductance; +: enhance; -: reduce.

General conclusions

The above studies suggest three points:

(1) Voltage threshold can be hyperpolarized by fluctuations of membrane potential. However, this change in voltage threshold due to a quick activation of fast sodium conductance is limited to the first spike in the spike train and is fluctuation-phase dependent. Therefore it is not related to the voltage threshold hyperpolarization observed during fictive locomotion, which is locomotion state dependent (Krawitz et al., 2000).

(2) A state-dependent hyperpolarization of voltage threshold could be produced by increasing sodium conductance or/and decreasing delayed rectifier potassium conductance in the initial segment. Increasing the initial segment sodium conductance can hyperpolarize the voltage threshold by an amount comparable to the experimental observations. Therefore, modulation of sodium conductance in the initial segment could be a major mechanism underlying the voltage threshold hyperpolarization during fictive locomotion.

(3) Hyperpolarization of voltage threshold could increase the output of motoneurone pools mainly through increasing the number of recruited motoneurones.

Improvements for future modeling

The single cell model used in this thesis was not a perfect model. The simplification of the dendrites ignored electrotonic properties of the branching and termination of the dendrites. The slope of secondary range of the f-I curve and the width of an action potential generated by the model were larger than those reported for real

References

1. Araki, T., and Terzuolo, C.A. (1962). Membrane currents in spinal motoneurones associated with the action potential and synaptic activity. *J Neurophysiol*, 25:772-789.

2. Astman, N., Gutnick, M.J., and Fleidervish., I. A.(1998). Activation of protein kinase C increases neuronal excitability by regulating persistent Na^+ current in mouse neocortical slices. *J Neurophysiology* 80: 1547-1551.

3. Avery, R.B. and Johnston, D. (1996). Multiple channel types contribute to the low voltage-activated calcium current in hippocampal CA3 pyramidal neurons. *J Neurosci.* 16:5567-82.

4. Azmitia, E., Gannon, E.P., Kheck, N., and Whitaker-Azmitia, P. (1996). Cellular localization of the 5-HT_{1A} receptor in primate brain neurons and glial cells. *Neuropsychopharmacology* 14:35-46.

5. Azouz, A., and Gray, C.M. (2000) Dynamic spike threshold reveals a mechanism for synaptic coincidence detection in cortical neurons in vivo. *Proc. Natl. Acad. Sci.* 97:8110-8115.

6. Baldissera, F., and Gustafsson, B. (1974a). afterhyperpolarization time course in lumbar motoneurones of the cat. *Acta Physiol. Scand.* 91:512-527.

7. Baldissera, F., and Gustafsson, B. (1974b). Firing behavior of a neuron model based on the afterhyperpolarization conductance time-course. First interval firing. *Acta Physiol. Scand.* 91:528-544.

8. Baldissera, F., and Gustafsson, B. (1974c). Firing behavior of a neuron model based on the afterhyperpolarization conductance time-course and algebraical summation. Adaptation and steady state firing. *Acta Physiol. Scand.* 92:27-47.

9. Barrett, J.N. and Crill, W.E. (1974). Influence of dendritic location and membrane prperties on the effectiveness of synapses on cat motoneurones. *J Physiol. (Lond)* 293:325-345.

10. Barrett, J.N. and Crill, W.E. (1974). Specific membrane properties of cat motoneurones. *J Physiol (Lond)* 239:301-324.

11. Barrett, E.F., Barrett, J.N., and Crill, W.E. (1980). Voltage-sensitive outward currents in cat motoneurones. *J. Physiol.* 304: 251-276.

12. Barrett, J.N. and Crill, W.E. (1980). Voltage clamp of cat motoneurone somata: properties of the fast inward current. *J. Physiol.* 304:231-249.

13. Bashor, D.P. (1998) A large-scale model of some spinal reflex circuits. *Biol. Cybern. 78, 147-157*

14. Bayliss, D.A., Umemiya, M., and Berger, A.J. (1995). Inhibition of N- and P-type calcium currents and the after-hyperpolarization in rat motoneurones by serotonin. *J Physiol (Lond)* 485:635-47.

15. Bennett, David J., Han Hultborn, Brent Fedirchuk, and Monica Gorassini (1998). Synaptic activation of plateaus in hindlimb motoneurones of decerebrate cats. *J. Neurophysiol.* 80: 2023-2037

16. Berger, A.J., and Takahashi, T. (1990). Serotonin enhances a low-voltage-activated calcium current in rat spinal motoneurons. *J Neurosci* 10:1922-8.

17. Bernstein, J. (1902). Untersuchungen zur thermodynamik der bioclektrischen ströme. *Pflügers Arch. Ges. Physiol.* 92:521-562.

18. Binder, M., Heckman, C.J., and Powers, R. (1996). The physiological control of motoneurone activity. In Handbook of Physiology. Section 12: Regulation and Integration of Multiple System. Rowell, L.B. and Shepherd, J.T. (eds). *American Physiology Society*, New York: Oxford, pp. 3-53.

19. Booth, V., Rinzel, J., and Keihn, O. (1997). Compartmental Model of vertebrate motoneurones for Ca^{2+}-dependent spiking and plateau potentials under pharmacological treatment. *J Neurophysiol* 78:3371-3385.

20. Bower, J.M. and Beeman, D. (1998). *The Book of GENESIS*, 2nd edition, Springer-Verlag New York.

21. Brock, L.G., Coombs, J.S., and Eccles, J.C. (1952). The recording of potential from motoneurones with an intracellular electrode. *J Physiol (Lond)* 117:431-460.

22. Brownstone, R.M., Gossard, J. P., and Hultborn, H. (1994). Voltage-dependent excitation of motoneurones from spinal locomotor centres in the cat. *Exp Brain Res* 102: 34-44

23. Brownstone, R.M., Jordan, L.M., Kriellaars, D.J., Noga, B.R., and Shefchyk, S.J. (1992). On the regulation of repetitive firing in lumbar motoneurones during fictive locomotion in the cat. *Exp Brain Res* 90:441-455.

24. Burke, R.E. (1981). Motor units: anatomy, physiology, and functional organization. In *Handbook of Physiology*, Sec. 1: *The Nervous System*, Vol. 2: *Motor Control*, Part 1 (V.B. Brooks, ed.) Bethesda, MD: American Physiological Society, pp 345-422.

25. Burke, R.E., Levine, D.N., Salcman, M., and Tsairis, P. (1974) Motor units in cat soleus muscle: Physiological, histochemical and morphological characteristics. *J. Physiol.* 238:503-514.

26. Cantrell, A.R., and Catterall, W.A. (2001). Neuromodulation of Na^+ channels: An unexpected form of cellular plasticity. *Nature Reviews (Neuroscience).* 2: 397-406.

27. Cantrell, A.R., Ma, J.Y., Scheuer, T., and Catterall, W.A. (1996). Muscarinic modulation of sodium current by activation of protein kinase C in rat hippocampal neurons. *Neuron* 16:1019-1026.

28. Cantrell, A.R., Scheuer, T., and Catterall, W.A. (1999). Voltage-dependent neuromodulation of Na^+ channels by D1-like dopamine receptors in rat hippocampal neurons. *J Neuroscience* 19 (13): 5301-5310.

29. Cantrell, A.R., Smith, R.D., Goldin, A.L., Scheuer, T., and Catterall, W.A. (1997). Dopaminergic modulation of sodium current in hippocampal neurons via cAMP-dependent phosphorylation of specific sites in the sodium channel α subunit. *J Neuroscience* 17(19):7330-7338.

30. Carlin, P.L. McCrea, D.A., and Durand, D. (1984) Dendrites and motoneuronal integration. In *Handbook of the Spinal Cord*, edited by R.A. Davidoff. Marcel Derker, Inc. Vol 2&3: pp. 243-267

31. Catterall, W.A. (1981). Localization of sodium channels in cultured neural cells. *J Neurosci* 1:777-783.

32. Catterall, W.A. (1992). Cellular and molecular biology of voltage-gated sodium channels. *Physiol. Rev.* 72, S15-S48.

33. Cestèle, S., Qu, Y., Rogers, J.C., Rochat, H., Scheuer, T. and Catterall, W. A. (1998). Voltage sensor-trapping: enhanced activation of sodium channels by b-scorpion toxin bound to the S3-S4 loop in domain II. *Neuron* Vol. 21, 919-931.

34. Chandler, S.H., Hsaio, C., Inoue, T., and Goldberg, L.J. (1994). Electrophysiological properties of guinea pig trigeminal motoneurones recorded in Vitro. *J Neurophysiol.* 71:129-145.

35. Clements, J.D. and Redman, S.J. (1989). Cable properties of cat spinal motoneurones measured by combining voltage clamp, current clamp and intracellular staining. *J Physiol (Lond)* 409:63-87.

36. Conradi, S. (1969). Observations on the ultrastructure of the axon hillock and initial axon segment of lumbosacral motoneurones in the cat. *Acta Physiol Scand suppl* 332:65-84.

37. Coombs, J.S., Curtis, D.R. and Eccles, J.C. (1957). The interpretation of spike potentials of motoneurones. *J Physiol (Lond)* 139:198-231.

38. Coombs, J.S., Curtis, D.R. and Eccles, J.C. (1957b). The generation of impulses in motoneurones. *J Physiol (Lond)* 139:232-249.

39. Cope, T.M. and Cleark, B.D. (1991). Motor-unit recruitment in the decerebrate cat: several unit prperties are equally good predictors of order. *J. Neurophysiol.* 66:1127-1138.

40. Crill, W.E., (1996). Persistent sodium current in mammalian central neurons. *Annu. Rev. Physiol.* 58:349-362.

41. Cullheim, S., Fleshman, J.W., Glenn, L.L., and Burke, R.E. (1987). Membrane area and dendritic structure in type-identified triceps surae alpha-motoneurones. *J Comp Neurol* 255:68-81.

42. Dai, Y., Jones, K.E., Fedirchuk, B., Krawitz, S., and Jordan, L.M. (1998a). Modeling the lowering of motoneurone Voltage threshold during fictive locomotion. In Neuronal Mechanisms for Generating Locomotor Activity. Kiehn O., Harris-Warrick R.M., Jordan L.M., Hultborn H. and Kudo N (Eds), pp 492-495. *Annals of the New York Academy of Sciences*, New York.

43. Dai, Y., Jones, K.E., Fedirchuk, B., and Jordan, L.M. (1998b). Computer simulation: A study of excitability of the cat lumbar motoneurones during fictive locomotion. *Society for Neuroscience Abstracts* 24:427.11.

44. Dai, Y., Bashor, D.P., Fedirchuk, B., and Jordan, L.M. (1999) Motoneuron threshold hyperpolarization: alteration of population output predicted by a large scale simulation. *Society for Neuroscience Abstracts* 25, 664.10.

45. Dai, Y., Jones, K.E., Fedirchuk, B., and Jordan, L.M. (2000). Effects of voltage trajectory on action potential voltage threshold in simulations of cat spinal motoneurones. *Neurocomputing*, Vol. 23-33: pp. 105-111.

46. Dai, Y., Jones, K.E., Fedirchuk, B., McCrea, D.A., and Jordan, L.M. (2001). A modeling study of locomotion induced hyperpolarization of voltage threshold in cat lumbar motoneurones. *J Physiology (Lond)*, to be submitted in Feb, 2001.

47. Dodge, F.A.J., and Cooley, J.W. (1973). Action potential of the motorneuron. *IBM Journal of Research and Development* 17:219-229.

48. Eccle, J.C. (1957b) Duration of AHP of motoneuron supplying fast and slow muscle. *Nature*, Vol. 179. pp 866-868

49. Eccles, J.C. (1957a). The physiology of nerve cells. The Johns Hopkins Press, Baltimore, Maryland.

50. Fedirchuk, B., McCrea, D.A., Dai, Y., Jones, K.E., and Jordan, L.M. (1998). Motoneurone frequency/current relationships during fictive locomotion in the cat. *Society for Neuroscience Abstracts* 24:652.15.

51. ffrench-Mullen, J.M., Plata-Salaman, C.R., Buckley, N.J. and Danks, P. (1994). Muscarine modulation by a G-protein alpha-subunit of delayed rectifier K^+ current in rat ventromedial hypothalamic neurons. *J Physiol (Lond)* 474:21-26.

52. Fleshman, J.W., Munson, J.B., Sypert, G.W. and Friedman, W.A. (1981). Rheobase, input resistance and motor-unit type in medial gastrocnemius motoneurones of the cat. *J Neurophysiol* 46:1326-1338.

53. Fleshman, J.W., Segev, I. and Burke, R.E. (1988). Electrotonic architecture of type-identified alpha-motoneurones in the cat spinal cord. *J Neurophysiol* 60:60-85.

54. Frankenhaeuser, B., and A.F. Huxley (1964). The action potential in the myelinated nerve fibre of Xenopus laevis as computed on the basis of voltage clamp data. *J Physiol. (Lond.)* 191:302-315.

55. Fuortes, M.G.F., Frank, K., and Becker, M.C. (1957). Steps in the production of motoneurone spikes. *J. Gen. Physiol. 40:735-752.*

56. Fyda, D.M., Vriend, J. and Jordan, L.M. (1999). Brainstem-evoked locomotion in the isolated neonatal rat brainstem-spinal cord preparation is associated with monoamine

release and requires region-specific activation of 5-HT7 and 5-HT2 receptors. *J Neuroscience*, submitted in Sept.

57. Gerin, C., Becquet, D. and Privat, A. (1995). Direct evidence for the link between monoaminergic descending pathways and motor activity. I. A study with microdialysis probes implanted in the ventral funiculus of the spinal cord. *Brain Res* 704:191-201.

58. Gerin, C. and Privat, A. (1998). Direct evidence for the link between monoaminergic descending pathways and motor activity: II. A study with microdialysis probes implanted in the ventral horn of the spinal cord. *Brain Res.* 794:169-173

59. Gold, M.S., Reichling, D.B., Shuster, M.J., and Levine, J.D. (1996). Hyperalgesic agents increase a tetrodotoxin-resistant Na^+ current on nociceptors. *Proc Natl Acad Sci USA* 93:1108-1112.

60. Gustafsson, B. (1984). Afterpotentials in transduction properties in different types of central neurones. *Arch Ital Biol* 122:17-30.

61. Gustafsson, B. and Pinter, M.J. (1984a). Relations among passive electrical properties of lumbar alpha-motoneurones of the cat. *J Physiol (Lond)* 356:401-431

62. Gustafsson, B. and Pinter, M.J. (1984b). An investigation of threhsold properties among cat spinal alpha-motoneurones. *J Physiol (Lond)* 357:453-483.

63. Halter, J.A., Carp, J.S., and Wolpaw, J.R. (1995). Operantly conditioned motoneurone plasticity: possible role of sodium channels. *J. Neurophysiol.* 73: 867-871.

64. Harris-Warrick, R.M., Johnson, B.R., Peck, J.H., Kloppenburg, P., Ayali, A. and Skarbinski, J. (1998). Distributed effects of dopamine modulation in the crustacean

pyloric network. In Neuronal Mechanisms for Generating Locomotor Activity. Kiehn O., Harris-Warrick R.M., Jordan L.M., Hultborn H. and Kudo N (Eds) pp 155-167. *Annals of the New York Academy of Sciences*, New York.

65. Heckman, C.J. (1994). Computer simulations of the effects of different synaptic input system on the steady-state input-output structure of motoneuron pool. *J. Neurophysiol.* 71:1717-1739.

66. Heckman, C.J. and Binder, M.D. (1991) Computer simulation of the steady-state input-output function of cat medial gastrocnemius motoneuron pool. *J. Neurophysiol.* 65:925-967.

67. Heckman, C.J. and Binder, M.D. (1993a). Computer simulation of motoneurone firing rate modulation. *J. Neurophysiol.* 69:1005-1008.

68. Heckman, C.J. and Binder, M.D. (1993b). Computer simulations of the effects of different synaptic input systems on motor unit recruitment. *J. Neurophysiol.* 70:1827-1840.

69. Heckman, C.J., and Binder, M.D. (1990). Neural mechanisms underlying the orderly recruitment of motoneurones. In: *The Segmental Motor System*, edited by M.D. Binder and L.M. Mendell. New York. Oxford University Press. P. 182-204.

70. Heckman, C.J., and Binder, M.D. (1993). Computer simulations of the effects of difference synaptic input systems on motor unit recruitment. *J. Neurophysiol.* 70:1827-1840.

71. Henneman, E., Somjen, G., and Carpenter, D.O. (1965). Functional significance of size in spinal motoneurones. *J. Neurophysiol.* 28:560-580.

72. Hevers, W. and Hardie, R.C. (1995). Serotonin modulates the voltage dependence of delayed rectifier and *Shaker* potassium channels in drosophila photoreceptors. *Neuron* Vol. 14, 845-856.

73. Hill, A.V. (1910) A new mathematical treatment of changes of ionic concentration in muscle and nerve under action of electric currents, with a theory as to their mode of excitation. *J. Physiol.* 40:190-324.

74. Hille, B. (1992). Ionic channels of excitable membranes (2^{nd} edition) Sinauer Associates Inc. Sunderland, Massachusetts.

75. Hochman, S. and McCrea, D.A. (1994a). Effects of chronic spinalization on ankle extensor motoneurones. I. Composite monosynaptic Ia EPSPs in four motoneuron pools. *J. Neurophysiol.* 71: 1452-1466.

76. Hochman, S. and McCrea, D.A. (1994b). Effects of chronic spinalization on ankle extensor motoneurones. II. Motoneurone electrical properties. *J. Neurophysiol.* 71: 1468-1479.

77. Hochman, S. and McCrea, D.A. (1994c). Effects of chronic spinalization on ankle extensor motoneurones. III. Composite Ia EPSPs in Motoneurones separated into motor unit types. *J. Neurophysiol.* 71: 1480-1490.

78. Hochman, S. and Schmidt, B.J. (1998). Whole cell recording of lumbar motoneurones during locomotor-like activity in the in vitro neonatal rat spinal cord. *J Neurophysiol.* 79:743-752.

79. Hodgkin, A.L. and Huxley, A.F. (1952a). Currents carried by sodium and potassium ions in the giant axon of Loligo. *J. Physiol. (Lond.)* 116:449-472.

80. Hodgkin, A.L. and Huxley, A.F. (1952b). The components of membrane conductance in the giant axon of Loligo. *J. Physiol. (Lond.)* 116:473-496.

81. Hodgkin, A.L. and Huxley, A.F. (1952c). The dual effect of membrane potential on sodium conductance in the giant axon of Loligo. *J. Physiol. (Lond.)* 116:497-506.

82. Hodgkin, A.L. and Huxley, A.F. (1952d). A quantitative description of membrane currents and its application to conduction and excitation in nerve. *J. Physiol. (Lond.)* 117:500-544.

83. Hsiao, C. F., Trueblood, P. R., Levine, M. S., and Chandler, S. H. (1997). Multiple Effects of Serotonin on Membrane Properties of Trigeminal Motoneurons In Vitro. *J. Neurophysiol.* 77:2910-2924.

84. Hsiao, C.F.; Negro, C.A.D., Peggy R. Trueblood, P.R., and Chandler, S.H. (1998). Ionic Basis for Serotonin-Induced Bistable Membrane Properties in Guinea Pig Trigeminal Motoneurons. *J. Neurophysiol.* 7:2847-2856.

85. Hultborn, H. and Kiehn, O. (1992). Neuromodulation of vertebrate motorneuron membrane properties. *Curr Opin Neurobiol* 2:770-775.

86. Jahnsen, H., and Llinás, R. (1984a). Ionic basis for the electroresponsiveness and oscillatory properties of guinea-pig neurons in vitro. *J Physiol (Lond)* 349:227-247.

87. Jahnsen, H., and Llinás, R. (1984b). Electrophysiological properties of guinea-pig thalamic neurons: An in vitro study. *J Physiol (Lond)* 349:205-226.

88. Jordan, L.M. (1983) Factors determining motoneuron rhythmicity during fictive locomotion. In *Neural origin of rhythmic movements.* A Roberts and B. Roberts eds. Society for Experimental Biology Symposium. 37, 423-444.

89. Kernell, D. (1965). High-frequency repetitive firing of at lumbosacral motoneurones stimulated by long-lasting injected currents. *Acta Physiol Scand* 65:74-86.

90. Kernell, D. (1968). The repetitive impulse discharge of a simple neuron model compared to that of spinal motoneurones. *Brain Res.* 11:685-678.

91. Kernell, D., and H. Sjöholm (1972). Motoneurone models based on 'voltage clamp equations' for peripheral never. *Acta Physiol. Scand.* 86: 546-562.

92. Kheck, N., Gannon, P., and Azmitia, E., (1995). 5-HT_{1A} receptor localization on the axon hillock of cervical spinal motoneurones in primates. *J. Comp. Neurol.* 355:211-220.

93. Kitai, S.T., and Surmeier, D.J. (1993). Cholinergic and dopaminergic modulation of potassium conductances in neostrial neurons. *Adv Neurol* 60:40-52.

94. Kjaerulff, O., and Kiehn, O. (2001). 5-HT modulation of multiple inward rectifiers in motoneurones in intact preparations of the neonatal rat spinal cord. *J. Neurophysiol.* 85: 580, in press.

95. Krawitz, S., Fedirchuk, B., Dai, Y., Jordan, L.M. and McCrea, D.A. (1997). Locomotion hyperpolarizes the voltage threshold of cat lumbar motoneurones. *Society for Neuroscience Abstract* 23, 298.4.

96. Krawitz, S., Fedirchuk, B., Dai, Y., Jordan, L.M. and McCrea, D.A. (2001). State-dependent hyperpolarization of Voltage threshold enhances motoneurone excitability during fictive locomotion in the cat. *J Physiol (Lond), J Physiol (Lond)*, in press.

97. Krnjevic, K., Puil, E. and Werman, R. (1978). EGTA and motoneuronal after-potentials. *J Physiol* (Lond) 275:199-223.

98. Larkman, P.M. and Kelly, J.S. (1998). Characterization of 5-HT-sensitive potassium conductances in neonatal rat facial motoneurones in vitro. *J Physiol (Lond)* 508:67-81.

99. Larkman, P.M. and Kelly, J.S. (1997). Modulation of Ih by 5-HT in neonatal rat motoneurones in vitro: Mediation through a phosphorylation independent action of cAMP. *Neuropharmacology* 36:721-733.

100. Larkman, P.M., Kelly, J.S., and Takahashi, T. (1995). Adenosine 3':5'-cyclic monophosphate mediates a 5-hydroxytryptamine-induced response in neonatal ratmotoneurones. *Eur J Physiol* 430:763-769.

101. Larkman, P.M., and Kelly, J.S. (1992). Ionic mechanisms mediating 5-hydroxytryptamine- and noradrenaline-evoked depolarization of adult rat facial motoneurones. *J Physiol (Lond)* 456:473-90.

102. Larkman, P.M., and Kelly, J.S. (1997). Modulation of IH by 5-HT in neonatal rat motoneurones in vitro: mediation through a phosphorylation independent action of cAMP. *Neuropharmacology* 36:721-33.

103. Larkman, P.M., and Kelly, J.S. (1998). Characterization of 5-HT-sensitive potassium conductances in neonatal rat facial motoneurones in vitro. *J Physiol (Lond)* 508:67-81.

104. Larkman, P.M., Penington, N.J., and Kelly, J.S. (1989). Electrophysiology of adult rat facial motoneurones: the effects of serotonin (5-HT) in a novel in vitro brainstem slice. *J Neurosci Methods* 28:133-46.

105. Lee, R.H. and Heckman., C.J. (2001). Essential role of a fast persistent inward current in action potential initiation and control of rhythmic firing. *J. Neurophysiol* 85: 472-475.

106. Lindsay, A.D., and Feldman, J.L. (1993). Modulation of respiratory activity of neonatal rat phrenic motoneurones by serotonin. *J Physiol (Lond)* 461:213-33.

107. Lux, H.D., Schubert, P., and Kreutzberg, G.W. (1970). Direct matching of morphological and electrophysiological data in cat spinal motoneurones. In: *Excitatory synaptic Mechanisms*, Andersen, P. and Jansen, J.K.S. (eds.) Universitetsforlaget, Oslo, pp. 189-198.

108. Mainen, Z.F., Joerges, J., Huguenard, J.R. and Sejnowski, T.J. (1995). A model of spike initiation in neocortical pyramidal neurones. *Neurone*, 15:1427-1439.

109. Marder, E. (1998). Computational dynamics rhythmic neural circuits. *Neuroscientist* 3:295-302.

110. McLarnon, J.G. (1995). Potassium currents in motoneurones. *Prog Neurobiol* 47:513-531.

111. Miller, R.J. and Fox, A.P. (1990). Voltage sensitive calcium channels. In *Intracellular Calcium Regulation*, ed F. Bronner, New York: Wiley-Liss. pp. 97-138.

112. Moore, J.W., Stockbridge, N., and Westerfield, M. (1983). On the site of impulse initiation in a neurone. *J. Physiology* 336:301-311.

113. Murakoshi, H., Shi, G., Scannevin, R.H. and Trimmer, J.S. (1997). Phosphorylation of the Kv2.1 K^+ channel alters voltage-dependent activation. *Mol Pharmacol* 52:821-828.

114. Mynlieff, M. and Beam, K.G. (1992). Characterization of voltage-dependent calcium currents in mouse motoneurons. *J Neurophysiol.* 68: 85-92.

115. Nishimura, Y., Schwindt, P.C., and Crill, W.E. (1989). Electrical properties of facial motoneurones in brainstem slices from guinea pig. *Brain Res.* 502:127-142.

116. Ole Kiehn (1991) Plateau potentials and active integration in the 'final common pathway' for motor behaviour. TINS Vol. 14, No. 12. pp 68-73

117. Örnung, G.O., Ottersen, O., Cullheim, S., and Ulfhake, B. (1998) Distribution of glutamate-, glycine- and GABA-immunoreactive nerve terminals on dendrites in the cat spinal motor nucleus. Exp. Brain res. 118:517-532.

118. Peretz, T., Levin, G., Moran, O., Thornhill, W.B., Chikvashvili, D. and Lotan, I. (1996). Modulation by protein kinase C activation of rat brain delayed-rectifier K^+ channel expressed in Xenopus oocytes. *FEBS Lett* 381:71-76.

119. Pinter, M.J. (1990). The role of motoneuron membrane properties in the determination of recruitment order. In: *The Segmental Motor System*, edited by M.D. Binder and L.M. Mendell. New York. Oxford University Press. P. 165-181.

120. Pinter, M.J., Curtis, R.L., and Hosko, M.J. (1983). Voltage threshold and excitability among variously sized cat hindlimb motoneurones. *J Neurophysiol* 50:644-657.

121. Powers, R. (1993) A viriable-threshold motoneurone model that incorporates time- and voltage-dependent potassium and calcium conductances. J. *Neurophysiol.* 70:246-262.

122. Powers, P.K. and Binder, M.D. (1996). Experimental evaluation of input-output models of motoneuron discharge. *J Neurophysiol.*75: 367-79.

123. Purkerson, S.L., Baden, D.G., and Fieber, L.A. (1999). Brevetoxin modulates neuronal sodium channels in two cell lines derived from rat brain. *Neurotoxicology* 20(6):909-920.

124. Rall, W. (1959) Branching dendritic trees and motoneurone membrane resistivity. *Exp. Neurol.* 2:503-532.

125. Rall, W. (1962a) Theory of physiological properties of dendrites. *Ann. N.Y. Acad. Sci.* 96:1071-1092.

126. Rall, W. (1962b) Electrophysiology of a dendritic neuron model. *Biophys. J.* 2(2): 145-167.

127. Rall, W. (1977). Core conductor theory and cable properties of neurons. In: *Handbook of Physiology – Section 1: The nervous system I*, Chapter 3 pp. 39-99. American Physiology Society, Bethesda, Maryland.

128. Rall,W. (1964) Theoretical significance of dendritic tree for input-output relation. In *Neural Theory and Modeling*, Reiss, R. ed., pp. 73-97, Stanford University Press.

129. Rall, W. (1969) Time constants and electrotonic length of membrane cylinders and neurons. *Biophys. J.* 9:1483-1508

130. Rall, W. (1989). Cable theory for dendritic neurones. In *Methods in Neuronal Modeling*. C. Koch and I. Segev (Eds.), The MIT Press, pp. 7-62

131. Rall, W., R.E. Burke, W.R. Holmes, J.J.B. Jack, S.J. Redman, and I. Segev (1992) Matching dendritic neuron models to experimental data. *Physiological Reviews* 72: S159-S186

132. Ramón, F., Moore, J.W., Joyner, R.W. and Westerfield, M. (1976). Squid giant axons: a model for the neuron soma? *Biophys J* 16:953-963.

133. Rashevsky, N. (1931) On he theory of nervous conduction. *J. Gen. Physiol.* 14:517-528.

134. Rasmussen, K., and Aghajanian, G.K. (1990). Serotonin excitation of facial motoneurons: receptor subtype characterization. *Synapse* 5:324-32.

135. Redman, S.J. (1976) A quantitative approach to integrative function of dendrites. In *Neurophysiology II*, vol. 10., R. Porter (Ed.), University Park Press, Baltimore, pp. 17-35.

136. Rekling, J.C., Funk, G.D., Bayliss, D.A., Dong, X.W., and Feldman J.L. (2000) Synaptic control of motoneuronal excitability. *Physiology Reviews* 80:767-852.

137. Risk, A., and Bawa, P. (1992). Recruitment of motor units in human forearm extensors. *J. Neurophysiol.* 68:100-108.

138. Safronov, B.V., Wolff, M. and Vogel, W. (2000). Excitability of the soma in central nervous system neurones. *Biophysical Journal* 78 (6) 2990-3010.

139. Safronov, B.V. (1999). Spatial distribution of Na^+ and K^+ channels in spinal dorsal horn neurones: role of the soma, axon and dendrites in spike generation. *Prog Neurobiol* 59:217-241.

140. Safronov, B.V., Wolff, M. and Vogel, W. (1997). Functional distribution of three types of Na^+ channel on soma and processes of dorsal horn neurons of rat spinal cord. *J Physiol* 503:371-385.

141. Safronov, B.V. and Vogel, W. (1995). Single voltage-activated Na^+ and K^+ channels in the somata of rat motoneurones. *J Physiol* 487:91-106.

142. Sah, P. (1996). Ca^{2+}-activated K^+ currents in neurons: types, physiological roles and modulation. *Trends Neurosci* 19:150-154.

143. Schiffmann, S.N., Desdouits, F., Menu, R., Greengard, P., Vincent, J.D., Vanderhaeghen, J.J. and Girault, J.A. (1998). Modulation of the voltage-gated sodium current in rat striatal neurons by DARPP-32, an inhibitor of protein phosphatase. *Eur J Neurosci* 10:1312-1320.

144. Schmidt, B.J. (1994). Afterhyperpolarization modulation in lumbar motoneurones during locomotor-like rhythmic activity in the neonatal rat spinal cord in vitro. *Exp Brain Res* 99:214-222.

145. Schmidt, B.J. and Jordan, L.M. (2000). The role of serotonin in reflex modulation and locomotor rhythm production in the mammalian spinal cord. *Brain Research Bulletin.* 53:689-710.

146. Schwindt, P.C. (1973) Membrane-potential trajectories underlying motoneurone rhythmic firing at high rates. *J. Neurophysiol.* 36:434-439.

147. Schwindt, P.C. and Calvin, W.H. (1972) Membrane potential trajectories between spikes underlying motoneurone rhythmic firing. *J. Neurophysiol.* 35:311-325.

148. Schwindt, P.C. and Crill, W.E. (1982) Factors influencing motoneurone rhythmic firing: results from a voltage-clamp study. *J. Neurophysiol.* 48:875-890.

149. Schwindt, P.C., and Crill, W.E. (1980). Properties of a persistent inward current in normal and TEA-injected motoneurons. *J Neurophysiol* 43:1700-24.

150. Schwindt, P.C., and Calvin, W.H. (1972). Membrane-potential trajectories between spikes underlying motoneurone firing rates. *J Neurophysiol* 35:311-325.

151. Schwindt, P.C., and Calvin, W.H. (1973a). Equivalence of synaptic and injected current in determining the membrane potential trajectory during motoneuron rhythmic firing. *Brain Res.* 59: 389-394

152. Schwindt, P.C., and Calvin, W.H. (1973b) Nature of conductances underlying rhythmic firing in cat spinal motoneurons. *J Neurophysiol* 43:1296-1318

153. Segev, I. (1992). Single neurone models: oversimple, complex and reduced. *TINS*, 15:414-421.

154. Stuart, G., Spruston, N., Sakmann, B. and Häusser, M. (1997). Action potential initiation and back propagation in neurones of the mammalian CNS. *Trends Neurosci*, 20:125-131.

155. Takahashi, T. (1990a). Inward rectification in neonatal rat spinal motoneurones. *J Physiol (Lond)* 1990 423:47-62.

156. Takahashi, T. (1990b) Membrane currents in visually identified motoneurones of neonatal rat spinal cord. *J Physiol (Lond)* 423:27-46.

157. Takahashi, T., and Berger, A.J. (1990). Direct excitation of rat spinal motoneurones by serotonin. *J Physiol (Lond)* 423:63-76.

129. Tegner, J., Hellgren-Kotaleski, J., Lansner, A., and Grillner, S. (1997). Low voltage-activated calcium channels in the Lamprey locomotor network: simulation and experiment. *J. Neurophysiol.* 77:1795-1812.

158. Traub, R.D. (1977). Motoneurones of different geometry and the size principle. *Biol. Cybern.* 25:163-176.

159. Traub, R.D. and Llinas, R. (1977). The spatial distribution of ionic conductances in normal and axotomized motoneurones. *Neuroscience* 2:829-849.

160. Traub, R.D., Wong, R.K.S., Miles, R. and Michelson, H. (1991). A model of a CA3 hippocampal pyramidal neuron incorporating voltage-clamp data on intrinsic conductances. *J Neurophysiol* 66 (2): 635-650.

161. Tsien, R.W., Lipscombe, D., Madison, D.V., Bley, K.R., Fox, A. P. (1998). Multiple types of neuronal calcium channels and their selective modulation. *Trends Neurosci.* 11:431-38.

162. Ulfhake, B., and Kellerth, J. (1981). A quantitative light microscopic study of the dendrites of cat spinal alpha-motoneurones after intracellular staining with horseradish peroxidase. *J. Comp. Neuroscience* 23:917-929.

163. Umemiya, M. and Berger, A.J. (1994). Properties and function of low- and high-voltage-activated Ca^{2+} channels in hypoglossal motoneurons. *J Neurosci.* 14(9): 5652-60.

164. Van Buren, J., and Frank, K. (1965). Correlation between the morphology and potential field of spinal motor nucleus in the cat. *Electroencephalogr. Clin. Neurophysiol.* 19:112-126.

165. VanderMaelen, C.P., and Aghajanian, G.K. (1980). Intracellular studies showing modulation of facial motoneurone excitability by serotonin. *Nature* 287:346-7.

166. VanderMaelen, C.P., and Aghajanian, G.K. (1982). Serotonin-induced depolarization of rat facial motoneurons in vivo: comparison with amino acid transmitters. *Brain Res* 239:139-52.

167. Viana, F., Bayliss, D.A. and Berger, A.J. (1993a). Calcium conductances and their role in firing behaviour of neonatal rat hypoglossal motoneurones *J Neurophysiol* 69(6): 2137-2149.

168. Viana, F., Bayliss, D.A. and Berger, A.J. (1993b). Multiple potassium conductances and their role in action potential repolarization and repetitive firing behaviour of neonatal rat hypoglossal motoneurones. *J Neurophysiol* 69(6): 2150-2163.

169. Wickens, J.R., and Wilson, C.J. (1998) Regulation of action-potential firing in Spiny neurons of the rat neostriatum in vivo. *J. Neurophysiol.* 79:2358-2364.

170. Westenbroek, R.E., Hoskins, L. and Catterall, W.A. (1998). Localization of Ca^{2+} channel subtypes on rat spinal motor neurons, interneurons, and never terminals. *J Neuroscience* 18 (16): 6319-6330.

171. White, S.R., and Fung, S.J. (1989). Serotonin depolarizes cat spinal motoneurons in situ and decreases motoneuron afterhyperpolarizing potentials. *Brain Res* 502:205-13.

172. Wickens, J.R., and Wilson, C.J. (1998) Regulation of action-potential firing in Spiny neurons of the rat neostriatum in vivo. *J. Neurophysiol.* 79:2358-2364.

173. Wilson, M.A. and Bower, J.M. (1989). The simulation of large-scale neural networks. In: *Methods in Neuronal Modeling*, Christof Koch and Idan Degev (eds.) The MIT press, pp.291-333.

174. Wollner, D.A. and Catterall, WA. (1986). Localization of sodium channels in axon hillocks and initial segments of retinal ganglion cells. *Proc natl Acad Sci* USA 83:8424-8428.

175. Zengel, J.E., Steven A. Reid, Geoge W. Sypert, and John B. Munson (1985). Membrane electrical properties and prediction of motor-unit type medial gastrocnemius motoneurons in the cat. *J. Neurophysiology* 53:1323-1344.

176. Zhang, L. and Krnjevic, K. (1987). Apamin depresses selectively the afterhyperpolarization of cat spinal motoneurones. *Neurosci Lett* 74:58-62.

177. Zhang, L. and Krnjevic, K. (1988). Intracellular injection of Ca^{2+} chelator does not affect spike repolarization of cat spinal motoneurones. *Brain Res* 462:174-180.

178. Zwaagstra, B. and Kernell, D. (1980). Sizes of soma and stem dendrites in intracellularly labeled alpha-motoneurones of the cat. *Brain Res.* 204:295-309.